APPROACHES TO INTERMOLECULAR STRUCTURE ELUCIDATION UTILIZING NMR AND DNP PARAMETERS

by

Candy Tsiao

Dissertation submitted to the Faculty of the

Virginia Polytechnic Institute and State University

in partial fulfillment of the requirements for the degree of

DOCTOR OF PHILOSOPHY

in

Chemistry

APPROVED:

H.C. Dorn, Chairman

M. Hudlicky

H.M. Bell

B.E. Hanson

D.G.I. Kingston

August, 1989

Blacksburg, Virginia

APPROACHES TO INTERMOLECULAR STRUCTURE ELUCIDATION UTILIZING NMR AND DNP PARAMETERS

by

Candy Tsiao

Committee Chairman: Harry C. Dorn
Chemistry

(ABSTRACT)

This thesis is divided into two parts. The first part involves the study of molecular structure utilizing lanthanide induced shift (LIS) and lanthanide induced relaxation (LIR) nuclear magnetic resonance (NMR). It the course of these studies, it was found that the trifluoroethoxy group is a good deactivating group towards lanthanide shift reagents (LSR) and can be used to selectively deactivate multifunctional molecules.

The second part of the thesis involves the utilization of liquid-liquid intermolecular transfer (LLIT) dynamic nuclear polarization (DNP) to study the microwave power needed to achieve saturation using deuterated and nondeuterated 2,4,6-tri-tert-butylphenoxy and galvinoxyl radicals, and ^{14}N labelled, nondeuterated and ^{15}N labelled, deuterated 4-hydroxy-TEMPO radicals. Also, selective ^{1}H DNP enhancements for taxol in solid-liquid intermolecular transfer (SLIT) DNP low-to-high field transfer experiments were obtained. Finally, the syntheses of compounds with both a LSR moiety and a nitroxide radical moiety in the same molecule were examined. LLIT DNP transfer experiments for the intramolecular LSR-nitroxide radicals molecular system and the intermolecular LSR-radicals systems were studied. Conclusions based on this study provide new insight regarding approaches for new LIS and DNP studies.

Dedication

This thesis is dedicated to my parents

Acknowledgements

Without the help of many people, I would never have completed my thesis. Much of the thanks goes to my research director, Dr. Harry Dorn. I couldn't have picked a better research director. Whenever I needed help, encouragement or just someone to talk to, he was always available.

and also deserve a large vote of thanks. Without their help in setting up the instrumentation, and their patience in teaching me how to operate the DNP instruments and answering my endless questions, most of the work in this thesis would have been completed. Thanks also go to rest of my research colleagues: , , , ,

and .

To many friends I have made during my tenure at VPI, thanks for the memories. To , thanks for keeping me going to aerobics and listening to my sometimes endless and pointless stories. I would also like to thank the faculty and staff of the chemistry department.

Almost last, I would like to thank my parents for believing in me and for their love and sometimes financial support.

Most of all, I would like to express deepest appreciation for . Without his love and support, especially the last year, I would never have finished my dissertation. I hope we'll have a long time to enjoy each others company. Thanks a whole lot.

TABLE OF CONTENTS

LIST OF FIGURES

LIST OF TABLES

Introduction

Using nuclear magnetic resonance (NMR) to determine structural information is an integral part of research for a chemist. One way to use NMR for structure studies involves lanthanide shift reagents (LSR) [1]. Lanthanide shift reagents can provide structure information via lanthanide induced shifts (LIS) or lanthanide induced relaxation (LIR). Both techniques rely on the distance relationship between the lanthanide metal and the nucleus of interest.

Dynamic nuclear polarization (DNP) is a double resonance technique which has been used to improve the sensitivity of NMR signals in liquids and solids [2,3]. This technique has also been used to probe stereo-specific interactions in liquids.

This dissertation is divided into 2 main parts which consist of six chapters. The first part of the dissertation deals with LSR. Chapter 1 is mainly a brief review of the theories involved in using LIS and LIR data to obtain structural information. Chapter 2 describes the results obtained utilizing LIS and LIR techniques to determine structural information in multifunctional molecules. In the course of these studies the trifluoroethyl moiety was found to be a good deactivating group towards lanthanide metal complexation, so that functional groups could be selectively deactivated. Chapter 3 starts the second part of the dissertation. It gives a brief review of the history of DNP, theories involved in static liquid DNP, the stable radicals used for DNP, the enhancements that have been observed for some of the nuclei utilizing DNP, and the recent development of flow DNP experiments. Chapter 4 deals with the synthesis of a few deuterated stable radicals used in the study of saturation power needed in DNP experiments. Chapter 5 details the DNP study of taxol utilizing the low-to-high field flow transfer DNP experiment. Chapter 6 describes the synthesis of LSR-radical systems used in the DNP studies to see if the LSR can selectively destroy or increase the DNP enhancements.

Chapter 1 - Lanthanide Shift Reagents

Since the initial development of lanthanide shift reagents (LSRs) by Hinckley in 1969 [4], numerous structural nuclear magnetic resonance (NMR) studies have been reported. Lanthanide shift reagents not only separate overlapping peaks in a spectrum to give a first order spectrum, but structural information (e.g. geometric information) can also be obtained. Two ways of obtaining structural information from LSR involve lanthanide induced shifts (LIS) and lanthanide induced relaxation (LIR). This chapter will discuss the types of LSR used and theories involved in using LIS and LIR for obtaining structural information.

Lanthanide shift reagents function as Lewis acids binding to nucleophilic functional groups present (e.g. amino, hydroxyl, carbonyl, etc.) in the molecule of interest. The most commonly used ligands for binding to lanthanide metals are β-dicarbonyl compounds. A general illustration is shown below:

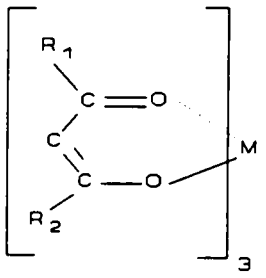

where M = Eu(III), Gd(III), Dy(III), Yb(III), etc.

and $R_1 = R_2$ = t-butyl (thd) [5]

R_1 = t-butyl, R_2 = heptafluoropropyl (fod) [6]

$R_1 = R_2$ = heptafluoropropyl (tfn) [7].

Fluorinated ligands are more useful for functional groups with decreased Lewis basicity and generally exhibit increased solubility in organic solvents [5]. The thd and fod ligands are widely used, because totally fluorinated ligands are harder to synthesize and keep anhydrous.

In addition to the LSRs indicated above, a number of other specialized shift reagents have been developed. These include chiral lanthanide shift reagents (for stereoisomer determinations) such as 3-(trifluoroacetyl)-d-camphor [8] or 3-(heptafluorobutyryl)-d-camphor [9]. For characterization of aromatic and olefinic compounds, binuclear shift reagent complexes are used. These include silver(I) heptafluorobutyrate used in conjunction with a lanthanide tris β-diketonate [10]. In 1980, a better binuclear reagent was developed which involved mixing silver β-diketonates (containing ligands of 6,6,7,7,8,8-heptafluoro-2,2-dimethyl-3,5-octanedione and 1,1,1-trifluoro-2,4-pentanedione) with lanthanide chelates of fod [11]. The binuclear complexes have silver atoms as a bridge between the soft Lewis base (olefin group) and the lanthanide ion.

In the simplest approach, the LIS provides a qualitative tool involving little theoretical interpretation of the data. In this case, the only requirement is for functional groups of sufficient nucleophilicity to complex with the lanthanide reagents which in turn reduce overlapping spectra to first order spectra. One example is the conversion of the ^{1}H NMR spectra of a straight chain aliphatic alcohol from second- to first-order as illustrated in Figure 1.1 [12]. Before the addition of LSR, the only hydrogens that can be identified are the H_G methylene hydrogens adjacent to the hydroxyl group and the H_A methyl hydrogens. As more LSR is added to the mixture, all of the methylene hydrogens are separated and one can determine that the alcohol is a seven carbon chain. With the use of LSR, the need for a NMR system with high field superconducting magnet is not crucial in obtaining structure information.

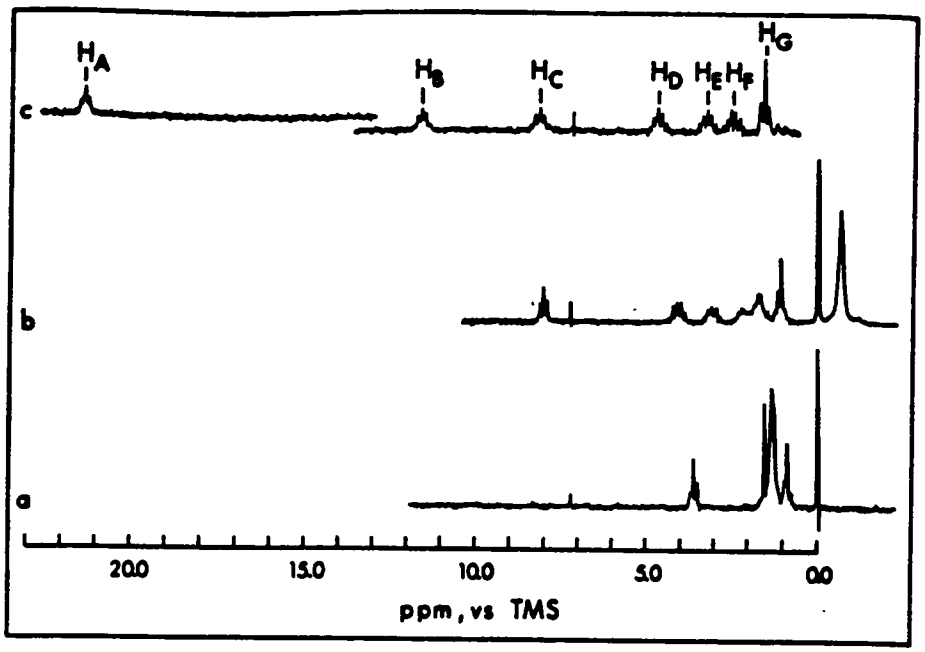

$$HO\text{-}CH_2\text{-}CH_2\text{-}CH_2\text{-}CH_2\text{-}CH_2\text{-}CH_2\text{-}CH_3$$

$$H_A \quad H_B \quad H_C \quad H_D \quad H_E \quad H_F \quad H_G$$

Figure 1.1 60 MHz ^1H NMR of 0.300 M 1-heptanol at various mole ratio: a) 0.00, b)0.19, c) 0.78, using $Eu(thd)_3$ as the LSR [12].

A more fundamental approach to the acquisition of geometric data is the use of LIS. Theoretically, this approach can provide a tool for solution structural analysis as powerful as x-ray crystallography is for solid state structural analysis. Unfortunately, this is not true in practice.

LIS is defined as the difference between the resonance frequencies of a substrate (S) and the shift of the lanthanide reagent-substrate adduct (LS). It is usually expressed in parts per million (Δppm). Two components contribute to the LIS observed in a LS system: the dipolar or pseudocontact term and the Fermi contact term. The first term describes all magnetic-dipolar types of interactions while the contact term accounts for the possible spin-delocalization within the complex. The dipolar term acts through space and represents the magnetic field exerts by the unpaired electrons on a nucleus via a dipole-dipole interaction, while the contact term acts through bonds and represents a polarization caused by covalent bond character between substrate and lanthanide reagents [13,1].

The dipolar shift can be calculated using the following equation: [14]

$$\Delta_{dip} = K_{ax} (3 \cos^2\theta - 1 / r^3) + K_{nonax} (\sin^2\theta \cos 2\omega / r^3) \qquad (1)$$

where r = the length of a vector joining the paramagnetic center and the nucleus

θ = the angle between the vector r and the z-magnetic axis

ω = the angle which the projection of r into the xy-planes makes with the x-magnetic axis (shown in Figure 1.2)

K_{ax}, K_{nonax} = constants which are functions of the magnetic anisotropy of the complex.

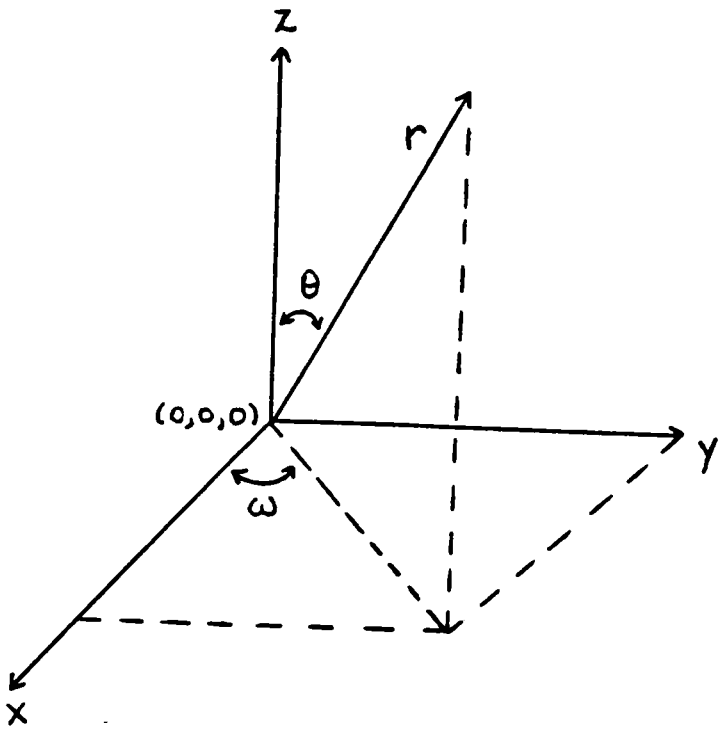

Figure 1.2 Definition of the parameters for the dipolar shift equation; the lanthanide ion is at the origin of the coordinate system.

In most cases, K_{nonax} is zero because the complex in solution is assumed to exist with axial symmetry. Therefore equation 1 reduces to

$$\Delta_i = K (3 \cos^2\theta_i - 1 / r_i^3) \qquad (2)$$

The above equation is called the McConnell-Robertson equation [15]. This equation is used most often to determine geometric information from LIS. As noted, the LIS obtained has an inverse r^3 relationship. By measuring the LIS, one can determine distance between the lanthanide metal and substrate's nuclei. Thus geometric information can be obtained.

The contact shift occurs by direct electron-nucleus magnetic interaction. The shift occurs by movement of unpaired electron spin density from the metal cation to the ligand via covalent bond formation. This mechanism operates through the metal cation-coordinating bond, therefore, it depends on the degree of covalency in this bond. This interaction is independent of the $3 \cos^2\theta - 1$ term and falls off rapidly with increasing distance except in conjugated systems, because they facilitate the delocalization of unpaired electrons [13].

The expression for the contact shift (Δ_c) is given by the following equation:

$$\Delta_c = \Delta_{\nu/\nu_0} = (A/h) \langle S_z \rangle / (\gamma B_o / 2\pi) \qquad (3)$$

where A/h = hyperfine coupling constant (Hz)

$\langle S_z \rangle$ = thermal average of the component along the field of the electron spin magnetization of the paramagnetic ion

Δ = magnetogyric ratio of the nucleus

B_o = applied magnetic field.

for lanthanide ions, the value of $\langle S_z \rangle$ in the ground electronic state is given by:

$$\langle S_z \rangle_J = - \beta J(J + 1) g_J (g_j - 1) B_o / 3 \kappa T \qquad (4)$$

where κ = Boltzmann constant

T = absolute temperature

β = Bohr magneton

J = quantum number for the total angular momentum

g_J = Lande g factor

Substituting equation 4 into equation 3, the contact shift becomes: [16]

$$\Delta_c = - 2\pi (A/h) \beta J(J + 1) g_J(g_J - 1) / 3 \kappa T \gamma$$

Since the unpaired electron spin in the atomic s orbital of the observed nucleus is induced through chemical bonds between the nucleus and the lanthanide ion, the hyperfine coupling constants are usually larger for those magnetic nuclei in closer proximity (through the bonds) to the lanthanide ion. Large contact shifts have been observed for ^{17}O, ^{14}N, and ^{31}P nuclei at the coordination sites and for ^{13}C nuclei near the coordination sites [17].

Even though there is a mathematical treatment for the contact shift, the measurements are rather uncertain and require a detailed evaluation of the molecular orbitals involved. Most of the time, investigators try to avoid dealing with this formalism. Studies have shown that ^1H LIS contributions come predominantly from the pseudo-contact term, except for aromatic systems [17]. The choice of the lanthanide metal used for LIS can also play a role in determining which term predominates. Eu^{3+} gives the largest contribution of contact component and Yb^{3+} has the smallest contact component for ^{13}C nucleus [17]. Therefore, Eu^{3+} is used most often for the shift studies of ^1H resonance since the pseudo-contact term

dominates, and Yb^{3+} is used for other nuclei. This avoids the problem of separating the pseudo-contact and contact components of the induced shifts.

Before the LIS can be used, the stoichiometry of the LS complex has to be determined. The optimum situation would result if only one equilibrium were involved where the formation of a 1:1 shift reagent-substrate complex, is observed as illustrated below:

$$L + S = LS \tag{6}$$

Unfortunately, other equilibria can occur such as the formation of a 1:2 shift reagent-substrate complex:

$$LS + S = LS_2 \tag{7}$$

and the formation of a shift reagent dimer:

$$2L = L_2 \tag{8}$$

Equations 7 and 8 can compete with equation 6 and complicate LIS measurements. Techniques such as X-ray crystallography, low-temperature NMR, infrared spectroscopy, circular dichroism, and mass spectrometry have been used to show that all three equilibria do exist [1]. Most of the time, the lanthanide metal and substrate are assumed to form a 1:1 adduct for the measurements of LIS. The other equilibria will cause a deviation in the plot of LIS especially at higher concentrations of LSR [13].

In theory to use LIS to calculate geometric information, one would prefer to use lanthanide metal cations or study nuclei that give predominantly pseudo-contact shifts.

Practically, this does not always work. In order to use LIS for geometric calculations, the following assumptions have to be made. [13,1]

1) The lanthanide reagent-substrate complex can be described by a single set of coordinates.
2) The "apparent" axial symmetry of the adduct in solution which makes the nonaxial contribution zero is assumed.
3) The diamagnetic shift upon addition of LSR to the substrate solution is negligible.
4) Contact interactions are negligible.
5) The principal magnetic axis passes through the lanthanide ion and the coordination center of the substrate.
6) Only a single stoichiometric complex species exits in solution in equilibrium with the uncomplexed substrate.

After applying the above assumptions, usually a computer program is used to match the measured LIS's with possible geometries until a match is found. Some of the programs that have been used for this purpose are: SIMULATION [18], CHMSHIFT [19], PDIGM [20], and MAXI [21]. Due to the problems and assumptions made in measuring LIS, many doubts remain as to how quantitative the results are.

Lanthanide Induced Relaxation (LIR)

As previously indicated, a second approach to obtain geometric information from LSR involves monitoring spin-lattice relaxations (T_1s) for the lanthanide-substrate complexes. Spin-lattice relaxation times are shortened by the paramagnetic lanthanide metal in the complexes and exhibits a $1/r^6$ dependency if dipolar interactions are assumed. Therefore, these perturbations can be used to calculate absolute distances from the paramagnetic metal

to the nucleus [22]. The advantage over the LIS in that the distance dependency rests on a more solid theoretical ground than the pseudo-contact shift equation and does not require assumptions as to the location of the principal magnetic axis [1].

The equation for spin-lattice relaxation time has two terms, dipolar and scalar, but in the presence of a paramagnetic lanthanide metal dipolar relaxation usually dominates [23]. The T_1 dipolar term can be expressed as: [24]

$$\frac{1}{T_{1M}} = \frac{2}{15} \frac{\gamma_I^2 g^2 J(J+1) \beta^2}{r^6} \left(\frac{3\tau_c}{1 + \omega_I^2 \tau_c} + \frac{7\tau_c}{1 + \omega_S^2 \tau_c} \right) \quad (9)$$

where T_{1M} = spin-lattice relaxation time of the given nucleus in the lanthanide metal complex

γ_I = nuclear magnetogyric ratio

g = Lande g factor

β = Bohr magneton

r = the distance between the paramagnetic lanthanide metal and the nucleus being monitored

ω_I = nuclear Larmor frequency

ω_S = electron Larmor frequency

τ_c = the overall correlation for the LSR complex.

τ_c can be expresses as:

$$1/\tau_c = 1/\tau_R + 1/T_{1e} + 1/\tau_M \quad (10)$$

where τ_R = rotational correlation time of the complex

T_{1e} = electron spin relaxation time

τ_M = life time of the lanthanide ligand complex.

Rotational correlation time for small molecules is typically 10^{-10} - 10^{-11} seconds. The life time of the complex is usually no shorter than 10^{-8} seconds, and the electron-spin relaxation time is 10^{-10} seconds for Eu^{2+} and Gd^{3+} ions and 10^{-13} seconds for Pr^{3+}, Eu^{3+}, and Yb^{3+}. Therefore, the electron-spin relaxation time typically determines the τ_c in the cases of Eu^{+3} and Yb^{+3} [25].

For lanthanide-ligand complexes with rigid structures, the overall correlation time is assumed to be the same for all the nuclei in the complex. For flexible substrate molecules, the intramolecular motions will contribute differently to the correlation times of nuclei at different sites. For many molecules that have been studied, the correlation times obtained are nearly equal for the nuclei in the complex. Therefore, equation 9 can rewritten in terms of the electron spin relaxation time to yield equation 11 [26]

$$1/T_{1M} = C\,(T_{1e} / r^6) \qquad (11)$$

where C = a constant.

This way r can be determine for a particular nucleus in the complex. From equation 11, the ratio of induced relaxation rates of the nuclei i and s can be given as:[25]

$$(1/T_{1M})_i / (1/T_{1M})_s = \langle r_i^{-6} \rangle / \langle r_s^{-6} \rangle \qquad (12)$$

Accordingly, analysis of relaxation data can provide structural information different from LIS data due to the lack of angle dependence term and no symmetry assumptions as shown by LaMar et al. [27] and Peters et al. [28].

Both LIS and LIR data can be used to determine molecular geometry if proper techniques are used and only one functional group is present in the molecule of interest. LSR studies of polyfunctional molecules often prove difficult due to uncertainties involving the location at which complexation occurs [29,30]. The preferred site of complexation is often difficult to determine with several factors including functional group basicity and steric environment playing a role. For example, it is expected that alcohols will complex more readily with LSR's than ketones based on the relative nucleophilicity of the respective functional groups (NH_2 > OH > ketone > ester > CN). However, tertiary alcohols coordinate more weakly than ketones. Also, small ring ethers (e.g. epoxides) complex more strongly than their acyclic counterparts.

When saturation of the preferred complexation site occurs, the LSR will begin to complex at the secondary site which has the effect of complicating rather than simplifying the spectra. Wright and Wei [31] found that for dimethoxy methyl benzoates, the o-methoxy groups exhibits a larger LIS than the ester even though the opposite would be predicted based on functional group nucleophilicity (Figure 1.3). This behavior is due to bidentate complexation between the o-methoxy group and the LSR and is not observed if the methoxy groups are meta or para. The same situation also applies for the isomers of methoxy methyl benzoate. The methoxy group in the ortho-isomer exhibits a larger LIS than the methoxy in the para-isomer due to bidentate complexation of the methoxy oxygen and the carbonyl oxygen of the ester group.

Although little has been reported in the area of functional group deactivation towards LSR complexation, there are some interesting examples in the literature.

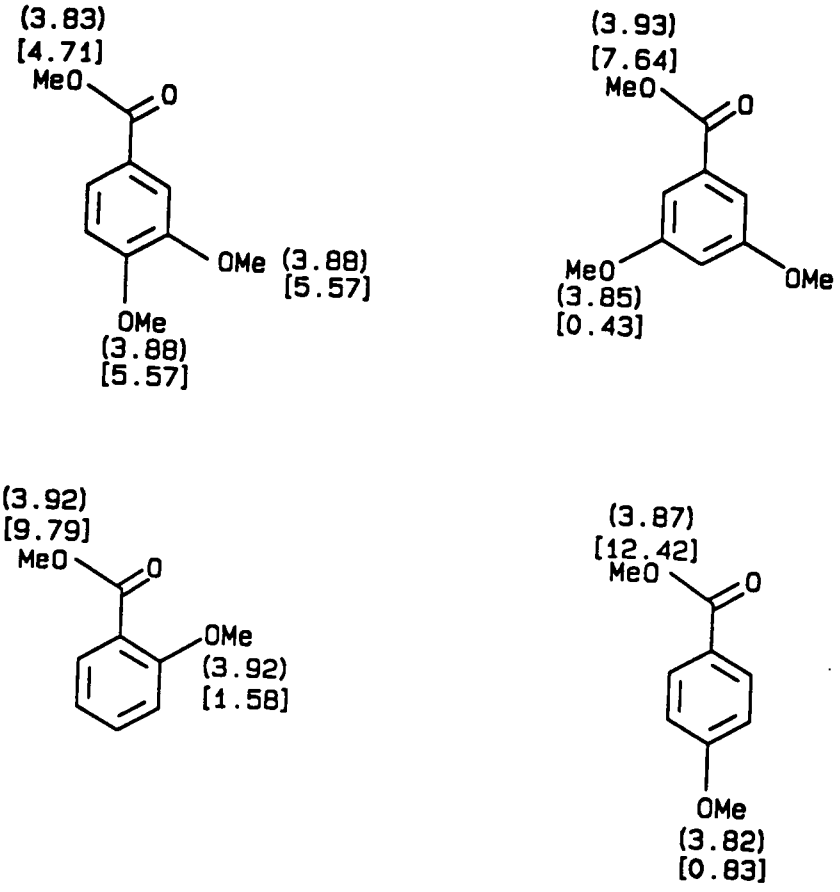

Figure 1.3 The NMR Chemical Shifts (ppm) and Lanthanide Induced Shifts (ppm) of Methoxybenzoates in $CDCl_3$ as Studied by Wright and Wei [31].

In 1970, Crump et al [32] reported that ethylene thioketal and trifluoroacetate groups could be used to deactivate oxygen containing functionalities (ketone and hydroxy groups) toward complexation with lanthanide shift reagents. This observation was utilized in assigning functional group positions in several of the Δ^5-Androsterenes. More recently, Raber and Propeck [33] reported that the t-butyldimethylsilyl ethers function acted as a steric blocking group toward LSR complexation. This work involved derivatizing several alcohols (primary, secondary, and tertiary) to form the trifluoroacetates, trimethylsilyl ethers, and t-butyldimethylsilyl ethers. They found that only t-butyldimethysilyl ethers were consistently capable of blocking complexation between the ether oxygen and the lanthanide metal. With trimethylsilyl ethers, complexation was hindered only in those cases where a tertiary alcohol was involved. Trifluoroacetate derivatives are less satisfactory due to the basic nature of the carbonyl oxygen which acts as a secondary binding site for the shift reagent. Also, the trifluoroacetate esters are prone to hydrolysis under the conditions of the LIS experiments [34].

Previously, Koller and Dorn [35] have reported that 2,2,2-trifluorodiazoethane (TFD) readily derivatizes alcohols, phenols, thiols and carboxylic acids by the reaction indicated below:

$$R\text{-}X\text{-}H + CF_3CH{=}N{=}N \xrightarrow{H^+} R\text{-}X\text{-}CH_2CF_3 + N_2\uparrow$$

R = alkyl, aryl

X = O, S, and $\underset{\underset{O}{\|}}{C}\text{--}O$

Also, Wild [36] has shown that ketones can be converted to bis(trifluoroethyl) ketals by the procedure outlined below.

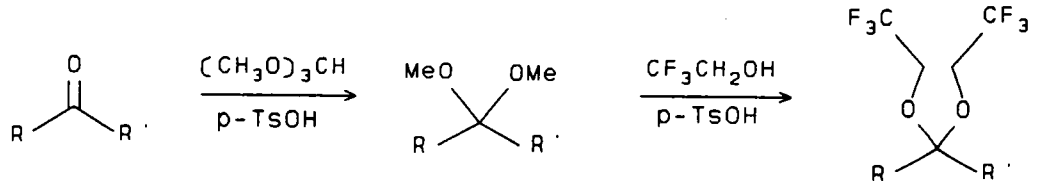

R, R' = alkyl, aryl

Preliminary studies indicate that the trifluoroethyl group acts as a deactivating group toward lanthanide shift reagents [35,36].

Besides using LIS, LIR can also be used to acquire structural information. McLennan and Lenkinski [26] in 1984 elegantly demonstrated the preferred site of complexation of $YbCl_3$ to adriamycin. The structure of adriamycin is shown below:

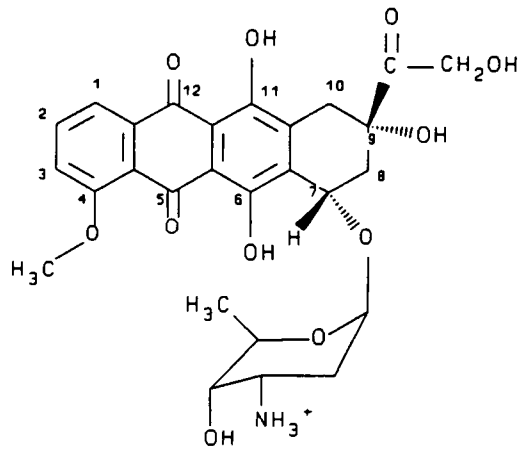

From the structure, there are several functional sites with at which Yb^{+3} metal could complex. When $YbCl_3$ was added to a solution of adriamycin in d_4-methanol, they observed 2 separate sets of signals in the adriamycin ^1H NMR spectra. One set for the complexed molecule and another set for the uncomplexed molecule. By measuring the T_1's of the hydrogens of the molecule, they determined that the Yb^{+3} metal chelates between C-11 and C-12 , the quinone and hydroquinone system. Even though McLennan and Lenkinski were able to determine distances for the complex of adriamycin and $YbCl_3$, they had to make several assumptions (such as there is only one stable conformation of adriamycin-metal complex) and use iterative procedures to determine which distances best fit the experimental data. The main reason they were able to determine the actual distances is due to the fact they observed two separate spectra corresponding to the complexed and uncomplexed species. If they had observed only one spectrum, the analysis would have been much more difficult.

Chapter 2

Lanthanide Induced Shift (LIS) and Lanthanide Induced Relaxation (LIR) Studies

Results and Discussion

Section 1: LIS Studies

We have shown previously [36] that when a ketone functionality is derivatized to the bis(trifluoroethyl) ketal, the ketal will not complex with lanthanide shift reagents. This seems to indicate that the trifluoroethyl group can act as a deactivating group toward LSRs. However, the initial studies dealt with monofunctional substrates. Polyfunctional molecules need to be studied to see if the trifluoroethyl group can indeed act as a selective deactivating functionality towards LSRs. This chapter will discuss the results of more detailed studies of the deactivating capabilities of the trifluoroethyl group and molecular information obtained for some of the compounds employed.

In works reported by Wild, 1,4-cyclohexanedione 1 was derivatized to the mono and bis(trifluoroethyl) ketals 2 and 3 [36]. In the present studies, LIS's have been obtained for these compounds.

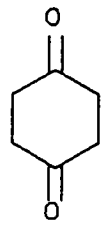

1

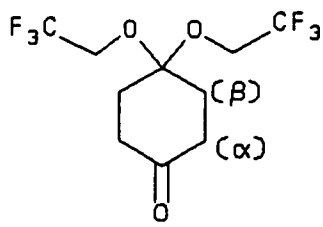

2

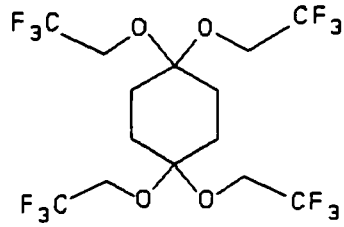

3

Figure 2.1 compares the complexing tendencies of 1 and 3 by observing the LIS exhibited by the ring hydrogens. As expected, dione 1 exhibits a high degree of complexation even at low LSR/substrate ratios. In contrast, the bisketal 3 exhibits no evidence of lanthanide metal complexation. The ^1H chemical shifts of the ring hydrogens exhibit no change as the concentration of the shift reagent is increased. Figure 2.2 presents the LIS data for compound 2. In this case, there are two unprotected types of hydrogens present in the substrate: those alpha to the carbonyl group (α) and those beta to the carbonyl group (β). As can be seen, both sets of hydrogens show evidence of complexation, however, the slope of the (α) hydrogens is greater than that exhibited by the (β) hydrogens. Table 2.1 gives the slopes for the (α) and (β) hydrogens and their LIS with increasing shift reagent concentration.

Next, the "ortho complexation effect" observed by Wright and Wei was examined to see if the same would occur with a trifluoroethyl group utilized for deactivation. The compounds 4,6-dimethyl-2-methoxyacetophenone (4), 2,6-dimethyl-4-methoxyacetophenone (5), 4,6-diemthyl-2-trifluoroethoxyacetophenone (6), and 2,6-dimethyl-4-trifluoroethoxyacetophenone (7) were synthesized and studied.

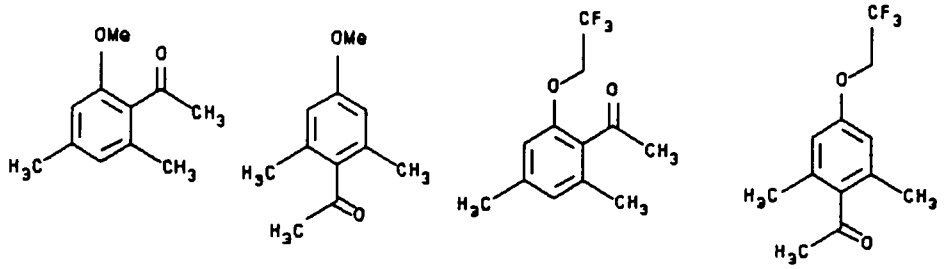

4 5 6 7

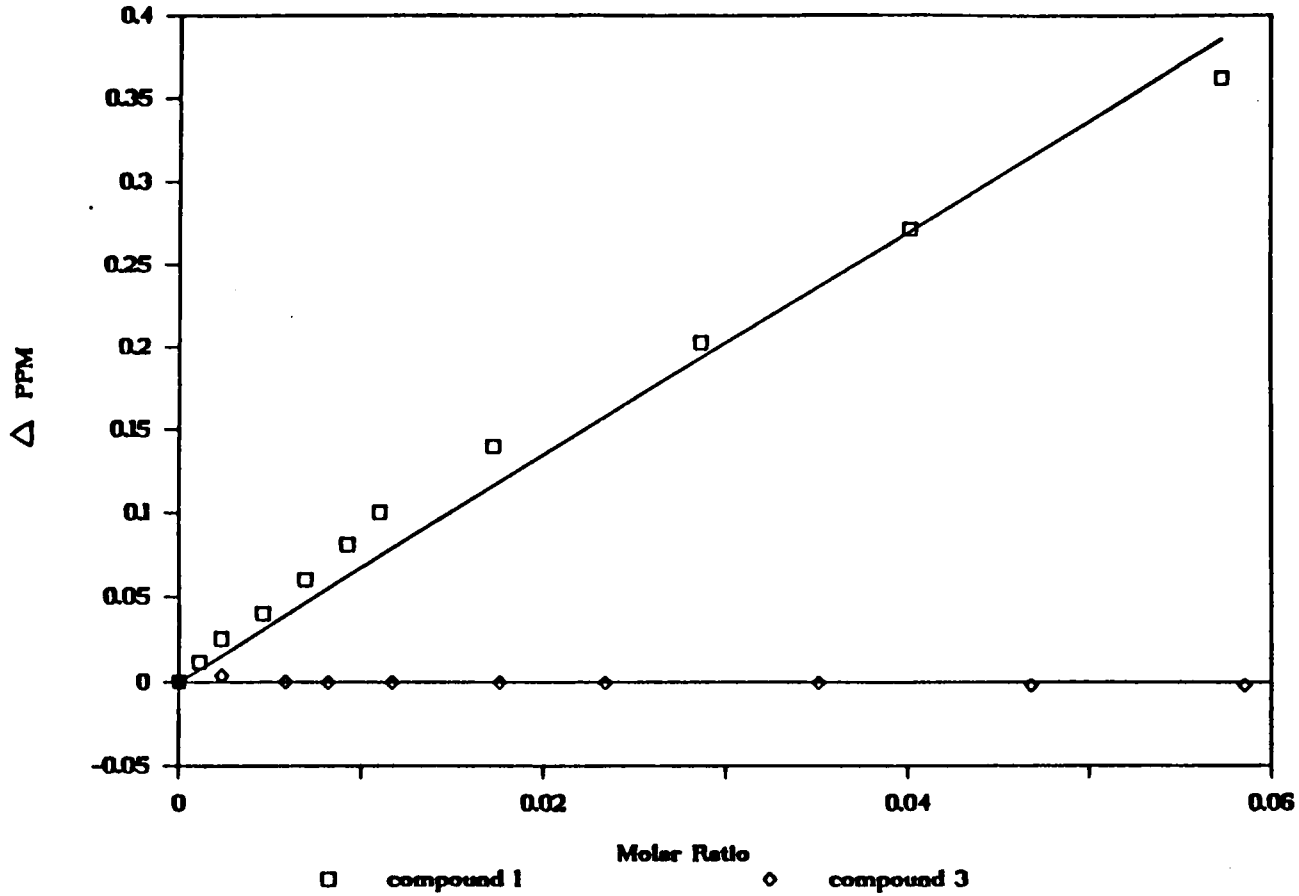

Figure 2.1 The changes in ^1H chemical shifts for compounds 1 and 3 as a function of added $Eu(fod)_3$.

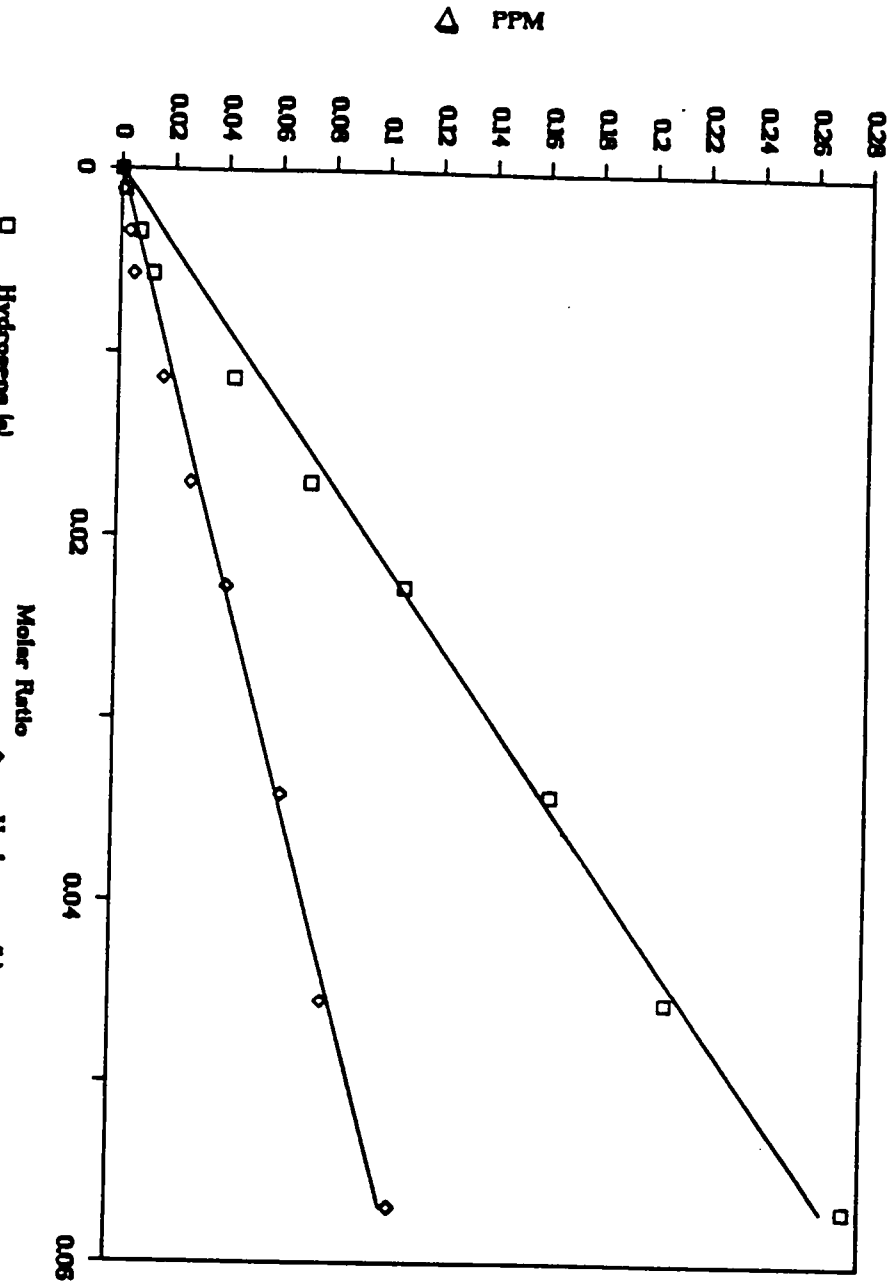

Figure 2.2 The changes in ^1H chemical shifts for the α and β hydrogens of compound **2** as a function of added $Eu(fod)_3$

Table 2.1 LIS (in ΔPPM) for Compound 2 as a Function of Added $Eu(fod)_3$ and Slopes

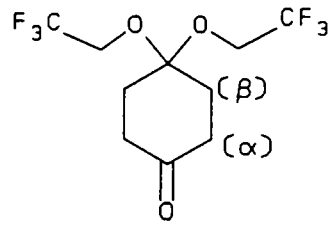

2

Molar Ratio [Eu]/[Substrate]	α-Hydrogen (Δ (δ PPM))	β-Hydrogens (Δ (δ PPM))
0	0	0
0.00114	0.0013	0.0005
0.00341	0.0072	0.0032
0.00569	0.0123	0.0051
0.01137	0.0433	0.0167
0.01706	0.0723	0.0277
0.02275	0.1078	0.0415
0.03412	0.1630	0.0628
0.04550	0.2074	0.0788
0.05687	0.2743	0.1049
Slopes[a]	4.68 ± 0.09	1.69 ± 0.09

a) The slopes calculated are the limiting slopes at low molar ratio

The LISs were measured using $Eu(fod)_3$ as the lanthanide shift reagent. The reason the 2,6-dimethyl-4-methoxyacetophenone (5) and 2,6-dimethyl-4-trifluoroethyoxyacetophenone (7) were included was to have a reference system that would not exhibit the "ortho" chelating effect. In this way, a comparison can be made to their ortho-isomers. The LIS's of compound 4 and compound 6 were measured as a 50/50 molar mixture of these two compounds. In this manner, both compounds 4 and 6 would equally compete for the available lanthanide shift reagents (LSR) under identical conditions. Whereas, the LIS's of compound 5 and compound 7 were measured separately. The methoxy group hydrogens and the methyl group hydrogens of the acetyl functionality were monitored in compounds 4 and 5. The methylene hydrogens of the trifluoroethoxy group and the methyl hydrogens of the acetyl functionality were monitored in compounds 6 and 7. Figure 2.3 compares the LIS of compounds 4 and 6 (the ortho-isomers) with increasing LSR concentration. As indicated in Figure 2.3, the methoxy hydrogens exhibit a higher degree of complexation relative to the methylene hydrogens of the trifluoroethoxy group. The reverse is true for the methyl hydrogens of the acetyl functionality of compound 4 and compound 6. Figure 2.4 and Figure 2.5 illustrates the LIS for compound 5 and compound 7, respectively. In those two figures, the methyl hydrogens of the acetyl functionality are closest to the only site of complexation and their slopes are much higher than the methoxy hydrogens or the methylene hydrogens. The slopes of the hydrogens measured for all four compounds are listed in Table 2.2. This data suggests that the 4,6-dimethyl-2-methoxyacetophenone (4) does exhibit the "ortho" chelation effect while 4,6-dimethyl-2-trifluoroethoxyacetophenone (6) does not exhibit any significant "ortho" chelation. The slope of the methoxy hydrogens is ~3 times as great as the methylene hydrogens of the trifluoroethoxy group. This is in contrast to the methyl hydrogens of the acetyl functionality of compound 4 are smaller by a factor of 2 than the methyl hydrogens of compound 6. These observations indicate the methoxy group is participating in the specific "ortho" chelation as illustrated below:

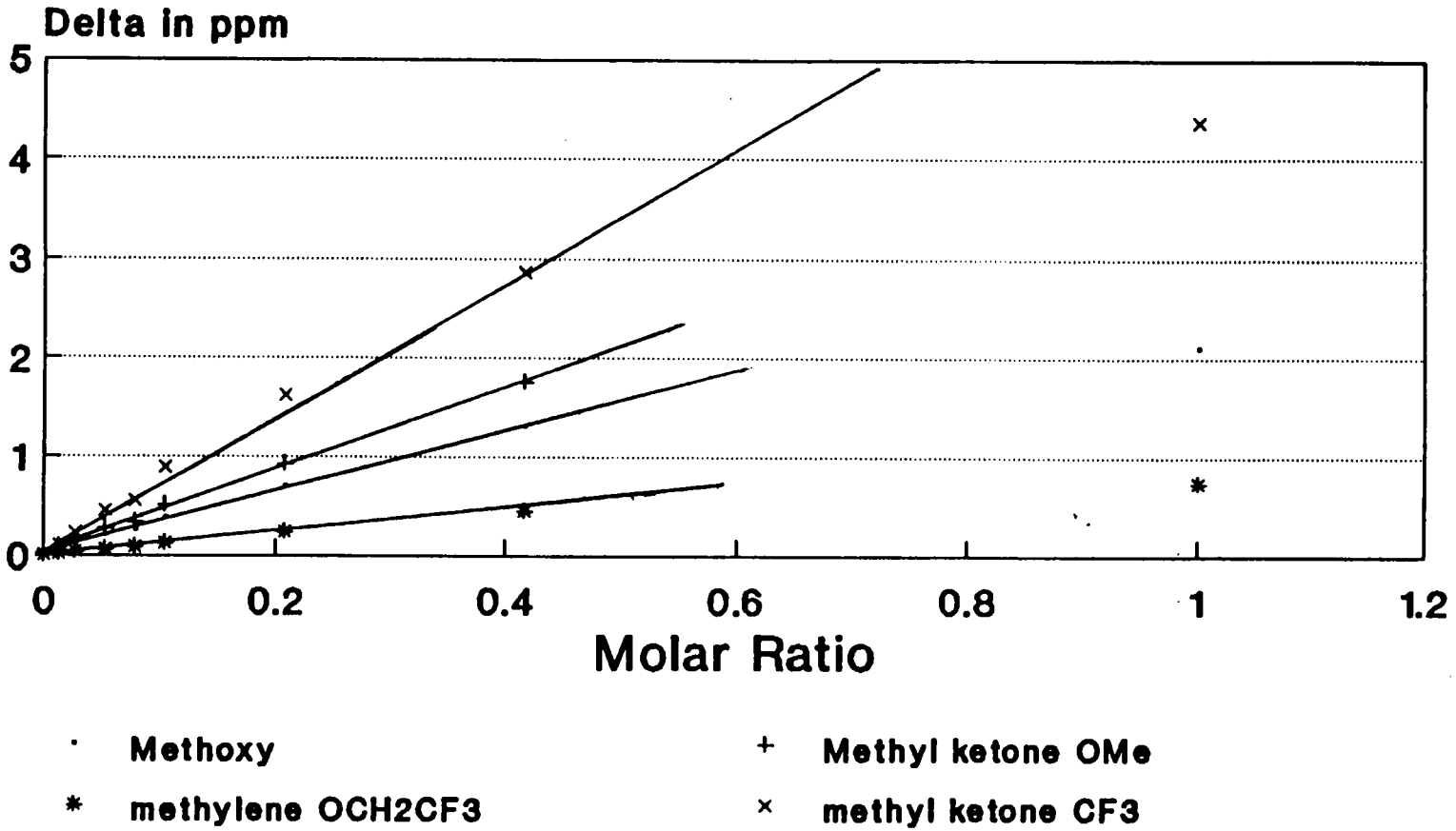

Figure 2.3 The changes in ^1H chemical shifts for compound 4 and 6 as a function of added $Eu(fod)_3$.

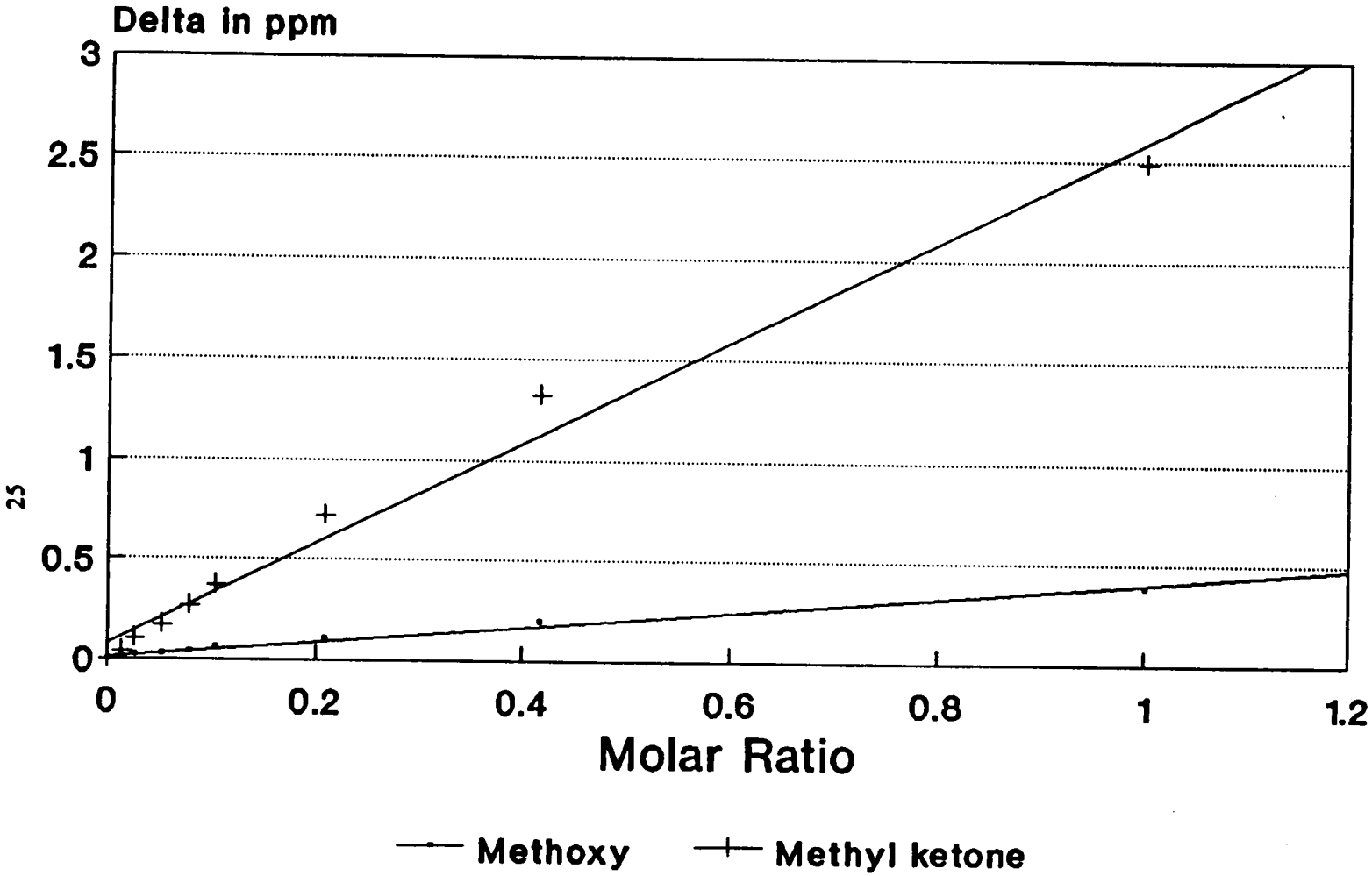

Figure 2.4 The changes in ^1H chemical shifts for compound 5 as a function of added $Eu(fod)_3$.

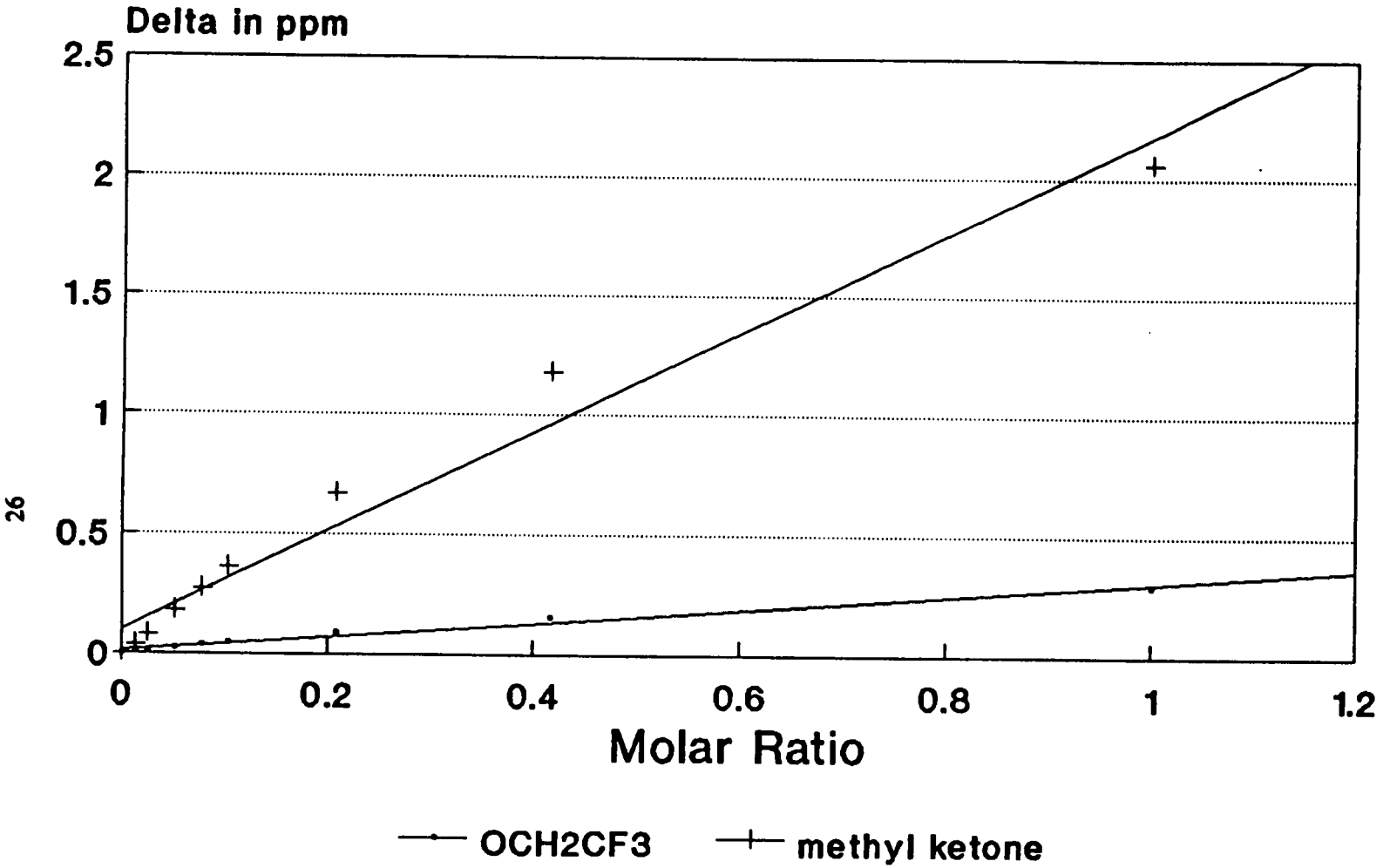

Figure 2.5 The changes in ^{1}H chemical shifts for compound 7 as a function of added $Eu(fod)_3$.

Table 2.2. The LIS ^{1}H NMR Limiting Slopes for the Hydrogens Monitored For Compounds 4 to 7.

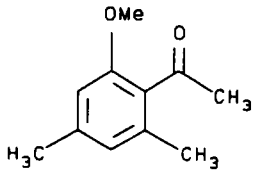

4

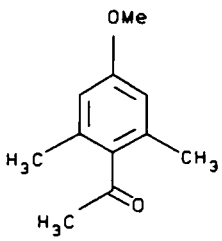

5

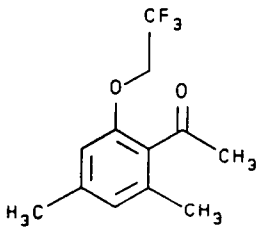

6

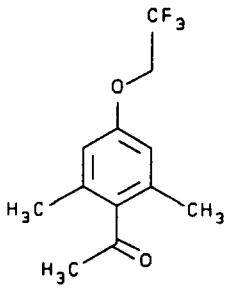

7

Compound	Methoxy Hydrogens (OMe)	Methylene Hydrogens (OCH_2CF_3)	Methyl Hydrogens (CH_3-C=O)
4	3.20 ± 0.05		4.31 ± 0.08
5	0.50 ± 0.01		3.25 ± 0.05
6		1.07 ± 0.01	7.14 ± 0.18
7		0.40 ± 0.01	2.96 ± 0.08

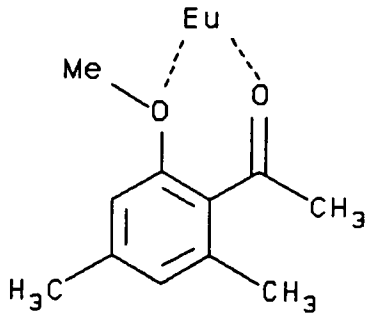

As reported by Wright and Wei [31], ortho ^{1}H NMR chelation increases the chemical shift for the methoxy functionality while decreasing the chemical shift of acetyl methyl functionality. In contrast, compound **6** contains a trifluoroethoxy group and does not exhibit specific "ortho" chelation, and with only apparent complexation site being the acetyl functionality. As a result, the methyl hydrogens for the acetyl functionality for compound **6** have a higher slope than its methoxy counterpart.

The slopes for compound **5** and **7** are similar which is expected for dominant complexation at only the carbonyl site. This is because these two compounds cannot form the specific "ortho" chelate with $Eu(fod)_3$ like compound **4**. Also, in each case the slopes of the methyl hydrogens of the acetyl functionality are almost the same. The methylene hydrogens of the trifluoroethoxy group exhibit a slightly smaller slope than the methoxy hydrogens which again is presumably due to the lack of complexation at the trifluoroethoxy site.

The reason that the methylene hydrogens of compound **6** have a higher slope (at least twice) than the analogous protons in compound **7** is due to the fact that the methylene hydrogens in compound **6** are closer to the complexation site than those in compound **7**. As stated before, the ^{1}H LIS is dominated by dipolar interaction and is distance dependent.

This is evident for compounds 6 and 7.

An interesting observation for these four compounds is that the acetyl functionality in the ortho-isomers seem to complex better (more) than the same functionality in the para-isomers. This is apparently due to steric effects. The acetyl functionality in the ortho-isomers is less sterically hindered toward complexation with the lanthanide shift reagents than in the para-isomers. This observation is also supported by the synthetic approach to these compounds. In the acylation of 3,5-dimethylanisole and 3,5-dimethyl-trifluoroethoxybenzene with $AlCl_3$ and acetic anhydride at room temperature, the ortho-isomers are always the major product in the acylation reaction. Even though the ratio of the products changes when going from the methoxy to trifluoroethoxy, 6 : 1 to 3 : 1, the ortho-isomers are still the predominant product.

After establishing that the trifluoroethyl group does act as a deactivating group for hydroxyl and carbonyl functionalities and can selectively deactivate one functional group in the presence of another, we undertook a study to establish isomer geometries utilizing this approach. (E) and (Z)-(2',2',2'-trifluoroethoxy)-4-phenyl-3-buten-2-one (8) were synthesized previously by Wild [36] in our lab by the reaction of 4-phenyl-3-butyn-2-one with sodium 2,2,2-trifluoroethoxide in refluxing 2,2,2-trifluoroethanol.

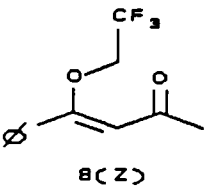

8(Z)

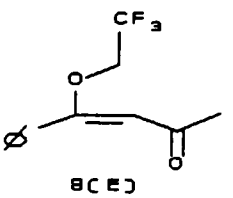

8(E)

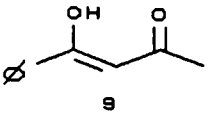

9

Compounds **8**(Z) and **8**(E) are the trifluoroethoxy derivatives of the β-diketone, 1-phenyl-2,4-butanedione. Compound **9**, shown in one of its tautomeric forms, has two active LSR complexation sites and is the parent difunctional molecule of compound **8**. Based on the LIS study of these TFE derivatives, the major isomer exists in the Z form. The ^{1}H NMR spectrum of compound **8** is shown in Figure 2.6(a). Assuming the carbonyl group is the only significant site for complexation, the induced shifts of the hydrogens α to the trifluoromethyl group as well as the ortho phenyl hydrogens should allow assignment of these isomers. For example, we believed that the ortho phenyl hydrogens are spatially closer to the complexation site for the E isomer. Figure 2.6(b) is a comparison of the shifts of the methylene hydrogens with the shifts of the ortho phenyl hydrogens. In directly comparing Figures 2.6(a) and 2.6(b), it can be observed that following the addition of 0.12 equivalents of Eu(fod)$_3$, the major methylene signal (the quartet at 4.31 ppm) has shifted downfield by ~ 0.9 ppm to 5.2 ppm. In contrast, the minor isomer's methylene signal has shifted downfield ~ 0.45 ppm from 4.15 to 4.6 ppm. The ortho phenyl hydrogens for the E-isomer resonate at 7.54 ppm in the absence of shift reagents. However, they are shifted to 8.1 ppm after the addition of LSR. In the case of the Z-isomer, these same hydrogens are shifted only 0.2 ppm from 7.6 to 7.8 ppm. This trend is further illustrated in Figure 2.7 and 2.8 where the LIS's for the ortho phenyl hydrogens and the methylene hydrogens are presented.

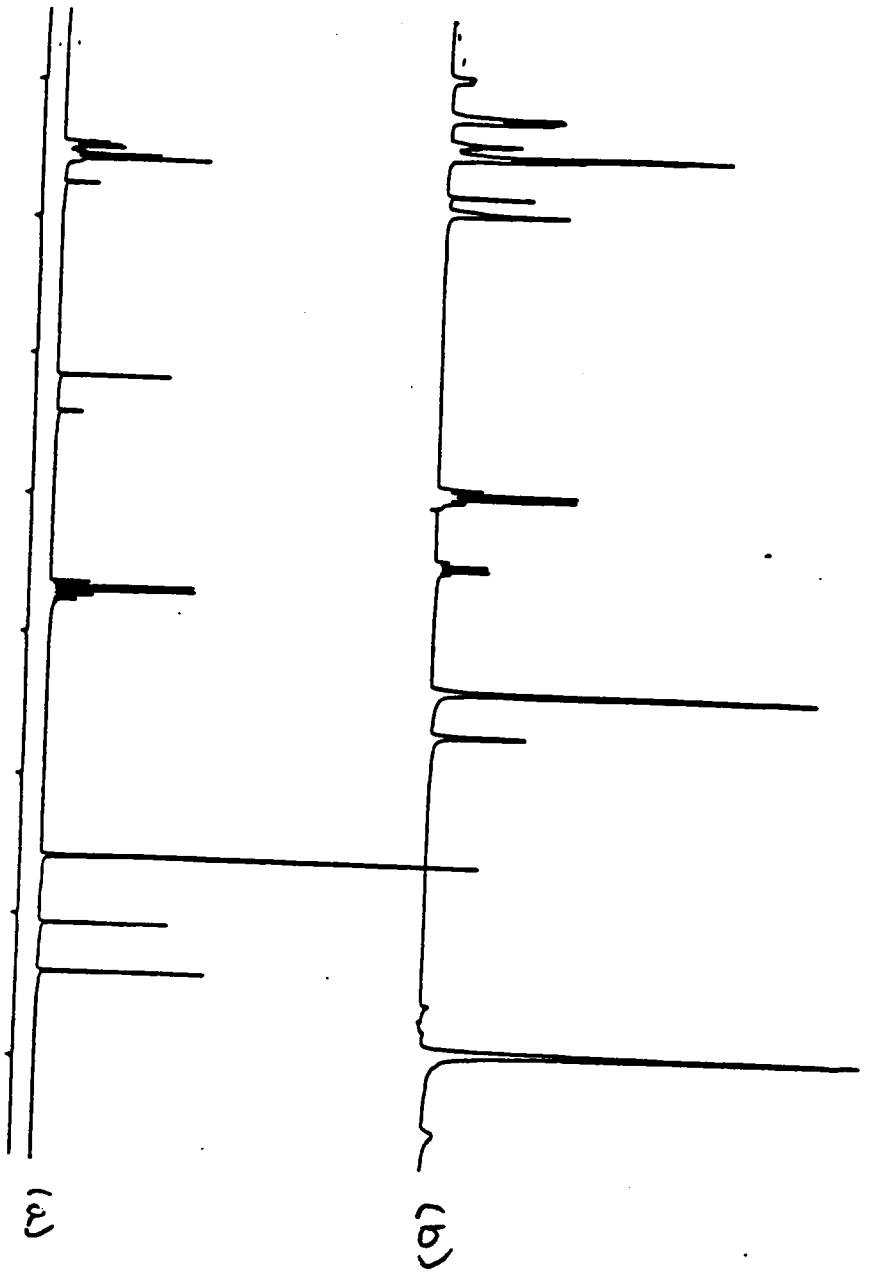

Figure 2.6 The ^{1}H NMR spectra of compound **8**: a) in absence of Eu(fod)$_3$ b) in 0.12 equivalent of Eu(fod)$_3$.

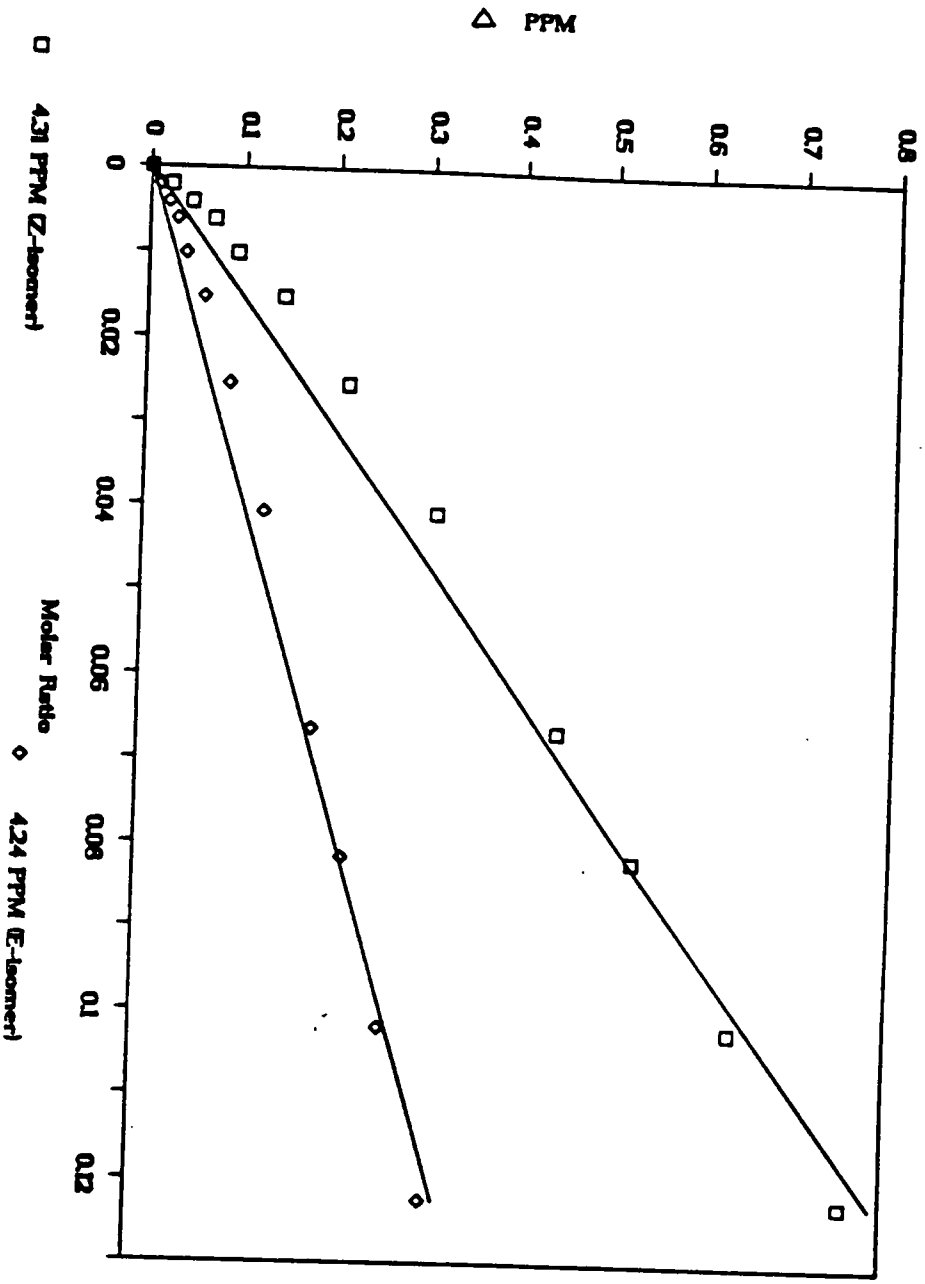

Figure 2.7 The changes in ^1H chemical shifts for the hydrogens α to the trifluoromethyl group of compound **8** as a function of added $Eu(fod)_3$.

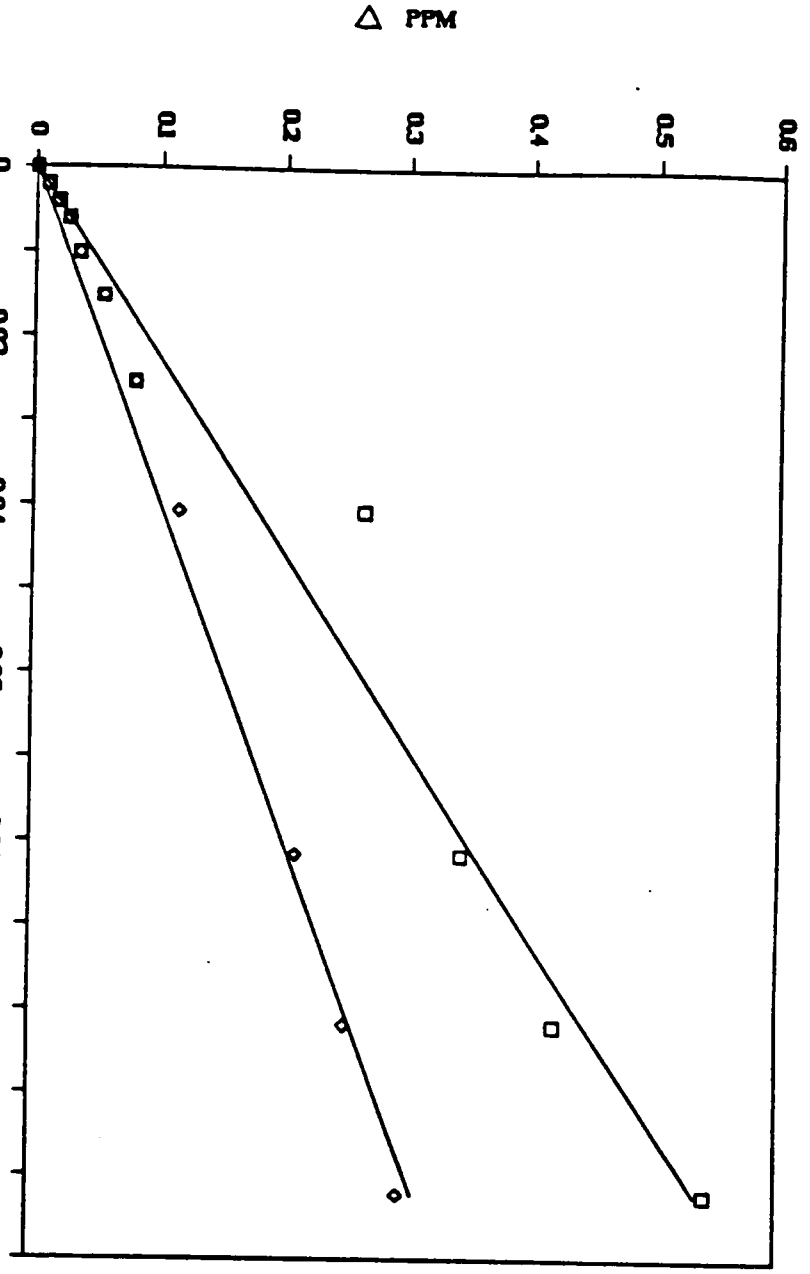

Figure 2.8 The changes in ^1H chemical shifts for the ortho phenyl hydrogens of compound **8** as a function of added Eu(fod)$_3$

Section 2: LIR Studies

LIS studies of the trifluoroethoxy group indicate that it is a good deactivating group toward Lewis acid complexation. LIR studies are performed to determine if relaxation rates ($1/T_1$) of nuclei are not affected in complexes involving the trifluoroethoxy group. As previously indicated, LIR is a also distance dependent parameter (the closer the nuclei is to the complexation site, the higher relaxation rate (shorter the T_1)).

The first compounds studied were 3,5-dimethyl-trifluoroethoxybenzene (**10**), 3,5-dimethyl-ethoxybenzene (**11**), and compound **7**.

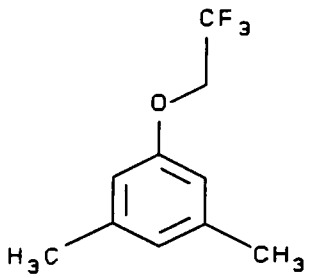

10

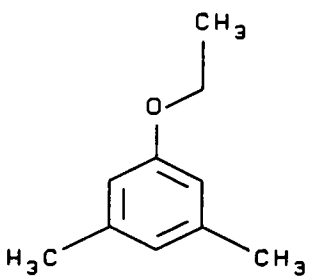

11

These were chosen due to the fact that compound **10** possess no complexation sites for LSR, compound **11** has a weak complexation site at the ethoxy functionality, and compound **7** has a strong complexation site at the acetyl functionality and a non-complexation site at the trifluoroethoxy group. The reason that the relaxation time (T_1) for the methylene hydrogens of the trifluoroethyl moiety is not measured is because the methylene hydrogens are coupled

with the 3 fluorine atoms and more than one T_1 is involved. The relaxation rates for compound **10** before and after the addition of LSR of 0.5 equivalent of $Yb(thd)_3$ are listed in Table 2.3. The relaxation rates did increase for all of the hydrogens monitored, however, all increased at the same rate. It is expected that the relaxation rates will increase as LSR are added due to the fact that LSR is a paramagnetic species with bulk relaxation properties [37]. When a paramagnetic species is introduced to a solution of substrate, the relaxation rate will increase even if the molecule possess no complexation sites. The fact that the relaxation rates for all hydrogens monitored in compound **10** increased by the same amount, indicates that the LSR is not complexing at a specific site in compound **10**. The LIR rates for compounds **11** and **7** are illustrated in Figure 2.9 and Figure 2.10, respectively. For compound **11**, the ethoxy group acts as a weak complexing site. The aromatic hydrogens ortho to the ethoxy group have the higher slope (0.65) compared to the aromatic hydrogen para to the ethoxy group (0.41), and the methyl hydrogens (0.55). The slopes of the hydrogens monitored in compound **7** are methyl hydrogens on the ring (1.92), aromatic hydrogens(0.64) and methyl hydrogens of the acetyl functionality (7.25). The methyl hydrogens of the acetyl functionality have the greatest slope compared to all hydrogens monitored in compounds **11** and **7** because they are situated next to the carbonyl group, a strong complexation site for lanthanide shift reagents.

Another compound, cyclohexenone **12**, was also monitored utilizing LIR studies. This compound was previously synthesized by Roy [38] by the reaction of 1-phenyl-1,3-butanedione with 2,2,2-trifluorodiazoethane (TFD) in the presence of $HBF_4{\cdot}OEt_2$. The structure of the compound is shown below:

Table 2.3 The Induced Relaxation Rates $(1/T_1)^a$ of 3,5-Dimethyltrifluoroethoxybenzene Without $Yb(thd)_3$ and With 0.5 Molar Ratio of $Yb(thd)_3$

PPM	No $Yb(thd)_3$ $(1/T_1)$ sec^{-1}	0.5 M $Yb(thd)_3$ $(1/T_1)$ sec^{-1}
2.31	0.27 ± 0.05	0.56 ± 0.05
6.57	0.13 ± 0.05	0.31 ± 0.05
6.69	0.15 ± 0.05	0.31 ± 0.05

a) Spin-lattice relaxation time (T_1) was measured using the inversion recovery pulse sequence (180°-τ-90°-acquire).

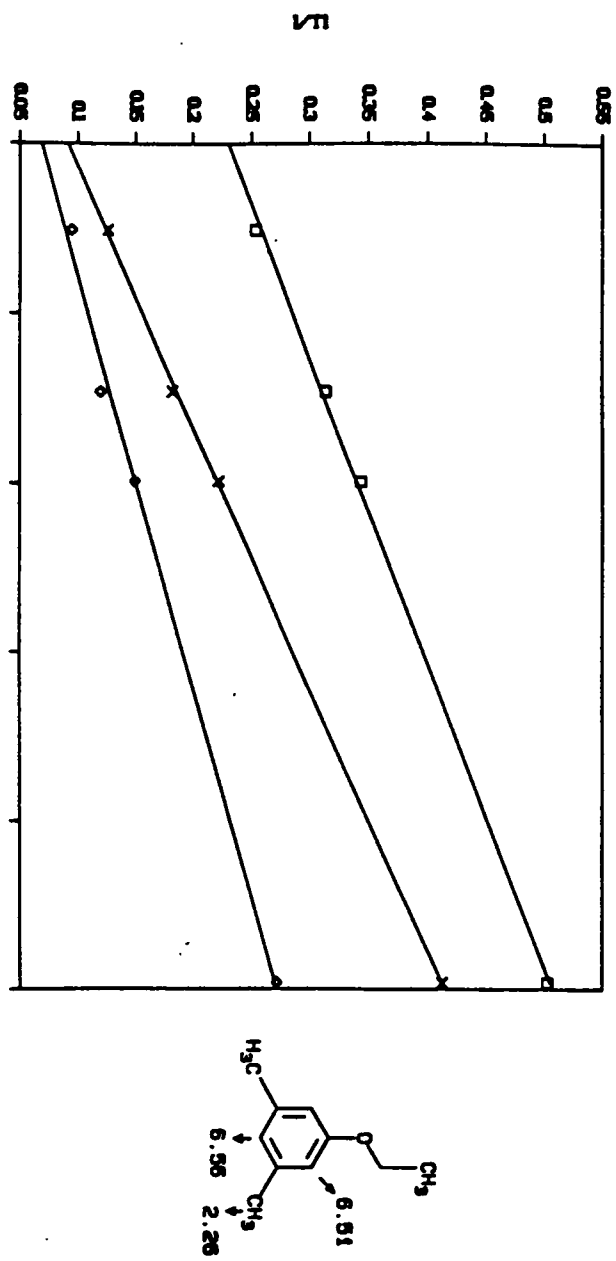

Figure 2.9 The ^1H induced relaxation rates for compound 11 as a function of added Yb(thd)$_3$.

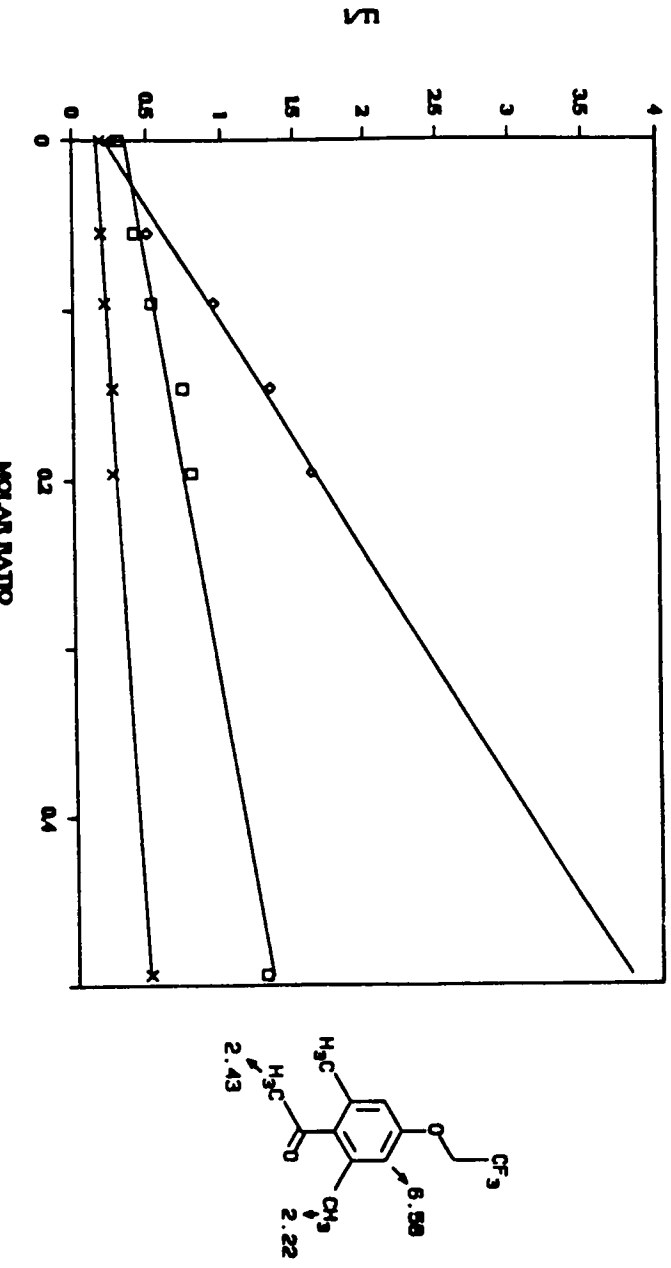

Figure 2.10 The ^1H induced relaxation rates for compound 7 as a function of added Yb(thd)$_3$.

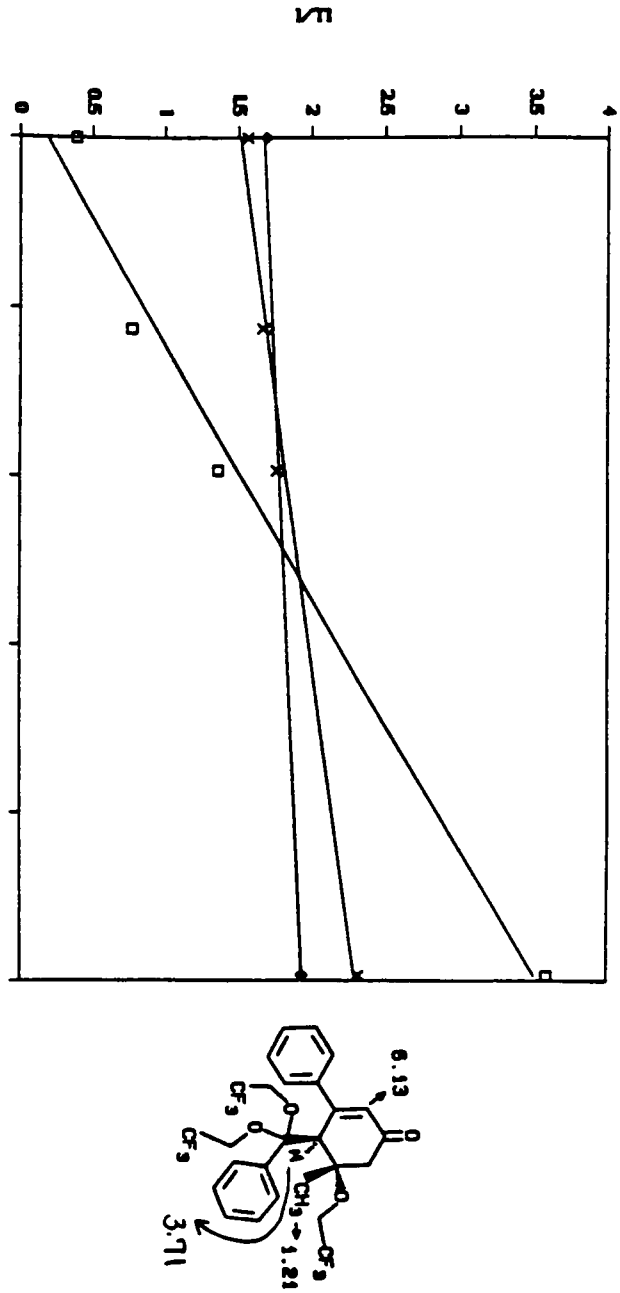

Figure 2.11 The ^1H induced relaxation rates for compound **12** as a function of added Yb(thd)$_3$.

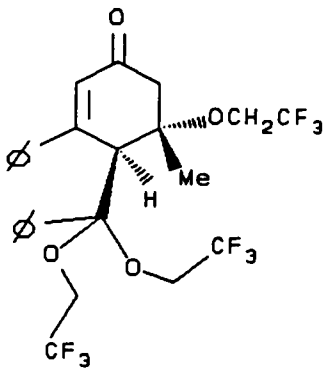

12

This compound contains one complexation site and two deactivated sites (i.e. trifluoroethyl ketal and ether). The LIR rates for the hydrogens proximate to these three sites are illustrated in Figure 2.11. The methine hydrogen (double bond) next to the carbonyl functionality has the greatest slope while the slopes for methyl hydrogens adjacent to the trifluoroethoxy group and the methine hydrogen adjacent to the trifluoroethyl ketal group are practically zero. The slopes of the various hydrogens as a function of added LSR for the four compounds studied above are listed in Table 2.4. The LIR studies of these four compounds indicate the trifluoroethyl group is a deactivating group toward LSR.

As previously stated, LIR can be used to determine structural information related to distance. This section describes an attempt to determine distance relationships for 4-t-butylcyclohexanol (13), 4-methylcyclohexanol (14), and 2-t-butylcyclohexanol (15). The LIR of all three compounds were measured using $Yb(thd)_3$ as the LSR. The LIR rates of compounds 14 and 13 are illustrated in Figures 2.12 and 2.13, respectively. The slopes suggest that the methyl hydrogens of the cis isomers of both compounds are situated closer

Table 2.4 The LIR Slopes For Compounds 10, 11, 7, and 12.

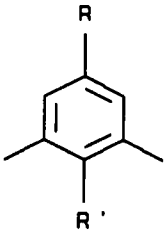

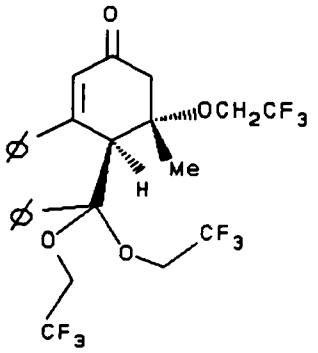

12

Compound	Slopes		
10 R = OCH_2CF_3, R'= H	0.58 (2.30 PPM)	0.36 (6.57 PPM)	0.32 (6.69 PPM)
11 R = OCH_2CH_3, R'= H	0.55 ± 0.02 (2.26 PPM)	0.40 ± 0.02 (6.56 PPM)	0.65 ± 0.01 (6.51 PPM)
7 R = OCH_2CF_3, R' = $CH_3C{=}O$	1.92 ± 0.17 (2.22 PPM)	7.25 ± 0.51 (2.43 PPM)	0.64 ± 0.05 (6.58 PPM)
12	1.57 ± 0.16 (1.21 PPM)	0.52 ± 0.06 (3.71 PPM)	6.67 ± 0.58 (6.13 PPM)

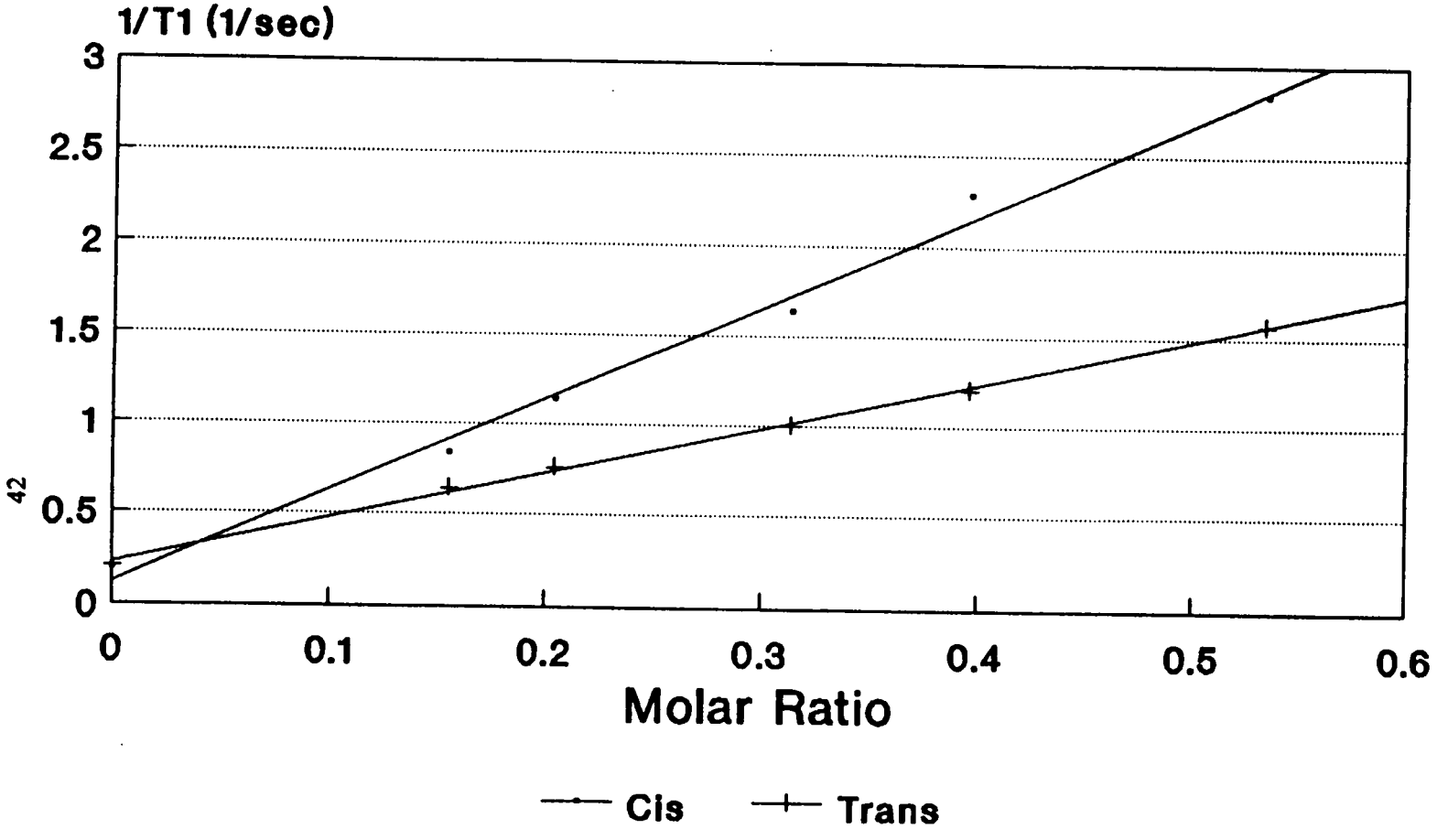

Figure 2.12 The ^{1}H induced relaxation rates for compound **14** as a function of added $Yb(thd)_3$.

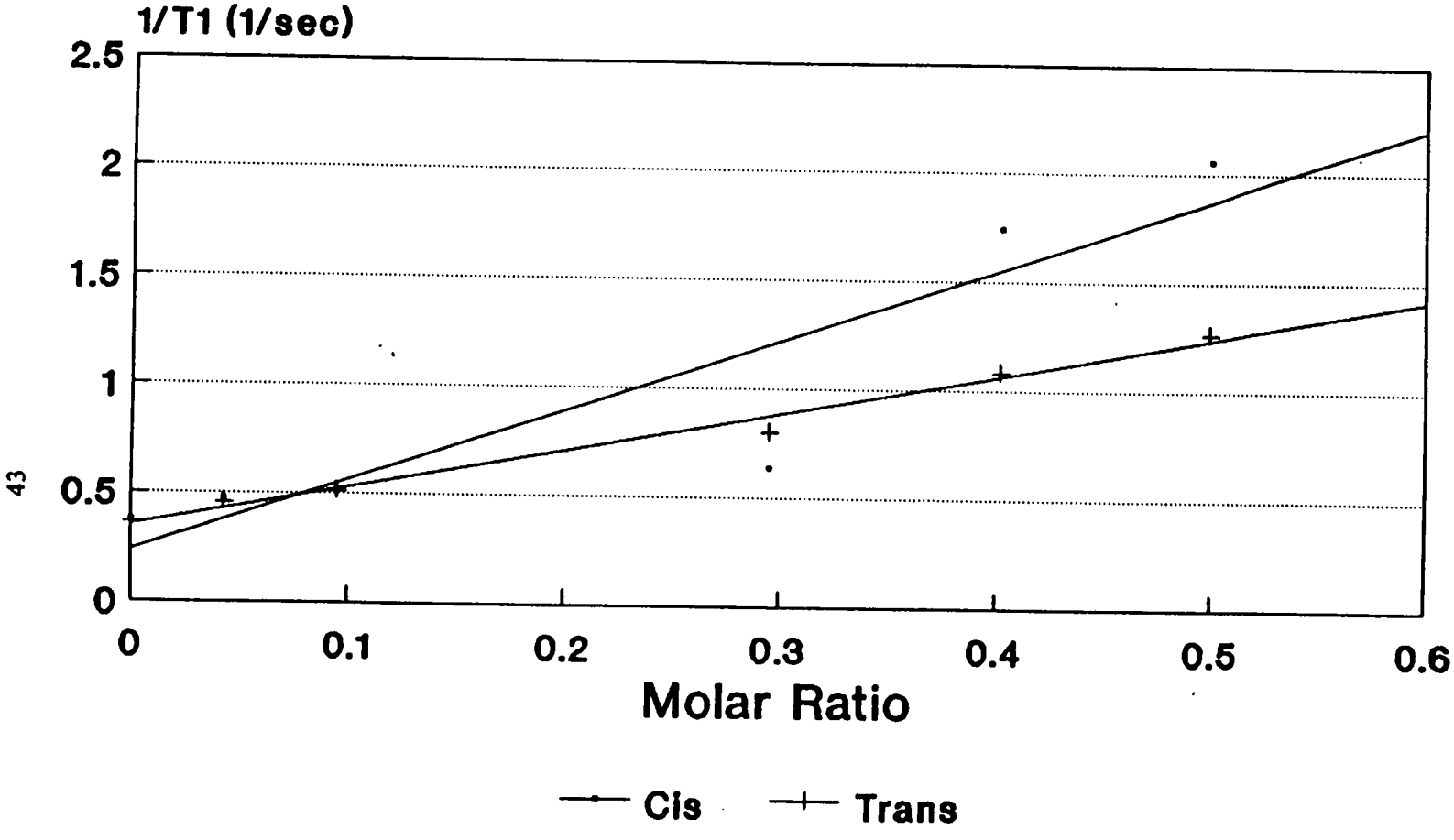

Figure 2.13 The ^1H induced relaxation rates for compound 13 as a function of added $Yb(thd)_3$.

to the hydroxyl functionality. The reverse is true for 2-t-butylcyclohexanol (**15**) as shown in Figure 2.14. The methyl hydrogens of the trans isomer in compound **15** are closer to the site of complexation on the hydroxy functionality. Figures 2.15 and 2.16 give graphic illustration of conformation and distances measured for compounds **13** and **15** respectively. Summaries of the slopes for all three compounds are listed in Table 2.5. From the slopes of all the isomers, the methyl hydrogens of trans-2-t-butylcylcohexanol appear closest to the metal complexation site, while those in trans-4-t-butylcyclohexanol are further away. Since only an "average" spectrum is observed for the complexed and uncomplexed molecule, the information that can be obtained from the LIR rates are only proportional to distances. Utilizing equation 12 from Chapter 1, ratios of the distances for the cis/trans isomers can be estimated. For comparison purposes, Drieding models of the three compounds were constructed, and the distances of the methyl hydrogens to the OH complexation site were measured. The measured distances, Drieding model ratios, and experimental ratios are listed in Table 2.6. Even though the values are not in quantitative agreement, the overall trend is very good. The LIR rate can be useful in obtaining qualitative structural information, however, this method does not directly provide distance information. Furthermore, assumptions must be made regarding the most stable conformation for the substrate-LSR complex. In addition, it is assumed that the equilibrium constants for complexation between the cis/trans isomers and the LIR are approximately equivalent.

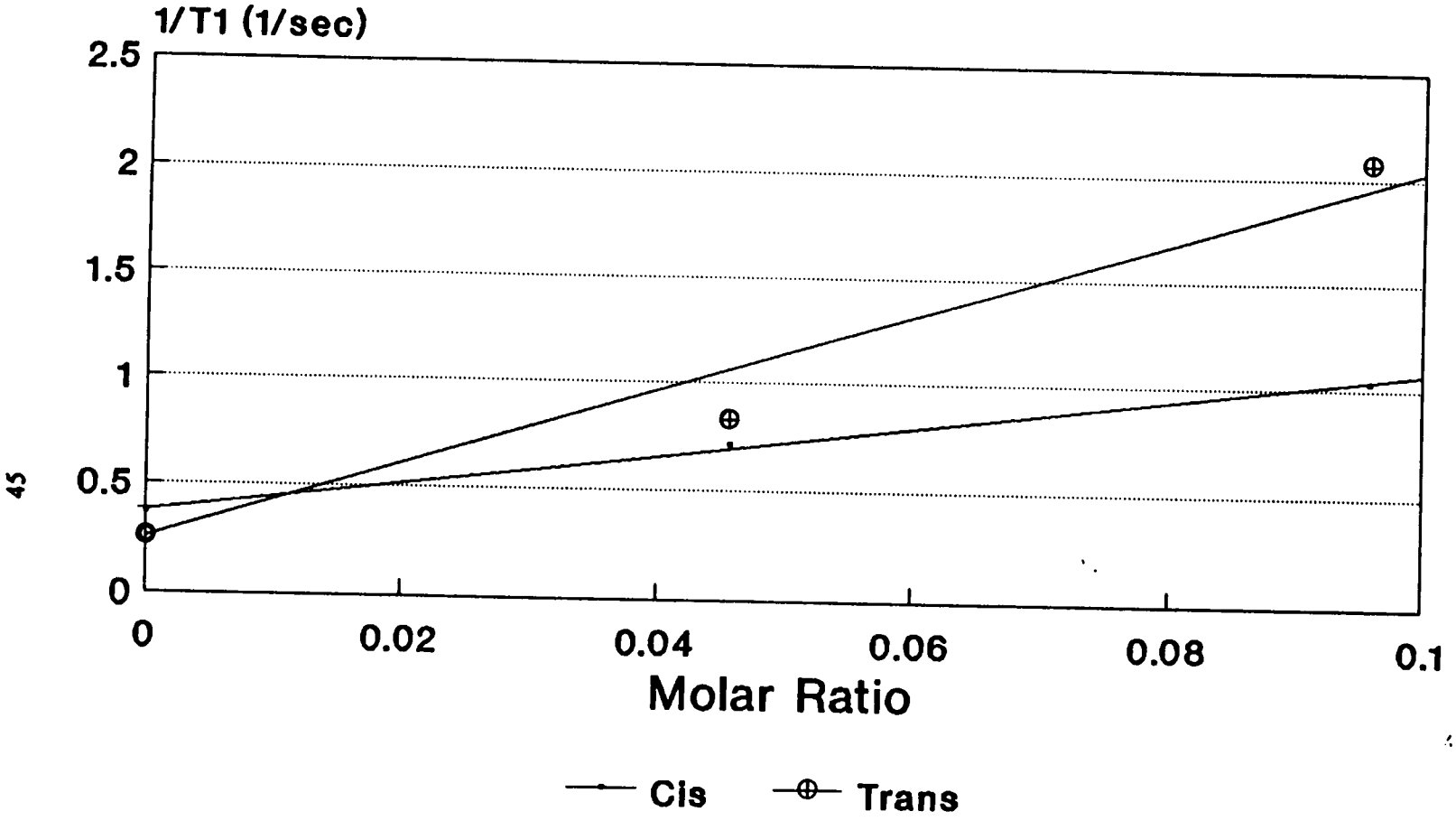

Figure 2.14 The ^{1}H induced relaxation rates for compound 15 as a function of added $Yb(thd)_3$.

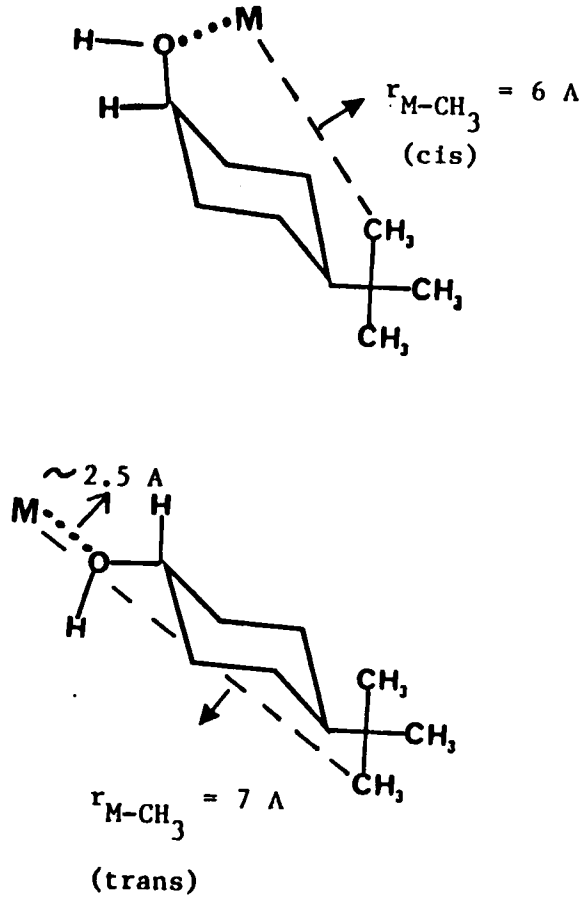

Figure 2.15 The Drieding complexation model for $Yb(thd)_3$-4-tert-butylcyclohexanol.

$Yb(thd)_3$ - 2-t-butyl Cyclohexanol

Complexation Model (Dreiding)

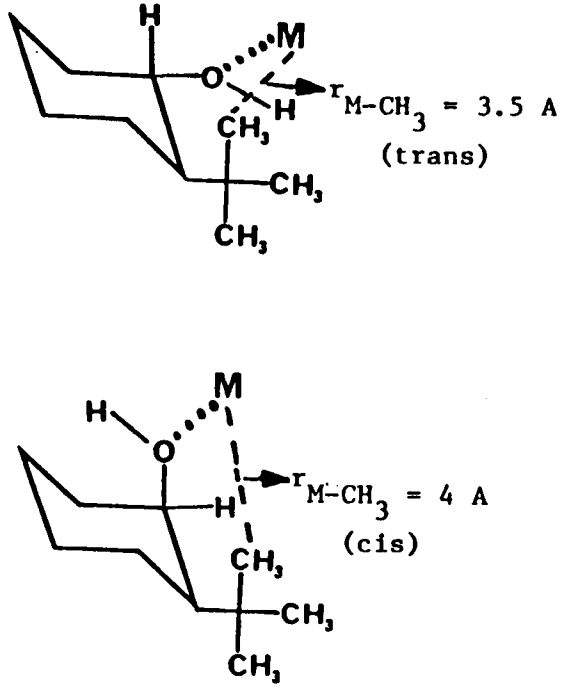

Figure 2.16 The Drieding complexation model for $Yb(thd)_3$-2-tert-butylcyclohexanol.

Table 2.5 The LIR[a] Slopes for the 4-Tert-butylcyclohexanol (13), 4-Methylcyclohexanol (14), and 2-Tert-butylcyclohexanol (15).

Compound	Slopes	
	Cis	Trans
13	3.50 ± 0.32	1.83 ± 0.13
14	5.11 ± 0.45	2.52 ± 0.10
15	7.03 ± 0.63	17.77 ± 8.38

a) T_1s were measured using inversion recovery pulse sequence

Table 2.6 Calculated T_1 Ratios vs. Experimental Values For 2-Tert-butyl, 4-Tert-butyl, and 4-Methyl Cyclohexanols

Compound	$r_{M\text{-}CH_3}$ (trans) Å	$r_{M\text{-}CH_3}$ (cis) Å	Geometry ratio from Drieding Model	Calculated T_1 ratio (cis/trans)	Experimental Values
2-t-butyl	3.5 ± 0.1	4.0 ± 0.1	0.9 ± 0.2	0.5 ± 0.2	0.40 ± 0.10
4-t-butyl	7.0 ± 0.1	6.0 ± 0.1	1.2 ± 0.2	2.5 ± 0.2	1.91 ± 0.10
4-methyl	7.0 ± 0.1	6.0 ± 0.1	1.2 ± 0.2	2.5 ± 0.2	2.02 ± 0.10

Experimental

Equipment. NMR data were obtained using either a Bruker WP-270 Spectrometer (^{1}H NMR 270 MHz/ ^{13}C NMR 67.5 MHz), or a Bruker WP-200 Spectrometer (^{1}H NMR 200 MHz/ ^{13}C NMR 50 MHz). Samples were dissolved in $CDCl_3$. Chemical shifts are referenced to either TMS or residual solvent ^{1}H resonances. Solvents were dried according to standard procedures. Starting materials and reagents were obtained from commercial sources.

Lanthanide Induced Shifts Studies. The experiments were conducted as follows. A 0.4 mL portion of the stock solution of a given compound was placed into a 5.0 mm NMR tube. The ^{1}H NMR of this solution was recorded. To this solution were added incremental amounts of the $Eu(fod)_3$ stock solution (1 μL or multiples thereof). After each addition, the ^{1}H NMR of the sample solution was recorded. Information gathered in this manner was used to determine the extent of complexation the various types of compounds undergo with $Eu(fod)_3$.

Lanthanide Induced Relaxation Studies. The experiments were conducted as follows. A 0.4 portion mL of the stock solution of a given compound was placed into a 5.0 mm NMR tube. The sample was deoxygenated by bubbling N_2 through the solution and sealing with Teflon® tape. The ^{1}H NMR of this solution was recorded and ^{1}H T_1s were measured using an inversion recovery pulse sequence (180°-τ-90°-acquire). To this solution was added incremental amounts of the $Yb(thd)_3$ stock solution (1 μL or multiples thereof). After each addition, the solution was deoxygenated and the ^{1}H NMR and T_1s were recorded and measured. Information gathered in this manner was used to determined the extent of relaxation the various types of compounds undergo with $Yb(thd)_3$.

4,6-dimethyl-2-methoxyacetophenone (4) and 2,6-dimethyl-4-methoxyacetophenone (5). 3,5-dimethylanisole (5 g, 0.0367 mol), $AlCl_3$ (11.0 g, 0.74 mol), and 10 mL of dry CS_2 were added to a 2-necked, 100 mL, round bottomed flask containing

a magnetic stir bar. The flask was fitted with an addition funnel and a water cooled condenser. The condenser was fitted with a gas trap to absorb the HCl gas given off during the course of the reaction. Acetic anhydride (3.75 g, 0.0367 mol) was added dropwise to the mixture. The reaction gave off gas immediately, turned yellow then brown, and became difficult to stir. After 2/3 of the acetic anhydride had been added, 5 mL of dry benzene was added to the flask in an effort to facilitate stirring. The remaining acetic anhydride was added with intermittent stirring. After this addition, the mixture was heated using a water bath (~ 50°C) for 1/2 hour. The mixture was then added to a 30 g ice/10 mL HCl solution. After the ice had melted, 20 mL of benzene was added. The organic layer was separated. The aqueous layer was extracted with 20 mL of benzene. The combined benzene layer was washed twice with 20 mL H_2O, dried over Na_2SO_4, and filtered. The resulting solution was distilled to remove of CS_2 and benzene. The ^1H NMR of the residue (5.53 g, yellow oil) indicated a small amount of starting material as well as ortho and para isomers of the desired product in the ratio of ~ 6 : 1. The isomers were separated using flash column chromatography (Kieselgel 60, > 230 mesh). Hexanes was used first to elute the starting materials, then the solvent was changed to 60% CH_2Cl_2/hexanes to separate the isomers. The chromatography yielded 3.8 g of compound 4, 0.3 g of compound 5 , and 0.6 g of the mixture for a total of 4.7 g (67%) products. Compound 4 afforded the following spectroscopic data. ^1H NMR δ 2.19 (s, 3H), 2.29 (s, 3H), 2.46 (s, 3H), 3.77 (s, 3H), 6.56 (s, 1H), 6.60 (s, 1H). Compound 5 afforded the following spectroscopic data. ^1H NMR δ 2.22 (s, 6H), 2.43 (s, 3H), 3.75 (s, 3H), 6.54 (s, 2H).

3,5-dimethyl-trifluoroethoxybenzene. 3,5-dimethylphenol (3.0 g, 0.236 mole) was dissolved in 25 mL of CH_2Cl_2 under N_2 in a 250 mL, 3-necked, round bottomed flask fitted with a water cooled condenser, an addition funnel, and a magnetic stir bar. The solution was cooled to 0°C with an ice-salt bath. After the addition of 0.25 mL of $HBF_4{\cdot}OEt_2$, 130 mL of 2,2,2-trifluorodiazoethane (0.298 M) was added dropwise over a period of 3 hours.

The resulting brown solution was washed twice with 50 mL of 5% $NaHCO_3$, 3 times with 50 mL of 5% NaOH, and 3 times with 60 mL of H_2O. The organic layer was dried over K_2CO_3 and the CH_2Cl_2 was removed *in vacuo*. The resulting brown liquid 4.0 g (80% crude yield) was used without further purification. The compound yielded the following spectroscopic data. ^1H NMR δ 2.30 (s, 6H), 4.31 (q, 2H, J = 8.1 Hz), 6.57 (s, 2H), 6.69 (s, 1H).

4,6-dimethyl-2-trifluoroethoxyacetophenone (6), and 2,6-dimethyl-4-trifluoroethoxyacetphenone (7). 3,5-dimethyl-trifluoroethoxybenzene (2.0 g, 9.8 mmol) , $AlCl_3$ (2.87 g, 21.5 mmol), and 8 mL of CS_2 were added to a 50 mL, 3-necked, round bottomed flask with stirring. The flask was fitted with an addition funnel and a water cooled condenser and gas trap. Acetic anhydride (1.10 g, 10 mmol) was then added dropwise to the dark brown mixture. The mixture became thick and difficult to stir. Following the addition of acetic anhydride, the mixture was stirred for 1/2 hour and heated using a water bath (~ 60 °C) for 1.5 hours. The resulting mixture was transferred to 15 g ice / 5 mL concentrated HCl solution. After the ice melted, 30 mL of CH_2Cl_2 was added. The organic layer was separated and the aqueous layer was extracted 3 times to a total of 20 mL of CH_2Cl_2. The combined CH_2Cl_2 layers were washed twice with 30 mL of water, dried over K_2CO_3, and filtered. The solvent was removed by distillation and 2.14 g of crude products (yellow oil) was recovered. ^1H NMR of the product indicates the ratio of ortho to para isomers is ~ 3 : 1. The isomers were separated by flash column chromatography (Kieselgel 60, > 230 mesh, 50% CH_2Cl_2/hexanes). The chromatography yielded 1.0 g of compound **6**, 0.3 g of compound **7** , and 0.5 g of the mixture for a total of 1.8 g (73% yield) of products. Compound **6** afforded the following spectroscopic data. ^1H NMR δ 2.24 (s, 3H), 2.32 (s, 3H), 2.49 (s, 3H), 4.36 (q, 2H, J = 8 Hz), 6.52 (s, 1H), 6.73 (s, 1H). Compound **7** afforded the following spectroscopic data. ^1H NMR δ 2.26 (s, 6H), 2.46 (s, 3H), 4.34 (q, 2H, J = 8 Hz), 6.60 (s, 2H).

Chapter 3 - Dynamic Nuclear Polarization

Dynamic Nuclear Polarization (DNP) is a nuclear electron double resonance or nuclear electron Overhauser effect. When the electron resonance (ESR) of a paramagnetic solute is saturated, drastic changes in the intensities of the lines of the nuclear magnetic resonance (NMR) spectrum of the solvent (or another solute) may occur. The observed NMR signal may be positively or negatively enhanced depending on whether scalar or dipolar dynamic coupling dominate the spin-lattice relaxation. Most chemical applications of DNP involve solutions of free radicals. The dynamic electron-nuclear interactions observed and their relation to molecular properties can be useful either for studying the solution structure of the free radicals themselves, or as a probe for motions and interactions between the radicals and solvent or another solute. Several excellent reviews have been written on DNP in liquids [2,39-41]. This chapter will give a brief history of the DNP experiment; describe the theories involved in measurement of DNP in liquids, some of the organic radicals used for DNP, and some of the nuclei that have been studied with DNP.

In 1953 [42], Overhauser predicted that in a system of two interacting spins, I and S, in a static magnetic field, H_o, the population of the energy levels (e.g. the polarization) of I is dependent on the polarization of S. A deviation from the equilibrium population of the Zeeman levels of S will produce a polarization of I which is DNP. This process originates from the relaxation processes involving both spins I and S and is often referred to as "Overhauser Effect". The system that Overhauser envisioned involved polarization of electrons in certain metals and observing their nuclear signal. Overhauser's prediction was realized by Carver and Slichter in the same year [43]. When they observed DNP using the metal lithium. Abragam in 1955 [44] extended Overhauser's prediction to nonmetal systems and predicted that the two spins can be either intra or intermolecular.

Since that time, various enhanced NMR signals have been observed in materials as diverse as chars [45], tars [46], metals [47], solutions containing transition metal ions [48], and solid free radicals [49]. Most of these systems have been probed to understand the spin-spin interactions.

In 1962, Richards and White [50] suggested the possibility of using DNP to increase the size of unobservable NMR signals. Simultaneously, Müller-Warmuth [51] and Poindexter [46] began using DNP to investigate the molecular motions and the collision dynamics in liquids. Using stable free radicals, induced DNP has been used for studying weak molecular complex formation [52], as between two aromatic molecules, for probing stereo-specific collisions in liquids [53] and aromaticity in non-benzoid compounds [54], and for measuring NMR signals which cannot ordinarily be seen with a high resolution NMR spectrometer [55].

As stated earlier, DNP is a double resonance technique in which the nuclear magnetic resonance is observed while the electron resonance is simultaneously irradiated. The polarization occurs when the applied radiation is at or near the electron Larmor frequency (ω_e). After saturating the electron resonance, the Boltzmann equilibrium distribution (which leads to the usual static spin polarization) is replaced by a dynamic distribution which corresponds to a much stronger nuclear polarization. This occurs as the electron spins attempt to reestablish the original Boltzmann distribution, which causes relaxation. One of the relaxation mechanisms is through polarization transfer from an electron to a nuclear spin. The mechanism and the magnitude of the polarization enhancement may be described considering a system of two interacting spins, a nuclear spin I and an electron spin S. When placed in an external magnetic field, the two spins (where $I = 1/2$) are distributed between the lower (α) and the higher (β) energy states according to the Boltzmann distribution. By irradiation with an appropriate frequency, transitions between the energy levels can be induced.

The energy level diagram for the spin system in the presence of an external magnetic field is given in Figure 3.1 [2]. W_1^S and W_1^I are the single quantum transition relaxation rates for the electron and the nucleus, respectively and W_o and W_2 are the zero and double quantum transition relaxation rates. When all transitions are allowed, the radiationless (non-allowed) W_o and W_2 transitions are responsible for DNP as they involve simultaneous flips of both electron and nuclear spins. The intensity of the NMR signal I_z is proportional to

$$I_z \propto (n_2 + n_4) - (n_1 + n_3) \tag{13}$$

where n_i $(i = 1,2,3,4)$ = the populations of the corresponding energy states.
At thermal equilibrium, $I_z = I_o$ which is proportional to the Boltzmann factor:

$$I_o \propto \exp(-\, h\, \omega_I / \kappa\, T) \tag{14}$$

when the electron spin transition is saturated, then $n_1 = n_3$, $n_2 = n_4$, and I_z is given by:

$$I_z \propto \exp[-\, h\, (\omega_S + \omega_I)/\kappa T] \tag{15}$$

The enhancement of the observed NMR transition A is

$$A \propto I_z / I_o \tag{16}$$

By dividing equation 14 into equation 15 and assuming $h\omega_I \ll 1$, the enhancement A becomes

$$A \propto I_z / I_o \approx \omega_S / \omega_I = |\gamma_S| / \gamma_I \tag{17}$$

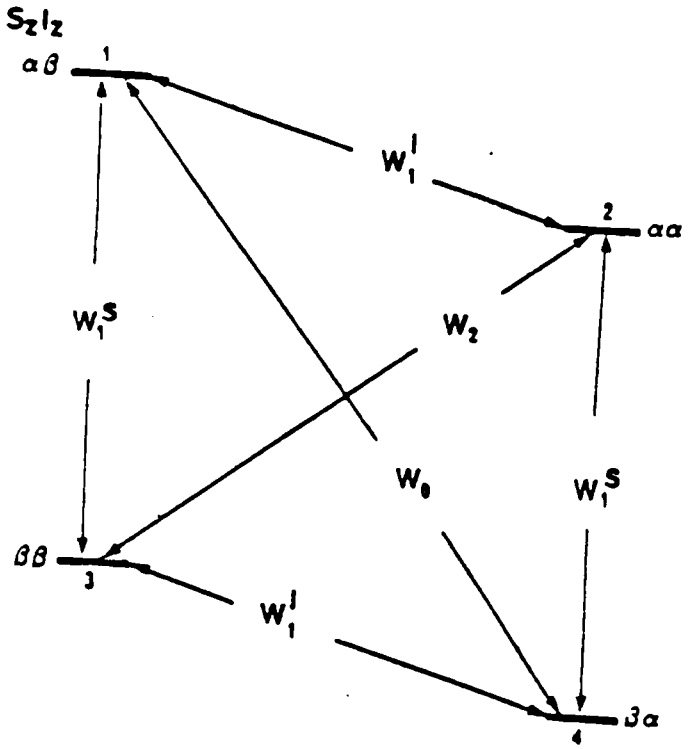

Figure 3.1 Spin level diagram for a coupled electron-nuclear spin system

Since DNP enhancement is a deviation from the static polarization ($I_z = I_o$), the DNP enhancement is usually expressed as:

$$A = (I_z - I_o) / I_o. \tag{18}$$

A more vigorous treatment of the DNP phenomenon, which takes into consideration the cross transition probabilities, leads to the basic equation for DNP: [2]

$$A = - \rho f s \, |\gamma_S|/|\gamma_I| \tag{19}$$

where ρ = coupling factor, which can range from -1.0 to +0.5

f = leakage factor, which has values from 0 to 1

s = saturation factor, which ranges from 0 to 1.

Each term will be discussed more extensively later.

The mechanism of DNP enhancement can be explained in terms of cross-relaxation transitions which occur after the electron spin system has been disturbed from its equilibrium value. Following saturation of the ESR transition, the coupled spin systems try to reestablish thermal equilibrium by either dipolar or scalar nuclear-electron interaction. For the electron spin system, which has been saturated, there will be more non-allowed relaxation transitions to the lower energy levels, which will induce more relaxation flips to the higher energy levels for the nuclear spin system. This produces a deviation of the equilibrium population of the nuclear spin system, i.e. a dynamic nuclear polarization.

The coupling factor, ρ, dictates the type of electron-nuclear interaction and can be described in terms of transition probabilities:

$$\rho = (W_2^D - W_o^D - W_o^{Sc}) / (W_2^D + W_o^D + W_o^{Sc} + 2W_1^D) \tag{20}$$

where D = dipolar coupling interaction

Sc = scalar coupling interaction.

In the case of pure dipolar coupling, $W_o^{Sc} = 0$, ρ is reduced to

$$\rho = (W_2^D - W_o^D) / (W_2^D + W_o^D + 2W_1^D) \tag{21}$$

Solomon has determined the expressions for W_1^D, W_o^D, and W_2^D [56]:

$$W_1^D = (\tau_c / 2h^2) < | F_1 | > / 1 + \omega_I^2 \tau_c^2) \tag{22}$$

$$W_o^D = (\tau_c / 8h^2) <F_o^2> (1 / 1 + (\omega_I - \omega_S)^2 \tau_c^2) \tag{23}$$

$$W_2^D = (2\tau_c / h^2) < | F_2 | > / 1 + (\omega_I - \omega_S)^2 \tau_c^2) \tag{24}$$

Where ω_I = resonance frequency of the nucleus

ω_S = resonance frequency of the electron

$< | F_1 | ^2 F_o^2 >$ and $< | F_2 | >$ average values for various part of the dipole-dipole perturbing Hamiltonian

τ_c = molecular correlation time

In equations 22-24, several points should be noted. First, as the external magnetic field is increased, both ω_S and ω_I increases and W_1^D, W_o^D and W_2^D approach zero. Second, since the electron resonance frequency is much larger than the nuclear frequency, W_o^D and W_2^D will decrease more rapidly with increasing applied field than W_1^D. As $H_o \rightarrow \infty$, the enhancement approaches zero. In order to determine the maximum value of ρ for the case of pure dipolar interaction, we assume extreme narrowing conditions, $\omega\tau_c \ll 1$. At which the ratios of the different dipolar transition probabilities are reduced to $W_o^D:W_1^D:W_2^D = 2:3:12$, and the coupling factor attains the maximum value of +0.5 for pure dipolar interaction. For pure scalar

interactions, $W_o^D = W_1^D = W_2^D = 0$, and the coupling factor is equal to -1.0. Therefore, the coupling factor can range from +0.5 to -1.0. The DNP enhancement for the electron-nuclear spin system can be positive or negative depending on whether dipolar or scalar coupling is the predominant interaction. Thus, the experimentally observed sign and magnitude of the DNP enhancement can provide information as to the type of electron-nuclear interaction.

The leakage factor, f, determines the relaxation efficiency of the electron spin relative to the nuclear spin and is defined in terms of transition probabilities as:

$$f = (W_o^D + W_o^{Sc} + 2W_1^D + W_2^D) / (W_o^D + W_o^{Sc} + 2W_1^D + W_2^D + W_{1o}) \qquad (25)$$

where W_{1o} = relaxation transition probabilities for the nuclear system other than that induced by dipolar and/or scalar electron-nuclear coupling.

Under dipolar dominated interaction, the equation reduces to:

$$f = (W_o^D + 2W_1^D + W_2^D) / (W_o^D + 2W_1^D + W_2^D + W_{1o}) \qquad (26)$$

The nuclear spin-lattice relaxation rates ($1/T_1$) in the absence and presence of a free radical can also be expressed in terms of transition probabilities:

$$1/T_{1no} = W_{1o} \qquad (27)$$

$$1/T_{1n} = W_o^D + 2W_1^D + W_2^D \qquad (28)$$

substituting into equation 26 yields:

$$f \approx 1 - (T_{1n} / T_{1no}) \qquad (29)$$

The leakage factor can be estimated by measurement of nuclear T_1's in the absence of radical (T_{1no}) and in the presence of radical (T_{1n}) and can range from 0 to 1.

The electron saturation factor, s, reflects the degree to which electron transitions that are saturated (e.g. s = 1 for complete saturation). The saturation factor can be defined as:

$$s = (s_o - s_z) / s_o \tag{30}$$

$$s_z = s_o / (1 + \alpha B_{1s}^2 T_{1s} T_{2s}) \tag{31}$$

where T_{1s} = electron spin-lattice relaxation time

T_{2s} = electron spin-spin relaxation time

B_{1s} = microwave magnetic field

α = a constant

Since B_{1s}^2 is proportional to the applied microwave power, P, substituting P into equation 19, gives the reciprocal enhancement as:

$$A^{-1} = (f\rho(|\gamma_S|/\gamma_I)^1 + 1/(\alpha P T_{1s} T_{2s})] \tag{32}$$

A plot of the reciprocal enhancement A^{-1} versus reciprocal power P^{-1} should give a straight line with an intercept $(A_\infty^{-1}) = f\rho(|\gamma_S|/\gamma_I)$The A_∞ value determined in this manner is the value of the enhancement for s = 1. Typically, A_∞ values are cited since observed enhancements are often smaller due to the higher power typically required for static DNP.

The potential enhancement using DNP is illustrated when one considers the ideal case where f = 1, s = 1; for dipolar dominant interaction with ρ = +0.5 and for ^1H observation, the A_∞ = -330. For scalar interaction with ρ = -1.0, the A_∞ = +660. The ^1H DNP enhancement is one of the lowest of all observable nuclei. In the case of ^{13}C, it can be +2600 for scalar interaction.

The most important factors governing the choice of radicals are stability, solubility in the solvent of interest, and ease of saturation of the EPR signal. Generally, dilute solutions (0.001 - 0.05 M) are employed, therefore, solubility is not a problem. In most cases, the stability of the radical is the most important criterion for deciding samples use. Some typical free radicals used in DNP experiments are illustrated in Table 3.1 [41].

Of the radicals shown in Table 3.1, only DPPH, GALV, PODS and DTBN can be obtained commercially as the radical. However, radicals derived from commercially available quinone or phenol precursors can generated quite easily. For example, TTBP is generated in a variety of hydro or fluorocarbon solvents by oxidation of 2,4,6-tri-tert-butylphenol with excess PbO_2 as shown below:

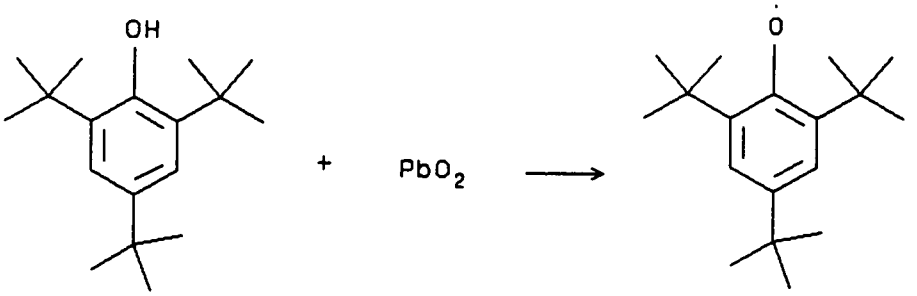

Table 3.1 Stable Radicals Used For DNP Experiments

Name	Structure
2,4,6-tri-tert-butylphenoxyl (TTBP)	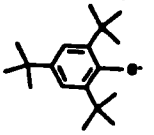
Galvinoxyl (GALV)	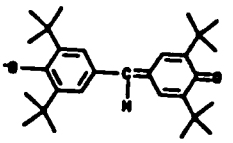
Diphenylpicrylhydrazyl (DDPH)	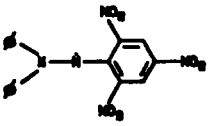
Tetrachlorosemiquinone (TCSQ)	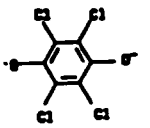
Bisdiphenylenephenylallyl (BDPA)	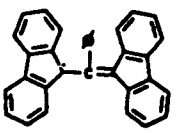
Peroxylamine disulfonate (PODS)	
Triphenylvedazyl (TPV)	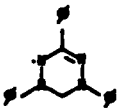
Triphenylpyrylyl (TPPY)	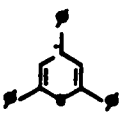
Wurster's blue perchlorate (WPBC)	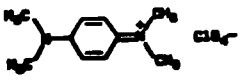
Di-tert-butylnitroxide (DTBN)	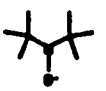
2,3-Dichloronaphthaquinone (DCNQ)	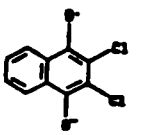

Also TCSQ can be obtained either by air oxidation of the corresponding hydroquinone or from tetrachloroquinone by reduction in base with glucose as illustrated below:

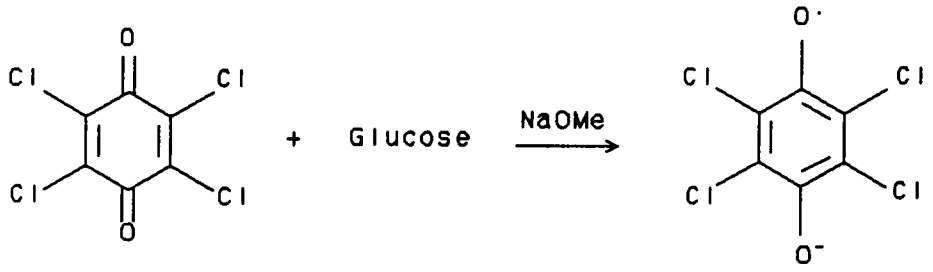

The disadvantage in generating radicals in situ is that most of these reactions do not go to completion, therefore, it is difficult to reproduce a given radical concentration. Therefore, radical concentration must be measured independently by ESR techniques.

Most of the nitrogen containing radicals are not widely used due to the fact that the EPR spectra are broad and difficult to saturate completely. They are mostly used at low applied fields where saturation is easier.

Most semiquinone radicals are not used except for TCSQ or DCNQ (due to the substituted chlorines) because their ESR spectra are also broad, making saturation difficult. Also, the radicals generated are anions and in non-polar solvents, they could exist as ion pairs making interpretation of the data more complicated.

TCSQ is classified as a percholoro radical and is the most widely used of this type. Due to the quadrupole moment of the chlorine nuclei, no hyperfine coupling of Cl with the radical (the electron) is observed as in cases for nitrogen or hydrogen [57]. The EPR signal of TCSQ is a sharp single line which is extremely easy to saturate. This makes it a popular

radical to use.

The nitroxide radicals (general structure shown below) has not been widely used

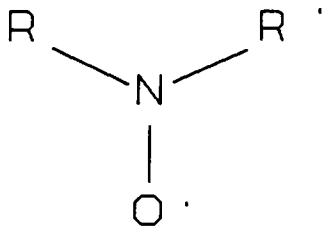

due to the three separate EPR signals (I = 1). However, they do have some advantages over other more commonly used radicals. First, the unpaired electron is highly localized on the N-O group rather than being delocalized over the entire molecule. Second, the groups R and R' can be varied to give a variety of organic functional groups without destroying the radical. Some nitroxide radicals that have been synthesized with different functional groups are illustrated in Table 3.2. Third, most of the nitroxide radicals are stable at room temperature, which permits a wide range of radical concentrations to be studied easily. And fourth, some nitroxide radicals are water soluble, which could make the observation of DNP in aqueous solutions possible. This could lead to studies of biological macromolecules utilizing DNP. Nitroxide radicals have already found uses in the study of biological macromolecules in the form of spin labels. Spin labelling is a spectroscopic technique which employs stable organic free radicals as structure probes or reporter groups in the investigation of biological macromolecules [58,59].

At the present time, the radicals most widely used for DNP studies are TTBP, GALV, DPPH, TCSQ, TPPY, and BDPA.

Table 3.2 Some Representative Nitroxide Free Radicals

Name	Structure
4-amino-TEMPO	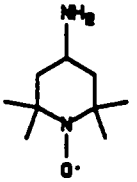
4-Hydroxy-TEMPO	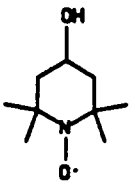
4-Oxo-TEMPO	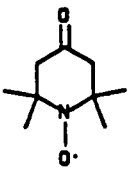
4-(Iodoacetamido)-TEMPO	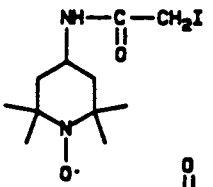
4-Phosphonoxy-TEMPO hydrate	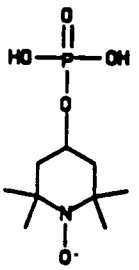
3-Carbamoyl-PROXYL	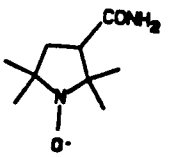
3-Carboxy-PROXYL	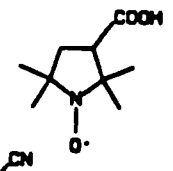
3-Cyano-PROXYL	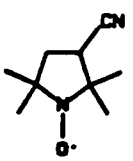

Some of the nuclei that have been studied utilizing DNP are ^{1}H, ^{2}H, ^{7}Li, ^{13}C, ^{19}F, ^{31}P and ^{119}Sn. Table 3.3 [2] gives the enhancement factors observed at low magnetic field for the nuclei mentioned above.

At low magnetic fields (<200 gauss), proton NMR enhancements generally extrapolate close to the dipolar limit. Some results at 74 gauss for a variety of radicals are shown in Table 3.4 [57] for mixed hydrocarbon-fluorocarbon solutions. Several observations can be made base on data from Table 3.4. First, the maximum observed enhancements cover a large range, but the extrapolated enhancements are around -330 (the dipolar limit for proton). Second, the radicals used cover a wide range of chemical types, and the extrapolated enhancements do not vary. Third, the chemical environment of the ^{1}H has little or no effect upon the ultimate enhancements. Therefore at low magnetic fields, the ^{1}H enhancement is dominated by dipolar coupling regardless of the free radical or solvent (solute) used.

The extrapolated ^{1}H enhancements for a variety of substituted methane systems at 3300 and 12,500 gauss are shown in Table 3.5 [60]. As expected, all enhancements are negative, indicating dipolar interactions. However, enhancements change markedly as the solvent molecule is changed. Also, as the viscosity of the solvent increases, the enhancement decreases due to the increased correlation time. Therefore, at high fields, the viscosity of the solvent or solute used can affect the ^{1}H enhancement observed. Even though ^{1}H enhancements are generally dipolar in nature, exceptions do occur. One is for $MnCl_2$ in aqueous solutions [48], where Mn^{+2} supplies the unpaired electrons and the proton NMR spectrum of water is observed. At the field of 10 gauss and very high RF power, a positive enhancement of 100 has been observed. Another case of predominant scalar coupling for ^{1}H is the acid proton of trifluoroacetic acid in solution containing the free radical 4,4,5,5-tetramethyl-2-(2-pyridyl)-Δ^2-imidazoline-1-oxyl (2-PYIN). The structure is shown below: [61]

Table 3.3 Experimentally Extrapolated Enhancements (A_∞) For Different Nuclei as Studied By DNP at Low Field

Nucleus	Spin	$\lvert\gamma_s\rvert/\gamma_I$	A_∞
^{1}H	1/2	658	-330
^{2}H	1	4290	-2000
^{7}Li	3/2	1694	-815 to +850
^{13}C	1/2	2617	-500 to +130
^{19}F	1/2	699	-280 to +460
^{31}P	1/2	1625	-760 to -60 (trivalent) +750 to +1600 (pentavalent)
^{119}Sn	1/2	-1766	-10 to -550
^{205}Tl	1/2	1140	+160

Table 3.4 ^{1}H DNP Enhancements at a Magnetic Field of 74 Gauss

Radical	Solvent	A_{∞}	A (observed)
PODS	DMSO	-310	- 22
GALV	Benzene	-325	-225
	Acetone	-315	-210
TTBP	Benzene	-310	-295
	Acetone	-315	-285
DPPH	Benzene	-310	- 55
	Acetone	-310	- 80
BDPA	Benzene	-300	-210
TCSQ	Acetone	-280	-210
TPV	Benzene	-310	- 75
	Acetone	-310	-105
TPPY	Benzene	-270	-140
	Acetone	-270	-170
WBPC	Acetone	-300	-130

Table 3.5 ^1H DNP Enhancements at Magnetic Fields of 3300 and 12,500 Gauss Using TTBP as the Radical

Solvent	A_∞ (3300 Gauss)	A_∞ (12,500 Gauss)
$CH_3\dot{O}H$	-200 ± 30	- 65 ± 20
$CH_3OH^\bullet$	-235 ± 35	- 90 ± 40
CH_3I	-256 ± 20	-121 ± 30
CH_2I_2	-102 ± 8	- 37 ± 15
CH_2Br_2	-141 ± 8	- 54 ± 15
CH_2Cl_2	-231 ± 17	-103 ± 15
$CHBr_3$	- 67 ± 5	- 21 ± 4
$CHCl_3$	-210 ± 10	- 85 ± 5
$CHFCl_2$	-265 ± 10	-134 ± 20

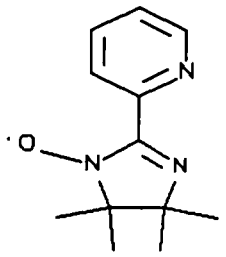

In this case, an extrapolated enhancement of more than +100 was obtained. This phenomenon was explained in terms of a strong solvent-solute interaction (i.e. hydrogen bonding formation at the imine site).

Few workers have tried to observe DNP for ^{2}H nuclei. However, Bates and co-workers [62] did observe very weak DNP for ^{2}H due to the fact of unfavorable bulk relaxation times resulting from quadrupolar relaxation and weak electron-nucleus coupling. The DNP they did observe was the result of dipolar interactions.

Even though lithium was the first DNP experiment to be performed, few studies were done using lithium until the 70's. DNP of ^{7}Li is interesting because the interaction of Li^{+} cations with both neutral free radical molecules and free radical anions or cations can be studied. The presence and strength of scalar coupling parallels the transmission of unpaired electron spin density from the radical to the nucleus during the molecular or ionic collisions or as a consequence of the formation of short-lived complexes. Very little scalar coupling was observed for lithium salts and neutral free radicals [63]. The exception is with nitroxide radical systems where scalar coupling predominates [64]. For the ^{7}Li nuclei in solutions containing free radical cation, WPBC, negative enhancements were observed also indicating weak scalar coupling [65]. Positive enhancements were observed with lithium salts and aromatic radical anions, such as naphthalene, biphenyl, phenanthrene, and anthracene [2]. Other radical anions differ from case to case. However, one conclusion that can be drawn

from the interaction between a lithium salt and a radical anion is that temperatures have to be relatively high (above room temperature) to observe large positive enhancements.

Attempts to quantitate DNP measurements of ^{13}C did not yield the desired results due to a lack of sensitivity owing to the low natural abundance and small magnetic moment of ^{13}C nuclei. One of the most complete experimental treatments of ^{13}C DNP was carried out by Natusch and Richards in 1966 [66]. At a field of 3300 gauss, they measured ^{13}C DNP enhancements for a variety of compounds using TTBP as the free radical. These results are shown in Table 3.6. A striking feature of Table 3.6 is that no numerical enhancements (quantitative) were reported (except for the one enriched sample) due to the fact that the equilibrium magnetization signals (M_0) could not be measured. Even though no numbers were given, trends can still be observed. In general, dipolar coupling dominates ^{13}C DNP except in cases of halo-substituted methanes (with the exception of CH_3I). It seems that the lone pair electrons of the halogen atoms participate in transfer of electron density from the radical to the ^{13}C nucleus.

In order to observe the equilibrium magnetization (natural abundance) signals and to obtain quantitative ^{13}C DNP enhancements, low field measurements have to be used. Grützedick and Müller-Warmuth in 1969 [67] obtained an extrapolated ^{13}C DNP enhancement of -450 with TTBP in benzene at 176 gauss at 294 K. It took them over a week to obtain the M_0 value for ^{13}C. Although quantitative enhancements have been measured, they do not approach the dipolar limit (-1300). This could due to the "three spin effect", in which hydrogens on the observed molecules with their large magnetic moments interact with ^{13}C, and the dynamic polarization of the hydrogens influence the observed ^{13}C enhancements. In order to overcome this, proton decoupling has to be employed.

Table 3.6 ^{13}C DNP Enhancements at a Magnetic Field of 3300 Gauss using TTBP as the Radical

Solvent	Sign of Enhancements	Remarks
C_6H_6	-	Very strong
C_6F_6	-	
C_6D_6	-	
C_6H_5-CH_3	-	
C_6H_5-CF_3	-	
C_6H_4-$(CH_3)_2$	-	
C_6H_{12}	-	
$Fe(CO)_5$	- 35	Enriched sample
$CHCl_3$	+	
$CHBr_3$	+	
CH_2Cl_2	+	
CH_2Br_2	+	
CH_2I_2	+	
CH_3I	-	
CCl_4	+	
CF_3CCl_3	-	
CH_3OH	-	
CH_3CN	-	^{13}CN resonance very strong
CH_3CH_2OH	-	
$(C_2H_5)_2CO$	-	
CS_2	-	

Dynamic nuclear polarization of fluorine has attracted much attention because it exhibits mixed scalar and dipolar interactions. Enhancements for theoretical scalar and dipolar interactions have been observed experimentally. The observed enhancements are governed both by the type of free radical and the type of fluorocarbon present. Tables 3.7 [61] and 3.8 [68] illustrate these effects. In Table 3.7, more negative enhancements were observed for the radicals TTBP and GALV. The reasoning behind this observation is that the bulky t-butyl groups on the radicals sterically shield the odd electron and inhibit its direct interaction with the molecule. With TPPY, TPV, and NNI radicals, which are fairly planar, scalar couplings are more likely because the odd electron is at the molecule's edge instead of shielded. From Table 3.8, it can be seen that aromatic fluorocarbons show more scalar couplings than saturated compounds. Also, scalar interaction generally increases with the degree of fluorination for aromatic fluorocarbons.

Measurements of ^{19}F DNP at four different fields with TTBP are shown in Table 3.9 [69]. The results follow predictions in that as the field strength increases, the enhancement decreases, in some cases it becomes positive.

For ^{31}P, enhancement factors have been found to be very sensitive to the chemical environment about the phosphorus atom. The extrapolated enhancements for phosphorus varied from -650 to +1610. Some of the experimental results are presented in Table 3.10 [70]. From the table, it can be seen that trivalent phosphorus always shows more scalar coupling than pentavalent phosphorus. The differences in enhancements are very dramatic when one compares alkylphosphates with the corresponding phosphites. The reasoning behind the observed differences are that the trivalent phosphorus' lone pair 3s electrons provide a means of introducing unpaired electron spin density. It is assumed that spin density is transmitted by polarization of the lone pair electrons during collisions with a radical, where the lone pair is sterically exposed. This does not apply to pentavalent phosphorus because the lone pair electrons are not available, and it is sterically difficult for a radical to approach

Table 3.7 ^{19}F DNP Enhancements in Hexafluorobenzene

Radical	A (observed)	A_∞
GALV	-165	-200
TTBP	-115	-150
DPPH	-0.3	- 2
BDPA	+ 16	+ 20
TCSQ	+165	+195
TPV	+ 95	+270
TPPY	+260	+300
WBPC	+135	+240
NNI[a]	+ 10	+450

a) NNI = Naphthalene negative ion

Table 3.8 ^{19}F DNP Enhancments using DPPH at a Magnetic Field of 74 Gauss

Compound	A_∞
CF_3CCl_3	-235
CHClFCHClF	-170
$CFCl_2CFCl_2$	-230
$CBrF_2CBrF_2$	-205
C_6H_5-CF_3	-185
perfluoro-n-hexane	-205
C_6F_6	- 3
C_6HF_5	- 95
1,2,3,4-tetrafluorobenzene	-130
1,2,4-trifluorobenzene	-155
o-difluorobenzene	-170
C_6H_5F	-170

Table 3.9 ^{19}F DNP Enhancements for Different Magnetic Field Strength Using TTBP as the Radical

Field (Gauss)	TCF[a]	TFT[b]	HFB[c]	OFN[d]
74	-235	-240	-135	-180
3050	- 55	- 27	- 21	- 22
3650	- 40	- 22	+ 11	- 20
8900	+ 5	- 7	+ 48	+ 39

a) TCF = CF_3CCl_3

b) TFT = α,α,α-trifluorotoluene

c) HFB = hexafluorobenzene

d) OFN = octafluoronaphthalene

Table 3.10 ^{31}P DNP Enhancements at a Magnetic Field of 74 Gauss Using BDPA as the Radical

Solvent	A_∞
$(C_6H_5)_3PO$	- 590
$(C_6H_5)_2P(O)Cl$	- 240
$(C_6H_5)P(O)Cl_2$	- 8
$P(O)Cl_3$	+ 895
$P(O)Br_3$	+ 670
$(OMe)_3PO$	- 650
$(OEt)_3PO$	- 415
$(OC_6H_5)_3PO$	- 590
$(OEt)_2P(O)Cl$	- 280
$(OEt)_2P(H)O$	+ 40
$(OC_6H_5)_2P(H)O$	+ 260
$(C_6H_5)_3P$	+ 860
$(C_6H_5)_2PCl$	+1040
PCl_3	+1610
PBr_3	+1300
$(OMe)_3P$	+1000
$(OEt)_3P$	+ 950
$(OC_6H_5)_3P$	+1050
$(OEt)_2PCl$	+ 790
$(C_6H_5)_2PH$	+1060

the phosphorus atom make direct contact. Several substituent effects can also be noted from Table 3.10. When Cl replaces a phenyl or alkyl group, scalar relaxation increases, but Br is less efficient than Cl. When OR is replaced by H, scalar coupling also increases.

High field measurements for ^{31}P hold the most promise for using DNP to obtain high resolution NMR spectra of nuclei with low NMR sensitivity. Dwek and Richards [71] in 1966 illustrated this point by using trimethylphosphite with 10^{-3} M TTBP at 12,500 gauss as shown in Figure 3.2. The enhancement is +35 and the resolution of the multiplet is very good considering that the sample was not spinning. This system works well for trivalent phosphorus, but enhancements for pentavalent phosphorus were not large enough to be useful. If a radical can be found that gives large enhancements for pentavalent phosphorus compounds, biological applications can be envisioned.

Most DNP NMR studies have utilized static liquid or solid [2,3] samples. As stated previously, the microwave magnetic field strength at the sample determines the efficiency of saturation at a given output power. The magnitude of the magnetic field (B_{1s}) varies as the square root of applied power ($P^{1/2}$), therefore, saturation can always be achieved at the expense of higher applied power.

In static DNP NMR studies, the NMR rf coil is placed within the microwave cavity. The NMR coil shields the microwave field thus reducing microwave efficiency as illustrated in Figure 3.3(a) and 3.3(b). In order to reach saturation, microwave power needs to be increased. In many cases, microwave power levels of 2 - 10 watts are required to achieve reasonable saturation levels ($s = 0.3 - 0.9$) in static DNP NMR studies. The increasing power needed for saturation in turn, can result in sample heating. More importantly, in this configuration, NMR detection is not optimized with respect to the rf coil.

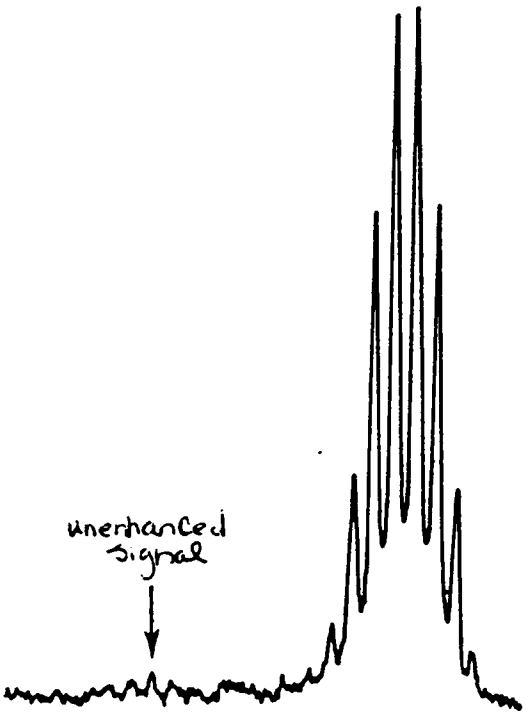

Figure 3.2 ^{31}P Spectrum of $P(OMe)_3$ with 10^{-3} M of TTBP.

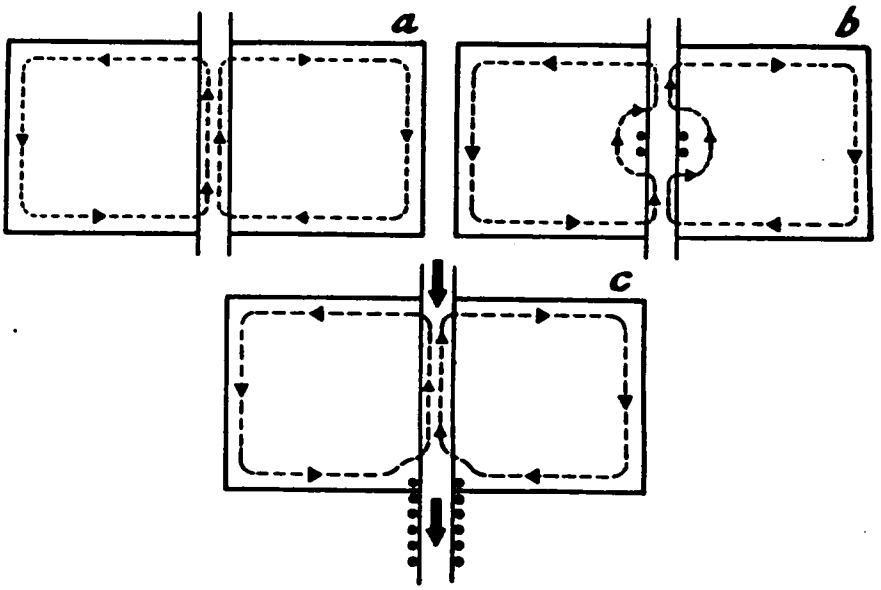

Figure 3.3 Microwave magnetic fields for:

a) Unperturbed microwave cavity
b) Typical static configuration for DNP-NMR
c) Flow configuration for DNP-NMR

Dorn et al [72] have recently shown that by using a flow sample, the microwave cavity and NMR rf coil can be separately optimized. Thus significantly reducing the microwave power needed to achieve saturation (.25 - 4.0 watts) as schematically illustrated in Figure 3.3(c).

A diagram of the flow DNP experiment is illustrated in Figure 3.4. The NMR observation region is normally at the same magnetic B_o field as the corresponding field for the ESR experiment. A flowing bolus enters the magnetic field and develops the nuclear Boltzmann magnetization on the order of 3-4 T_{1n}'s. The analogous condition holds for the free radical system, but requires a shorter time period for developing S_o (~ 3-4 t_{1s}). The ESR transition frequencies are irradiated in region A and polarization builds up with a time constant dependent on the nuclear spin-lattice relaxation time, T_{1n}. The bolus is then transferred from region A to C where the NMR signal is monitored. In this configuration, the free radical used is dissolved directly into the sample solvent. This system has been termed a liquid-liquid intermolecular transfer (LLIT) DNP experiment.

A variation on the LLIT DNP experiment is termed solid-liquid intermolecular transfer (SLIT) DNP experiments. The configuration for SLIT DNP is shown in Figure 3.5. [73] For SLIT DNP, the free radicals are immobilized on a surface such as silica gel instead of dissolved in the solvent system. The flowing bolus enters region A and develops the Boltzmann magnetization in the same manner as the LLIT DNP. At the same time period, the microwave field (B_{1s}) irradiates the ESR transition(s) of the immobilized radical, and the polarization builds up in the flowing bolus with a time constant T_{1n}. In region B and C, the polarized bolus relaxes at a relatively slow spin-lattice relaxation rate (T_{1no}^{-1}). The volume element of region B is relatively small and the corresponding transfer time (τ_B) is short ($\tau_B < T_{1no}$). The NMR signal for the polarized sample bolus is monitored using FTNMR as in LLIT DNP experiments. For SLIT DNP, the transfer time of the sample bolus to region C is dependent on T_{1no} instead of T_{1n} as in LLIT DNP.

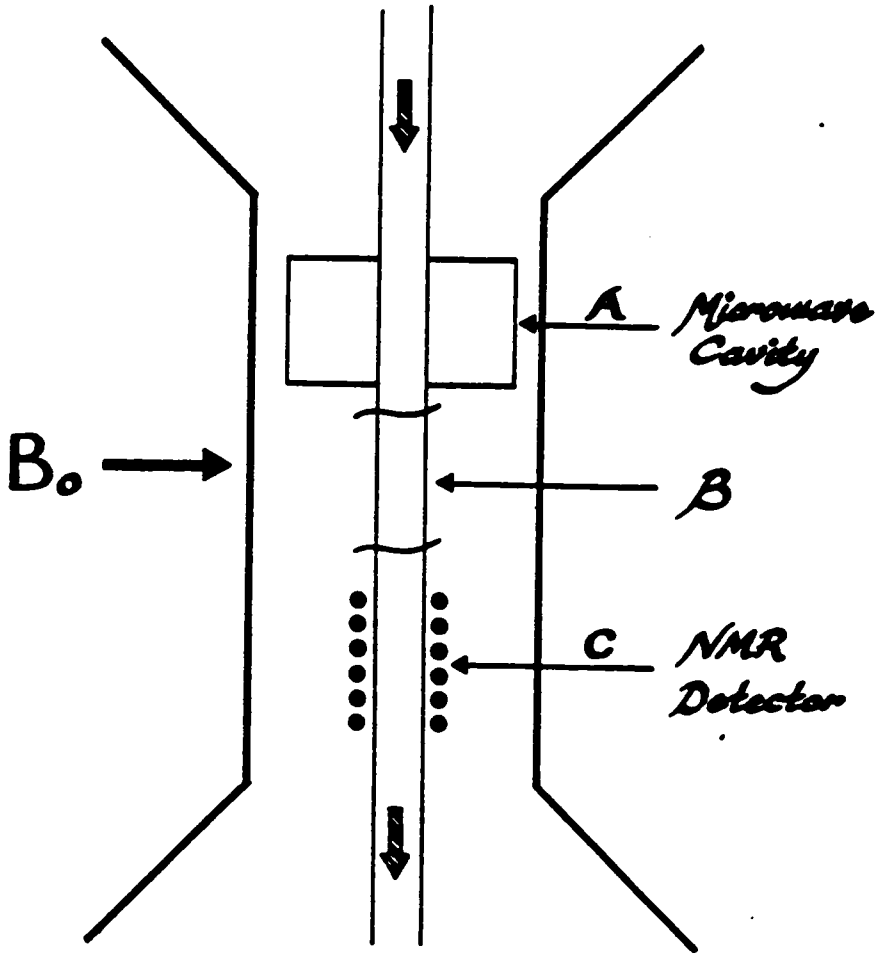

Figure 3.4 LLIT DNP-NMR experiment apparatus

Region A: microwave cavity, saturation volume
Region B: transfer volume
Region C: NMR observation volume

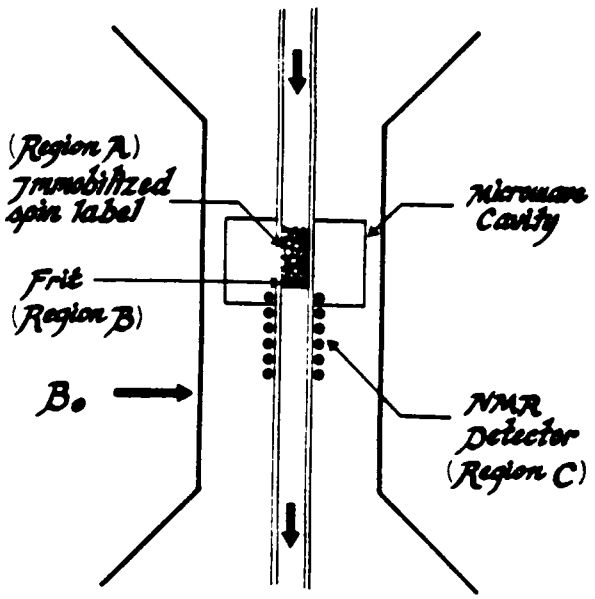

Figure 3.5 SLIT DNP NMR experiment apparatus

As mentioned previously, one major difference between SLIT and LLIT DNP experiments is that in the former, free radicals are immobilized on a support and not dissolved in the flowing bolus. This offers several advantages. First, broadening of NMR signals associated with the presence of paramagnetic species in solution will not occur. Second, free radicals cannot contaminate the flowing bolus. This is important if the sample is to be recovered. Another difference between LLIT and SLIT DNP is the time dependence of transfer (region B). In LLIT DNP, the transfer time is dependent on T_{1n} (spin-lattice relaxation time in the presence of free radicals), where in SLIT, this is dependent on T_{1no} (spin-lattice relaxation time in the absence of free radicals). This makes transfer time less restrictive for SLIT than for LLIT DNP in that T_{1no} is longer than T_{1n}.

The advantage of LLIT DNP over SLIT DNP for this system is in the magnitude of the observed enhancements as illustrated in Figure 3.6. This is due to the fact that τ_c for SLIT DNP is much longer than for LLIT DNP because the radicals are immobilized, and according to equations 22 - 24, as τ_c increases, enhancement decreases. The solvent sample being monitored is benzene and the radical used is 4-hydroxy-TEMPO.

More recently, Dorn et al. [74] have demonstrated the feasibility of flow transfer from low to high magnetic fields. The low to high magnetic field flow experiments were performed with instrumentation schematically illustrated in Figure 3.7. As can be seen in Figure 3.7, the experiments were performed using SLIT ^{1}H DNP. In the low to high magnetic field SLIT DNP transfer experiment, the observed magnetization for a flowing bolus at the high magnetic field detector is crucially dependent on the flow rate. At very low flow rates or static conditions, the observed NMR signal is dominated by the high magnetic field thermal Boltzmann-equilibrated magnetization (M_0^H). However, at high flow rates, the high magnetic field contribution to the total magnetization decreases dramatically since the spin-lattice relaxation time (T_{1no}) is relatively long compared to the residence time (τ_c) in region C. For high flow rates, a significant fraction of the observed signal can result from low

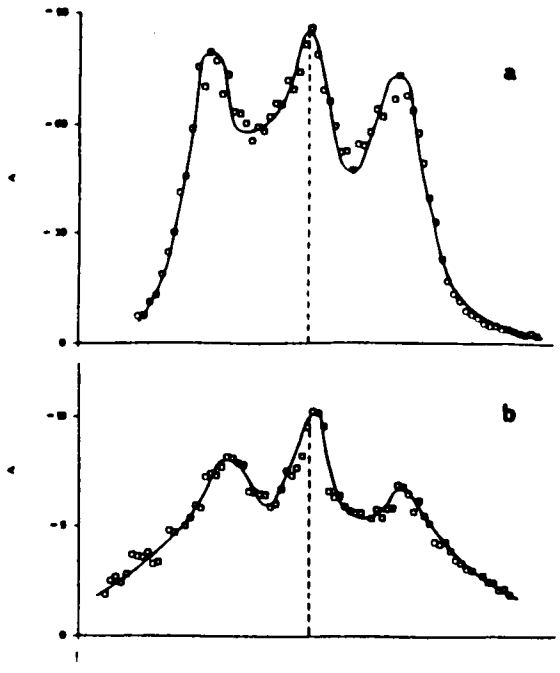

Figure 3.6 Comparison of observed enhancements for LLIT and SLIT DNP experiments.

a) LLIT DNP
b) SLIT DNP

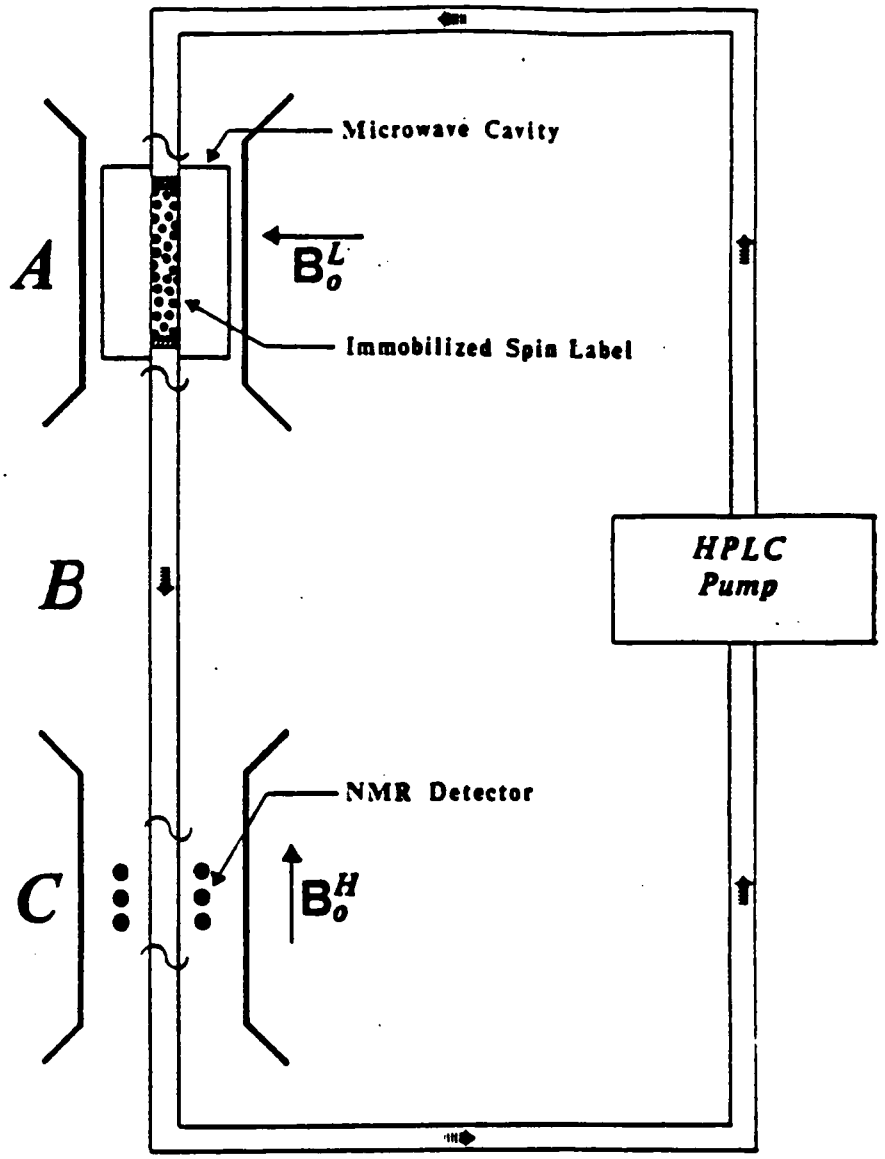

Figure 3.7 The SLIT DNP transfer experiment apparatus.

field thermal Boltzmann magnetization (M_0^L). That is, the bolus residence time in region A (τ_a) is long relative to T_{1n}.

After exiting region A, the bolus is transferred to the high magnetic field detector (region C). For high flow rates, the bolus is transferred via region B in a time period short relative to T_{1no}. At present a transfer time of 0.5 second has been achieved. Assuming T_{1no} is no shorter than 3 - 5 seconds, the low field magnetization will tend to dominate the monitored magnetization at sufficiently high flow rates (e.g. 5 - 10 mL/min).

The mathematical model for the low-to-high magnetic field transfer experiment has been developed by Tsai and Dorn [75]. Assuming τ_a, τ_b, and τ_c, are the average bolus residence times in regions A, B, and C, respectively, simplified equations 33 and 34 below can be derived [3].

$$\frac{\langle M_Z^{DNP}\rangle - \langle M_Z^{HL}\rangle}{\langle M_0^L\rangle} = A\,(1-E_{1a}) \qquad (33)$$

$$\frac{\langle M_Z^{DNP}\rangle - \langle M_Z^{HL}\rangle}{\langle M_0^H\rangle} = \frac{E_{1bc}\,A(1 - E_{1a})}{K} \qquad (34)$$

where $\langle M_Z^{DNP}\rangle$ = the monitored enhanced flow magnetization in the presence of the microwave fields B_{1e}

$\langle M_Z^{HL}\rangle$ = the monitored flow magnetization in the absence of a microwave field

$\langle M_0^L\rangle$ = the low field monitored flow magnetization

$\langle M_0^H\rangle$ = the static thermal Boltzmann high field magnetization.

$E_{1a} = e^{-\tau_a / T_1}$

$E_{1bc} = e^{-(\tau_b + \tau_c) / T_1}$

K = a constant which is the ratio (B_0^L/B_0^H).

For the present experiments K = 14.3.

Since $\langle M_Z^{DNP} \rangle$, $\langle M_Z^{HL} \rangle$, and $\langle M_0^H \rangle$ can be measured in a given experiment, the enhancement A can be obtained as a function of flow rate. The A values can then be extrapolated to f = 1, and s = 1, as a function of radical concentration and microwave power, respectively.

The immobilized nitroxide radicals used for the flow transfer experiments are not the same as those used in the SLIT DNP flow studies. Silica gel, the support system, is first reacted with dichlorosilane under N_2 in refluxing benzene. Then, 4-hydroxy-TEMPO is added to react with the silica gel supported silyl chloride. To obtain different radical concentrations in the immobilized system, the reacted silica gel is mixed with unreacted (clean) silica gel to achieve different radical concentrations.

Chapter 4

Saturation Studies

Results and Discussion

Although structural information can be obtained from LIS and LIR studies as illustrated in Chapter 2, the methods used to obtain this information are not trivial. Once the LIS or LIR data have been measured, other techniques or computer programs have to be used to match the data. This is a time consuming process. Many times, the information obtained cannot be used directly as illustrated in the study of the cyclohexanol series, where only ratios of the distances are obtained. In some cases, one is fortunate and direct distances can be calculated as in McLennan and Lenkinski's study [26].

Another method that could be used to obtain structural information is dynamic nuclear polarization (DNP). As previously described in Chapter 3, DNP has been used to probe stereo-specific collisions in liquids, to study weak molecular complex formation and to measure NMR signals in system with low natural abundance and magnetic moments. All of these are direct observations and could provide structural information that may not be obtainable by LIS or LIR studies.

As previously noted, a flow system for DNP can decrease the power needed for saturation. Another way to use less power for saturation is to narrow the line width of the ESR signals for the free radicals used. By substituting hydrogens on the radicals with deuterium, narrower line widths of the ESR signals can be observed. This is due to the fact that hyperfine coupling is significantly reduced between the electron and deuterium. In the case of nitrogen containing systems such as the nitroxide radicals, substituting ^{15}N for ^{14}N

results in a decrease of the ESR triplet to a doublet. This is because ^{15}N is an I = 1/2 nuclei and ^{14}N is an I = 1 system.

This chapter will discuss substituting deuteriums for some of the hydrogens present in the galvinoxyl and 2,4,6-tri-tert-butyl phenoxyl radicals, and the effect this has on the DNP experiment. Also, the results of substituting ^{15}N for ^{14}N and deuteriums for hydrogen in the nitroxide radical, 4-hydroxy-TEMPO will be examined. The structures for the compounds studied are illustrated in Figure 4.1. The LLIT DNP system was used to obtain ^1H DNP enhancements at $\omega_e/2\pi$ = 9.5 GHz and $\omega_n/2\pi$ = 14 MHz.

The d_3-TTBP compound was synthesized according to the procedure of Stillson et al [76] with the exception that d_6-phenol, D_2SO_4 and d_6-benzene were used instead of their protonated counterparts. The reaction scheme is shown below:

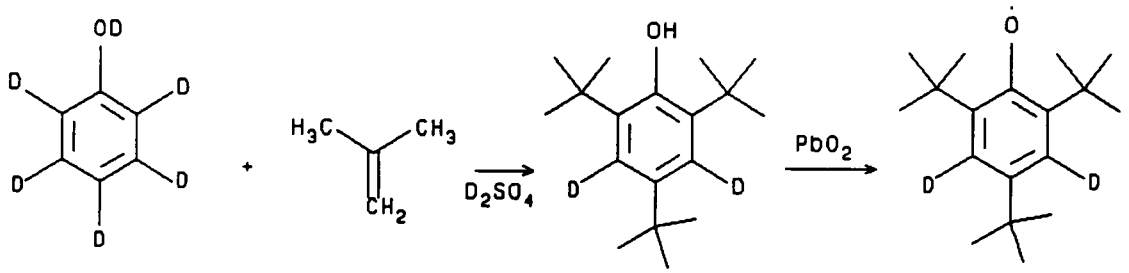

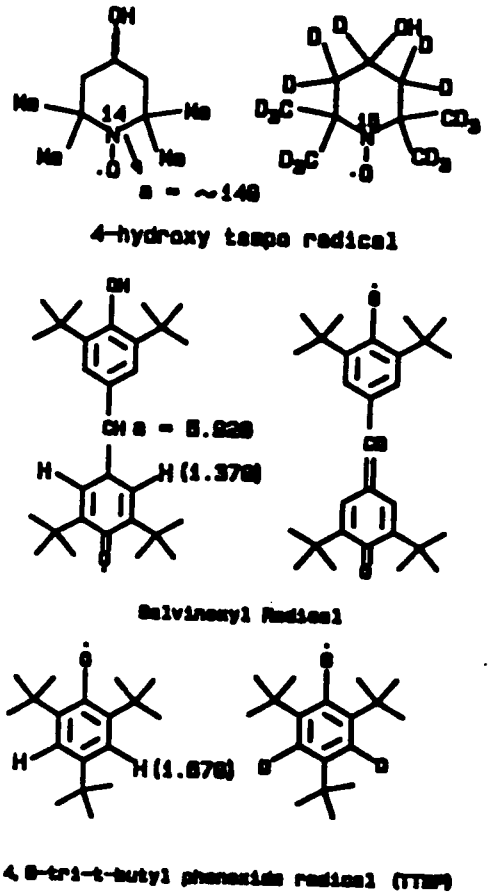

Figure 4.1 The compounds used for LLIT DNP saturation studies.

Figure 4.2 shows the superimposed ESR spectra for the deuterated and undeuterated TTBP radicals at a concentration of 1 x 10^{-2}M. The dotted spectrum is the deuterated TTBP radical and the solid spectrum is the undeuterated TTBP radical. The line width for the deuterated TTBP is somewhat but not significantly more narrow than the protonated analog. The saturation plot (S-plot) of both deuterated and undeuterated TTBP is shown at the concentration of 10^{-2}M in Figure 4.3. From equation 20, Chapter 3, the intercept of the S-plot is the inverse of DNP enhancement at s = 1. The intercept for the deuterated TTBP in Figure 4.3 is 0.38, which corresponds to a DNP enhancement of 66. For the undeuterated TTBP, the intercept is 0.28 which gives a DNP enhancement of 89. The S-plot for TTBP seems to indicate that deuteration of the aromatic hydrogens on TTBP does not reduce the power needed for saturation and in fact, it may degrade the enhancement. The specific reason for the lower enhancement for the deuterated analog is unclear at this time.

For galvinoxyl, deuterium substitution was carried out at the methine position between the two phenyl rings. The procedure was similar to the one published by Kharasch et al [77]. with the exception that d_2-paraformaldehyde is used instead of 37% formaldehyde solution and d_1-C_2H_5OD and 40% NaOD/D_2O were also used. The reaction scheme is shown below:

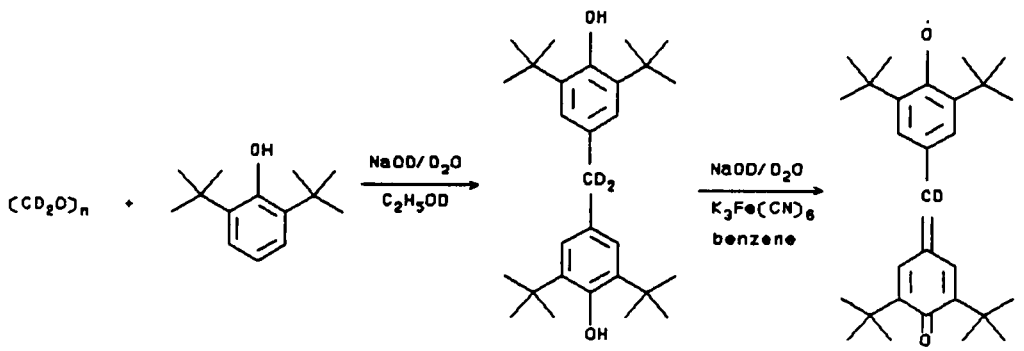

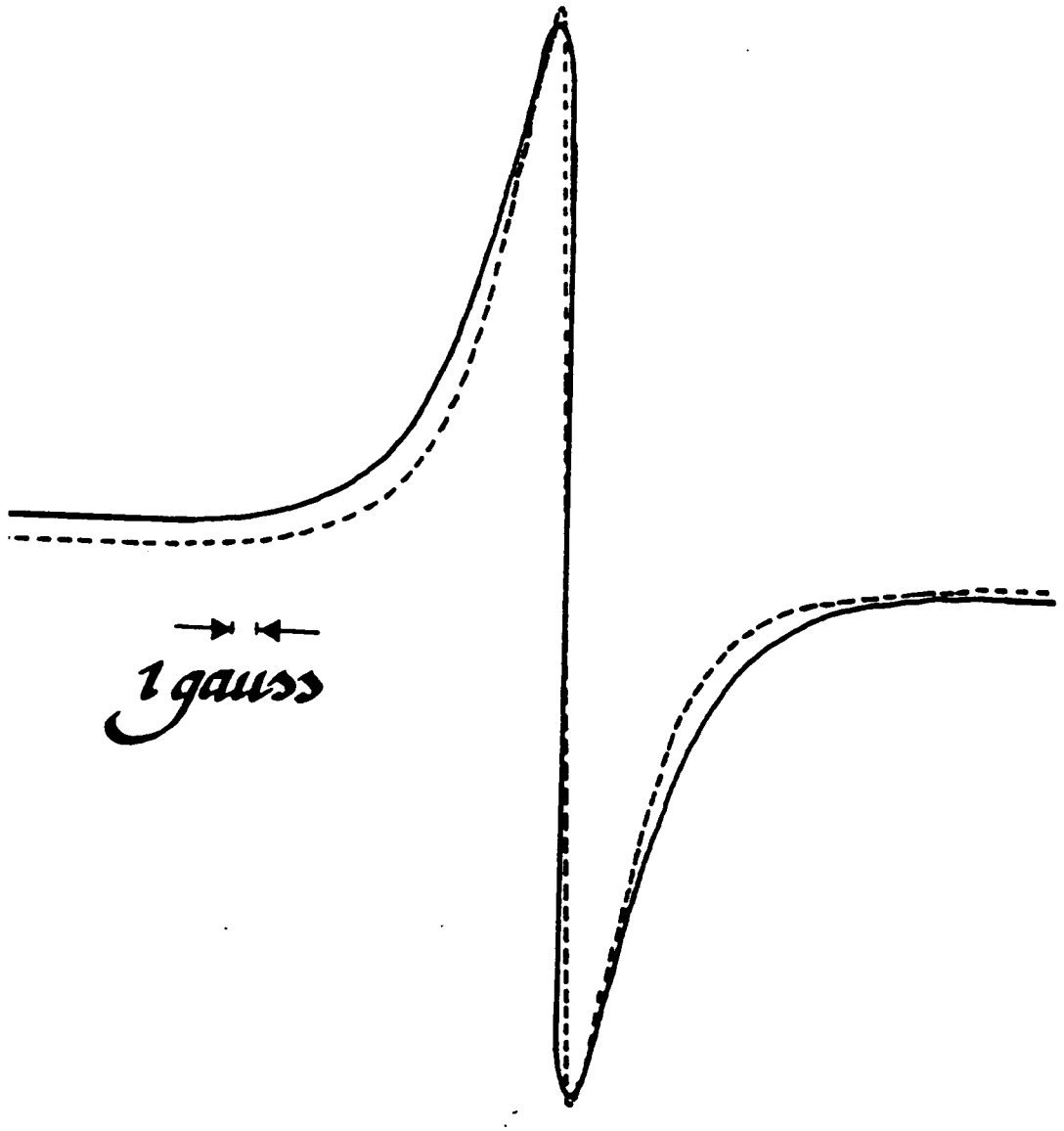

Figure 4.2 ESR spectra of TTBP radical at 1 x 10^{-2}M

----- : deuterated TTBP
——— : undeuterated TTBP

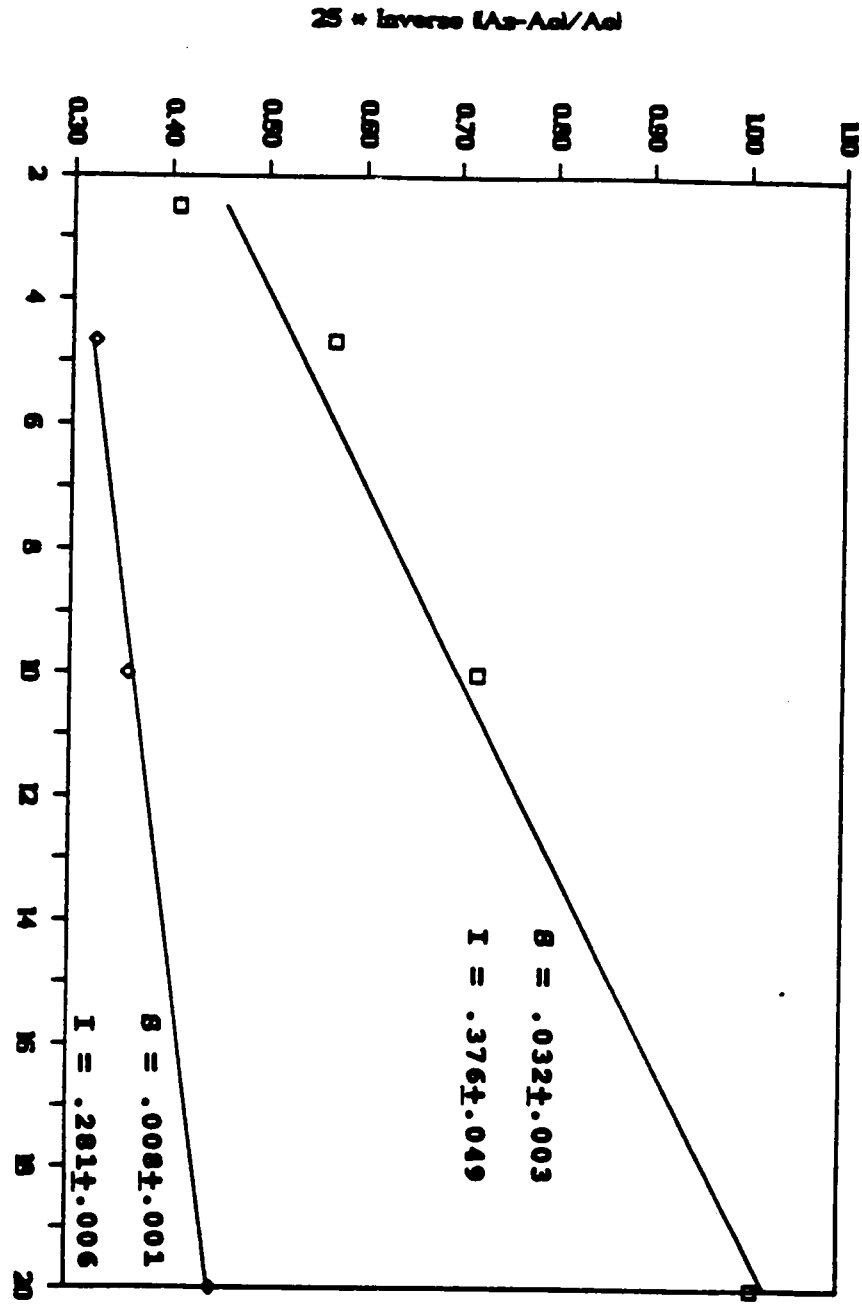

Figure 4.3 The S-plots of deuterated and undeuterated TTBP at 5 x 10^{-2} M.

The ESR spectra for the deuterated and undeuterated GALV radical is shown in Figure 4.4. Again S-plots were obtained for both cases and are presented in Figure 4.5. The GALV S-plots give lower enhancements than those obtained for the TTBP radical system at a given power. In the TTBP case, an enhancement can still be observed at 0.05 watts of power. For GALV radicals, the minimum power needed for an observed enhancement is 0.1 watt. The extrapolated enhancements, for s = 1, are not as good as the TTBP radicals. For the deuterated GALV radical, the intercept is 0.64 which corresponds to an extrapolated enhancement of 39, and for the undeuterated GALV radical, the intercept is 0.62 with an extrapolated enhancement of 40. Therefore, deuteration of the methine hydrogen in the GALV radical does not appear to offer any advantage. In fact, the GALV radical is not as good as TTBP radical in terms of the ultimate enhancement for benzene. It should be noted that we assume electron-electron exchange dominates the separate transition for the undeuterated GALV radical system at this concentration (5×10^{-2}M).

The nitroxide radical is a special case. The ESR of any nitroxide radical is usually a triplet (I = 1). Most studies have suggested that one has to saturate all three signals of the ESR spectrum to obtain any useful information [78]. In addition, as pointed out by Bates [79] the extrapolated enhancements cannot be directly obtained because of electron-electron exchange between the three transitions. However, this is not necessarily the case. For example, consider Figure 4.6 at high concentration of a ^{14}N (I=1) nitroxide radical, electron-electron exchange will dominate and the extrapolated enhancements will approach the appropriate dipolar limit (e.g. -330). However, at low ^{14}N nitroxide radical concentration (no electron-electron exchange), the dipolar limit is reduced by 1/3 (e.g. -110). In contrast, a ^{15}N (I = 1/2) labelled nitroxide radical will have an extrapolated enhancement reduced by a factor of 1/2 (e.g. -165) at low radical concentrations. Thus ^{15}N and deuterated 4-hydroxy tempo

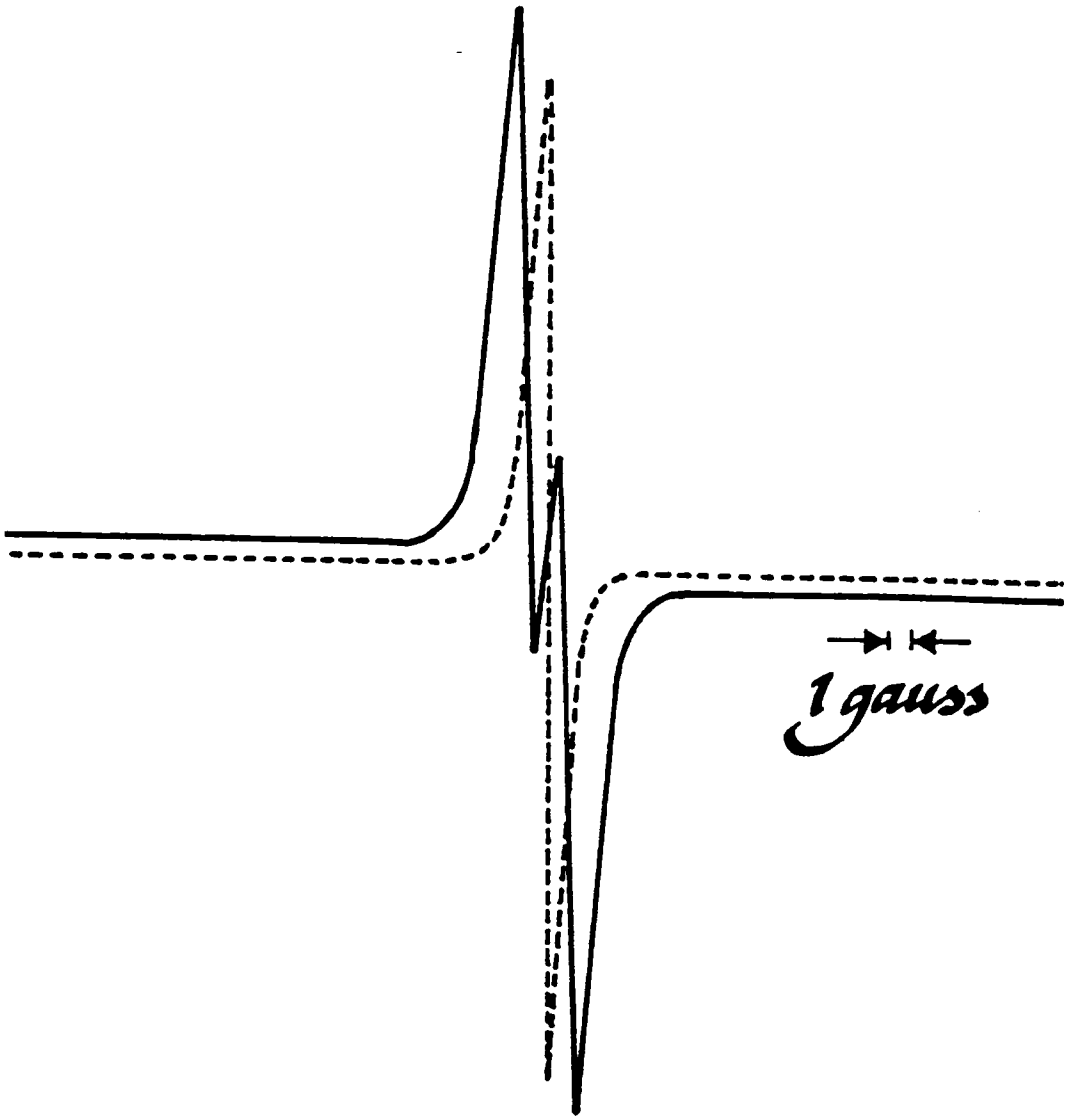

Figure 4.4 ESR spectra of GALV radical at 5 x 10^{-2} M

----- : deuterated GALV
——— : undeuterated GALV

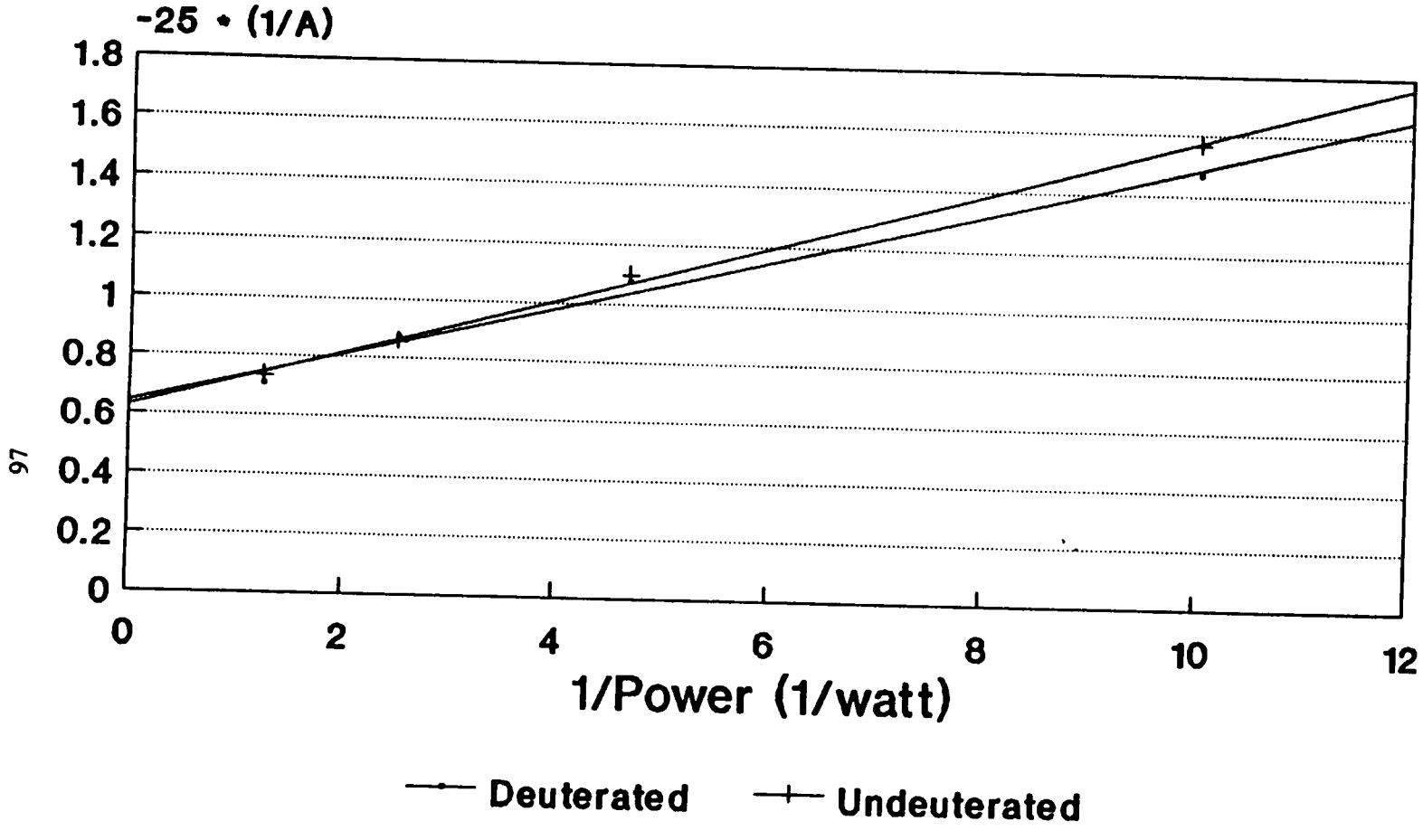

Figure 4.5 The S-plots of deuterated and undeuterated GALV radical at 5 x 10^{-2} M.

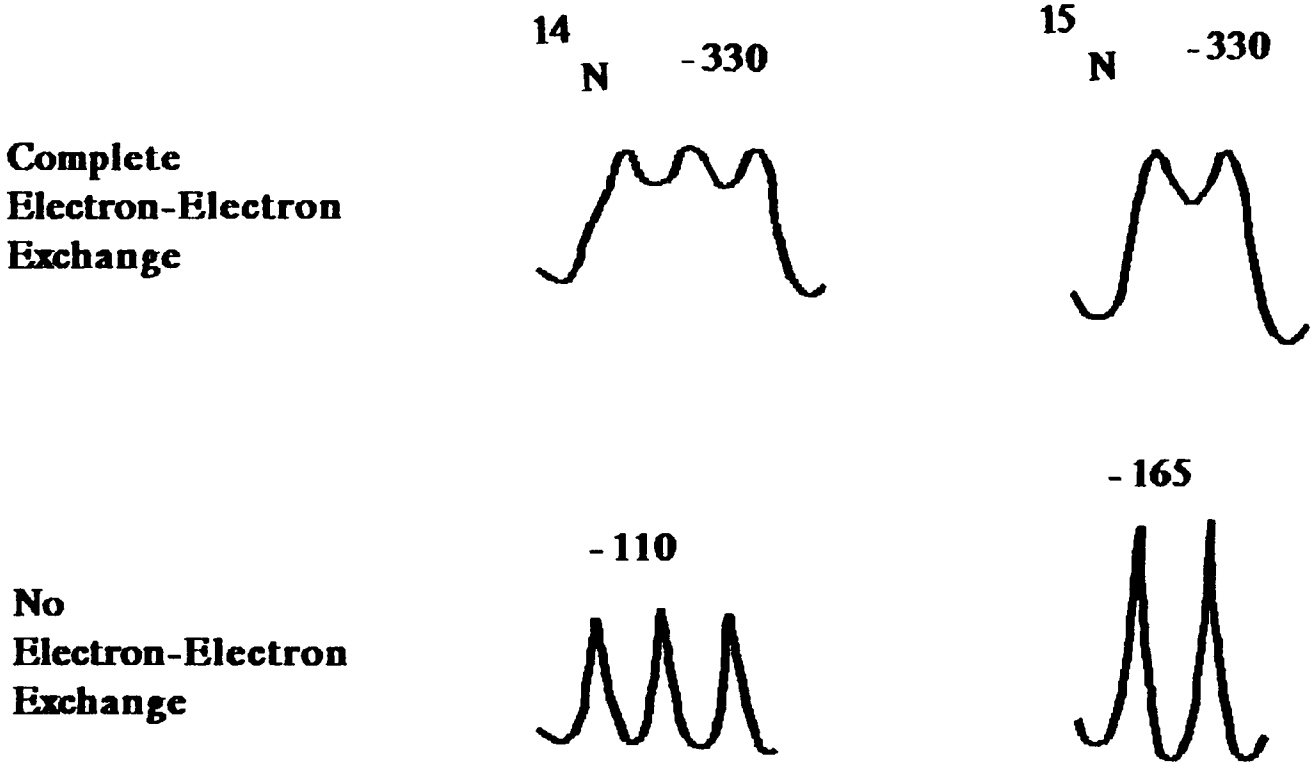

Figure 4.6 The extrapolated enhancements for ^{14}N and ^{15}N labelled nitroxide radical at complete electron-electron exchange and at no electron-electron exchange.

was purchased from MSD Isotopes. The S-plots of the undeuterated, ^{14}N tempol and deuterated, ^{15}N tempol at 10^{-2} M are shown in Figures 4.7 and 4.8. The intercept for the undeuterated, ^{14}N tempol radical is 0.32 with an extrapolated enhancement of 78, and for deuterated, ^{15}N tempol radicals, the intercept is 0.38 and the extrapolated enhancement is 66. Differences in enhancements were not observed until the concentration of tempol was decreased to 5 x 10^{-4} M. At this concentration, the deuterated, ^{15}N tempol gives a much higher observed enhancement than the undeuterated, ^{14}N tempol. The ESR spectra of 10^{-1} and 1 X 10^{-3} M of the tempol radicals are shown in Figure 4.9. When 4-hydroxy-TEMPO is at low concentration, the ESR spectrum is the expected triplet. At higher concentration, the triplet collapses into a broad singlet due to complete electron-electron exchange. At a concentration of 10^{-2} M, both the deuterated, ^{15}N and undeuterated, ^{14}N 4-hydroxy-TEMPO start to broaden to a singlet, and the enhancements obtained are very similar. At low concentration, the enhancements are dramatically different. Figures 4.10 and 4.11 illustrate this observation. Instead of S-plots, field plots are shown where the field is swept to observe all three signals or two signals of the tempol radical (the saturation for this case is s = 1). As can be seen from Figure 4.10, the deuterated, ^{15}N 4-hydroxy-TEMPO gives a higher observed enhancement than the undeuterated, ^{14}N 4-hydroxy-TEMPO (-110 vs. -90) at a concentration of 10^{-2} M, which is ~ 1.2 times greater. For Figure 4.11, the same plot at 8 x 10^{-4} M the observed enhancements are -29 vs. -17 for deuterated,^{15}N and undeuterated,^{14}N 4-hydroxy-TEMPO, respectively. The difference is almost twice. The theoretical dipolar limit for ^{1}H DNP enhancement is -330. If there is no electron-electron exchange, the theoretical enhancements for the deuterated, ^{15}N 4-hydroxy-TEMPO would be -330/2 = -165 for each of the doublet. For undeuterated, ^{14}N 4-hydroxy-TEMPO it would be -330/3 = -110. The importance of this observation is that at low nitroxide radical concentration, the use of ^{15}N substituted radicals can give much higher enhancements than the ^{14}N nitroxide radicals. In addition, using a mixture of 50/50 ^{14}N and ^{15}N labelled nitroxide radicals can provide information on

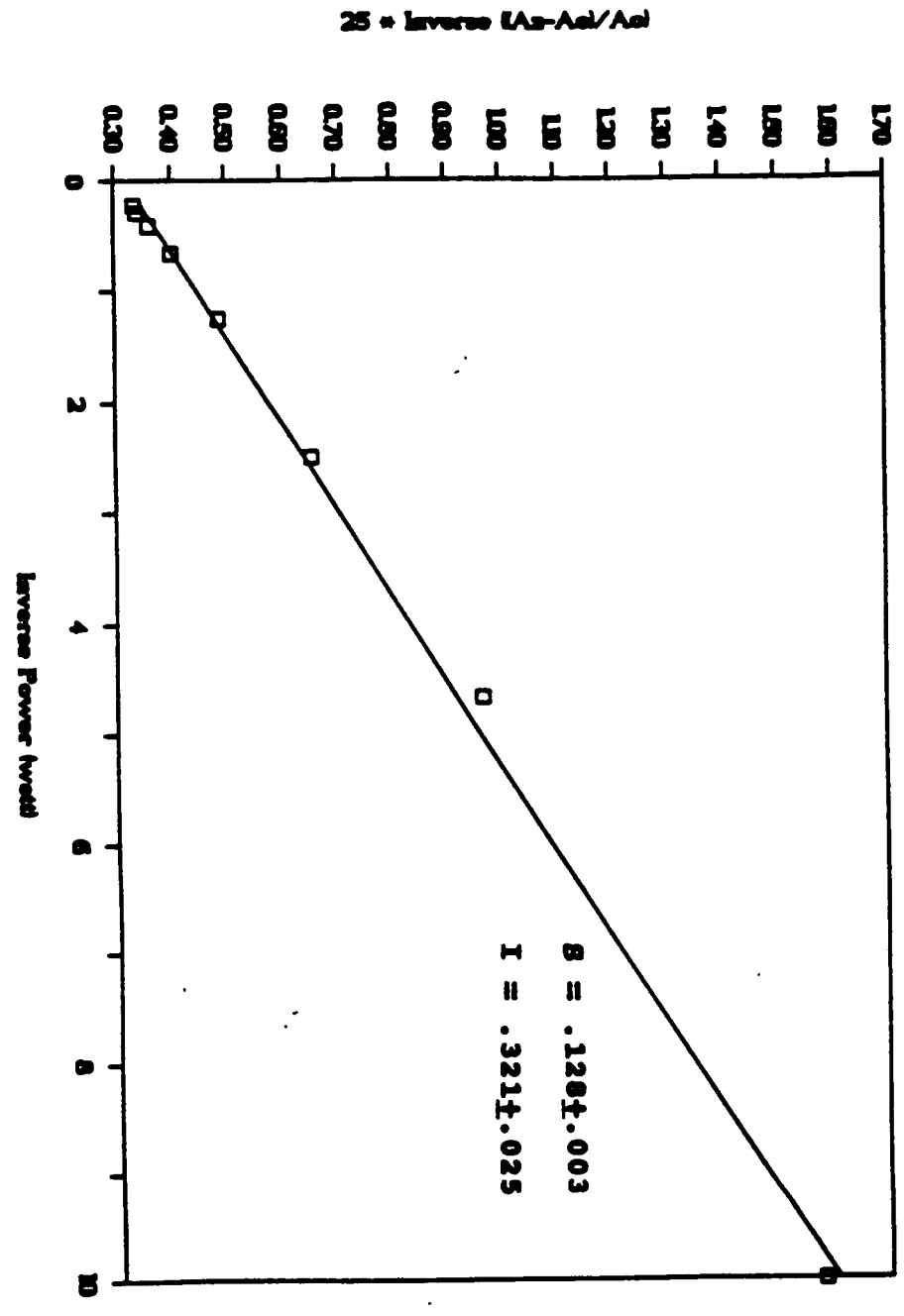

Figure 4.7 The S-plots of ^{14}N, undeuterated 4-hydroxy-TEMPO at 1 x 10^{-2} M.

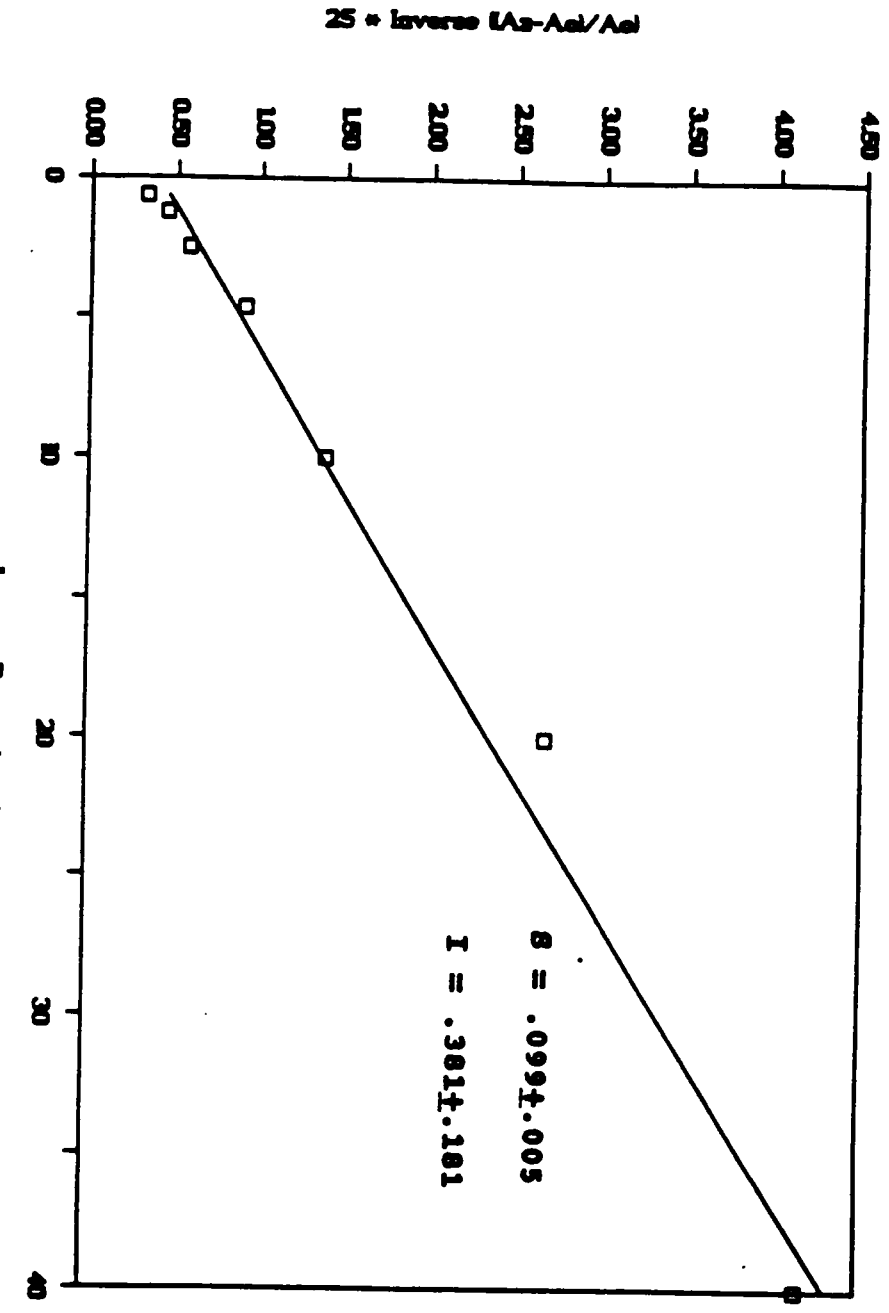

Figure 4.8 The S-plots of ^{15}N, deuterated 4-hydroxy-TEMPO at 1 x 10^{-2} M.

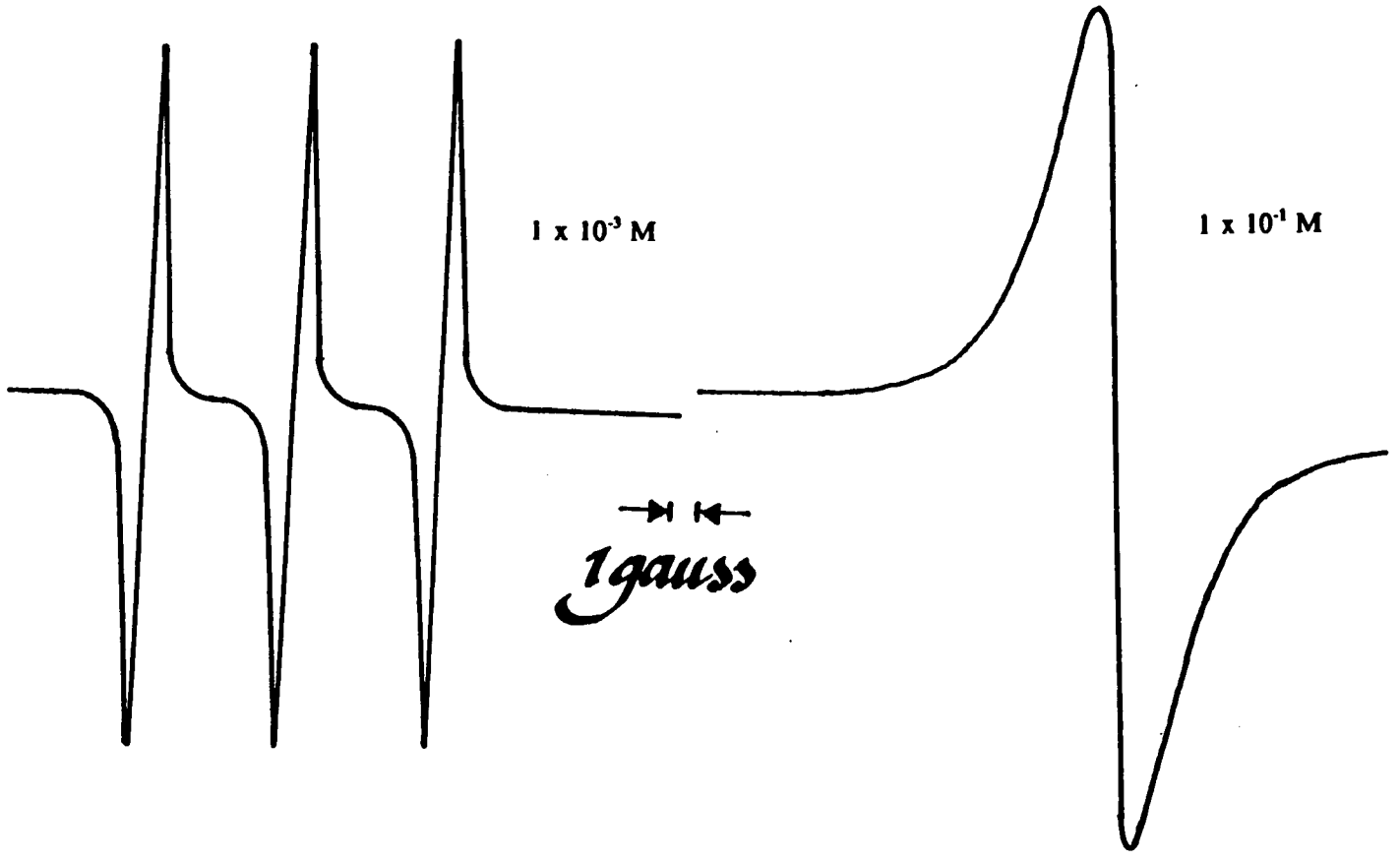

Figure 4.9 ESR spectra of 4-hydroxy-TEMPO at 1 x 10^{-3} M and 1 x 10^{-1} M.

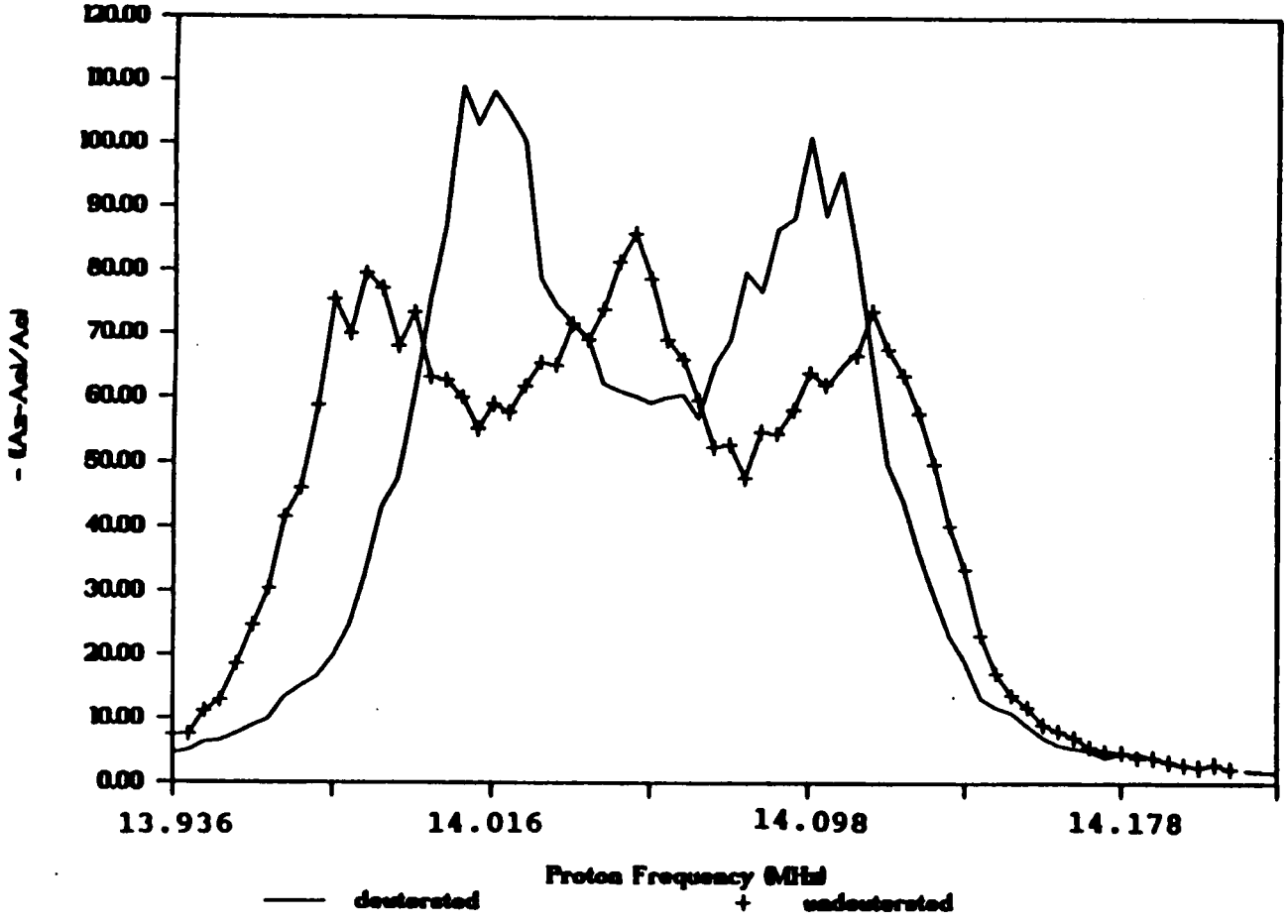

Figure 4.10 The field plots of ^{15}N, deuterated and ^{14}N, undeuterated 4-hydroxy-TEMPO at 1 x 10^{-2} M.

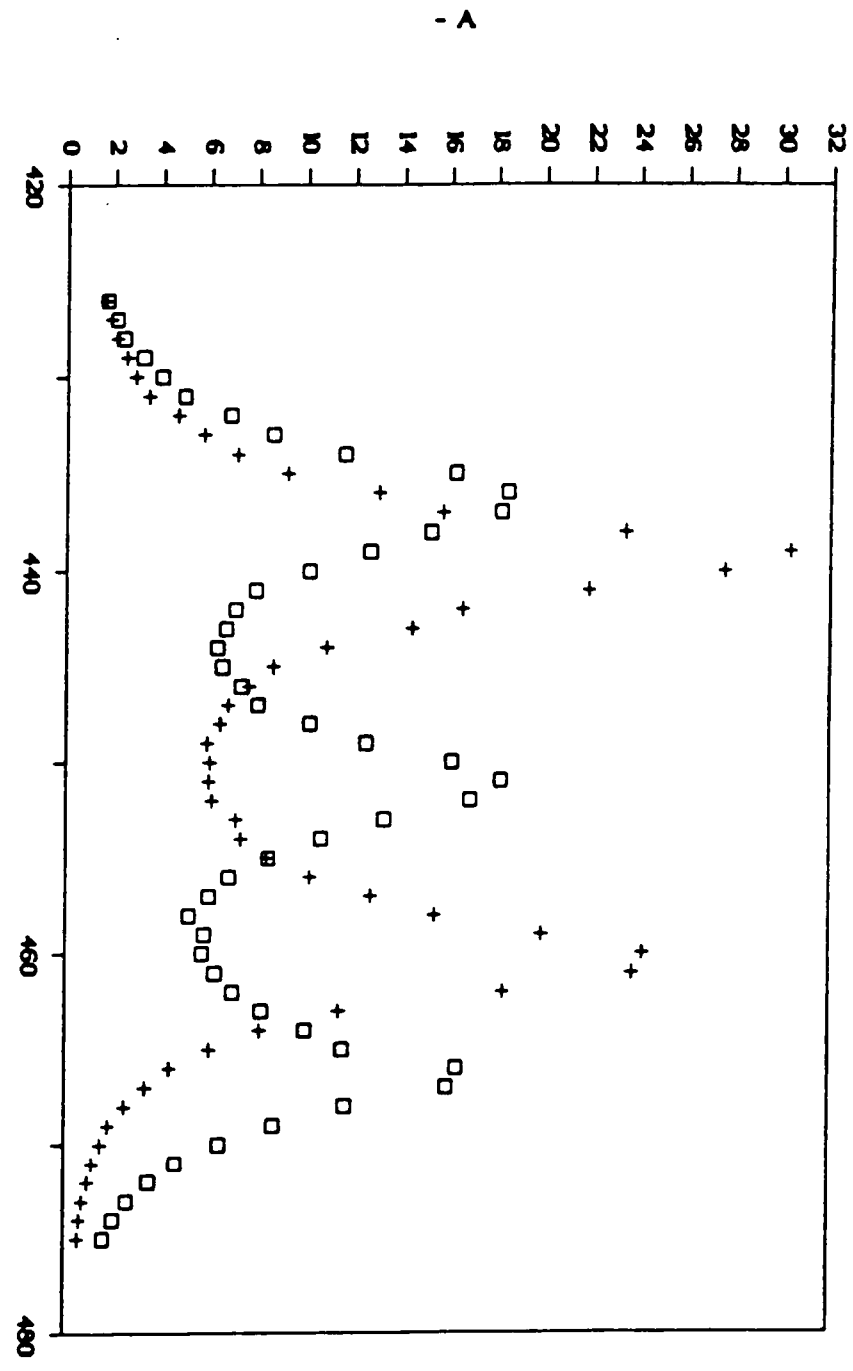

Figure 4.11 The field plots of ^{15}N, deuterated and ^{14}N, undeuterated 4-hydroxy-TEMPO at 8×10^{-4} M.

the amount of electron-electron exchange present in a given experiment. For the case of no electron-electron exchange, the ratio of the enhancements for ^{15}N to ^{14}N labelled nitroxide radicals would be 1.5 (e.g. -165/-110). In Figure 4.12, the field plot of a 50/50 mixture of ^{15}N, deuterated and ^{14}N, undeuterated 4-hydroxy-TEMPO at the concentration of 1 x 10^{-4}M is illustrated. In this case, the ratio of the enhancements calculated is ~ 2. This is more than the 1.5 predicted for no electron-electron exchange. The reason we believe the ratio is not 1.5 is due to the fact we are not comparing just ^{14}N and ^{15}N labelled 4-hydroxy-TEMPO. The ^{15}N labelled 4-hydroxy-TEMPO we used was also deuterated. The hyperfine coupling between hydrogen and the ^{14}N in the undeuterated, ^{14}N labelled 4-hydroxy-TEMPO was not taken into account. Therefore, the ratio we obtained for our 50/50 mixture studies is higher than the predicted. It would be useful if in the future the ^{15}N labelled, undeuterated 4-hydroxy-TEMPO or ^{14}N labelled, deuterated 4-hydroxy-TEMPO is used for the mixture studies.

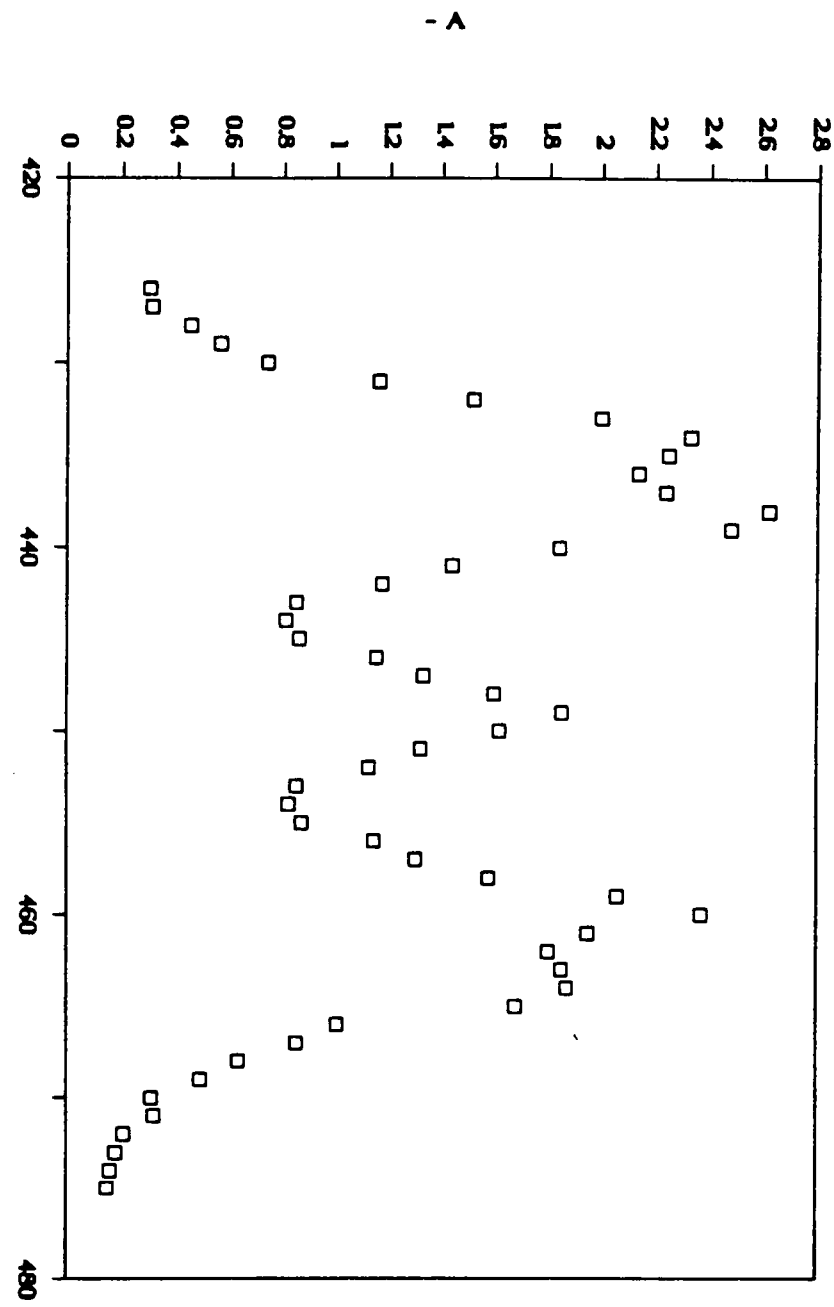

Figure 4.12 The field plot of a 50/50 mixture of ^{15}N, deuterated and ^{14}N, undeuterated 4-hydroxy-TEMPO at 1 x 10^{-4} M.

Experimental

Equipment. The ESR data were obtained with a Varian E-3 spectrometer operating at B_0 = 3.3 KG. Samples were dissolved in benzene.

Flow DNP Experiments. The experiments were performed using a modified Varian E-3 spectrometer at Bo = 3.3 KG. The Klystron microwave source (ω_s = 9.3 GHz) had a maximum power output of 4.4 watts with a Hughes TWT amplifier Model 8010. The NMR coil had a total length of 10 mm (18 turns, #30 Cu wire) and was virtually out of the microwave TE_{102} cavity (~ 1 - 2 mm at the end of the lower region cavity). The cell was made of ceramic. The active cell volume of the NMR detector is ~ 20 μL. For these conditions, the quality factor (Q) of the cavity was not significantly degraded by the presence of the NMR coil assembly (Q is approximately 1700 in the presence or absence of NMR rf coil). The ^{1}H NMR (14 MHz) signal was detected by the rf coil and a wideband JEOL FX-200 spectrometer console. No attempt was made to improve the Bo homogeneity of the Varian ESR magnet, ^{1}H NMR line widths of ~ 600 Hz were routinely obtained. A Waters M-45 pump was used for these experiments.

d_2-2,4,6-Tri-tert-butylphenol. d_6-Phenol (1.0 g, 0.01 mol), D_2SO_4 (0.1 g), and 5 mL of d_6-benzene were added to a 10 mL, 2-necked, round bottomed flask fitted with a water cooled condenser, thermometer and a pipette for gas (isobutylene) addition. The reaction was maintained at 65 ± 5°C while the isobutylene was bubbled into the mixture. After 7 hours, the reaction was complete (by NMR). The solution was cooled to room temperature and shaken with 2% NaOH until the aqueous layer was basic. The organic layer was washed with water until no longer basic. After drying over $MgSO_4$, the solvent was removed *in vacuo*. The residue was a white slush. This material was recrystallized from 95% ethanol to give 1.8 g of white crystals (68% yield). The crystals had a M.P. = 128 - 130°C. The compound afforded the following spectroscopic data. ^{1}H NMR δ 1.28 (s, 9H), 1.43 (s, 18H), 5.01 (s,

broad, 1H). The radical is formed by addition of a 10% molar excess of PbO_2 to the solution.

d_1-ethanol (C_2H_5OD). Tetraethylorthosilicate (104.2 g, 0.5 mol) and D_2O (40g, 2.0 mol) were added into a 250 mL, 1-necked, round bottomed flask. A magnetic stir bar was added, the flask was stoppered and allowed to stir at room temperature for 24 hours. The resulting white mixture was vacuum distilled @ 5 mm Hg. The receiver was cooled with a dry ice/acetone bath. 75 mL of the desired product was collected.

4,4'-Methylene bis(2,6-di-tert-butylphenol) (Galvinoxyl precursor). d_2-paraformaldehyde (1.0 g), 2,6-di-tert-butylphenol (3.22 g, 0.156 mol) and 30 mL of d_1-C_2H_5OD were added to a 100 mL, 3 necked, round bottomed flask under N_2. The flask was fitted with a water cooled condenser and an additional funnel. The reaction mixture was heated (Variac dial set at 30) and 4 mL of 40 % NaOD/D_2O was added dropwise. After the addition, the reaction was heated for 10 hours. After cooling, the reaction mixture was allowed to stir overnight at room temperature. The purple mixture was filtered and the solids were washed twice with 5 mL of C_2H_5OD. This yielded 2.0 g of a yellow solid which was used without further purification. The compound afforded the following spectroscopic data. ^1H NMR δ 1.39 (s, 36H), 5.02 (s, broad, 2H), 7.00 (s, 4H).

Galvinoxyl radical. A mixture of $K_3Fe(CN)_6$ (3.09 g), 2 mL of 40 % NaOD/D_2O, 10 mL D_2O and 62 mL d_6-benzene were combined in a 250 mL, 2 necked, round bottomed flask fitted with an addition funnel and a water cooled condenser under N_2. A solution of 4,4'-methylene bis(2,6-di-tert-butylphenol) (1.09 g, 0.0026 mol) in 15 mL d_6-benzene was added dropwise over a period of 30 minutes. As the precursor was added, the mixture went from yellow to reddish brown. The solution was stirred for 1 hour. The water layer was separated from the organic layer. and the latter was washed with water until the water layer remained clear. The organic layer was dried over $MgSO_4$ and the solvent removed *in vacuo*. The bluish purple solids were recrystallized from 100% ethanol to gave 0.70 g of the desired product (64% yield). M.P. 155 - 156 °C. The ESR of the compound was taken.

Chapter 5

Solid-Liquid Intermolecular Transfer (SLIT) DNP Flow Transfer Studies Utilizing Taxol

Results and Discussion

As mentioned in the introduction of Chapter 3, most of the previous static DNP studies used relatively low magnetic fields (e.g. 0.005 - 1.4 T) because of technical and phenomenological difficulties [2,3,39-41]. Several groups have suggested the possibility of polarizing a bolus in low magnetic fields, but monitoring the enhanced magnetization at high magnetic fields [40,80]. An obvious advantage of this approach is the increased chemical shift dispersion achievable at the higher magnetic fields for DNP-enhanced signals. Also, the experiment has a sensitivity advantage in comparison with the low field DNP experiment. The obvious extension of the SLIT or LLIT DNP experiments is to flow the polarized sample from the low magnetic field into the high magnetic field.

Dorn et al. [74] have demonstrated the feasibility of flow transfer from low to high magnetic fields. The low to high magnetic field flow experiments were performed with the instrumentation schematically illustrated in Figure 3.7. In the low to high magnetic field SLIT DNP transfer experiment, the observed magnetization for a flowing bolus at the high magnetic field detector is crucially dependent on the flow rate. At very low flow rates or static conditions, the observed NMR signal is dominated by the high magnetic field thermal Boltzmann-equilibrated magnetization (M_0^H). However, at high flow rates, the high magnetic field contribution to the total magnetization decreases dramatically since the spin-lattice relaxation time (T_{1no}) is relatively long compared to the residence time (τ_c) in region C. For high flow rates, a significant fraction of the observed signal can result from the low field thermal Boltzmann magnetization (M_0^L). That is, the bolus residence time in region A (τ_a) is long relative to T_{1n}.

After leaving region A, the bolus is transferred to the high magnetic field detector (region C). For high flow rates, the bolus is transferred via region B in a time short relative to T_{1no}. In this work, a transfer time of ~ 0.5 second was achieved. Assuming T_{1no} no shorter than 3 - 5 seconds, the low field magnetization will tend to dominate the monitored magnetization at sufficiently high flow rates (e.g. 5 - 10 mL/min).

The mathematical model for the low-to-high magnetic fields transfer experiment has been developed by Tsai and Dorn [75]. Assuming τ_a, τ_b, and τ_c, are the average bolus residence times in regions A, B, and C, respectively, simplified equations 33 and 34 have been derived [75].

Since most of the systems studied using flow transfer DNP have been small molecules (e.g. benzene, $CHCl_3$), it was important to establish the validity of the approach for more complex molecules. Specifically, could DNP enhancements even be observed for large molecules, since correlation times for large molecules increase and the condition for maximum DNP enhancement ($\omega_e\tau_c \ll 1$) is not readily fulfilled. In addition, the question of whether there would be different enhancements occur at different sites in a complex molecule would also be answered. To this end, a joint study with D.G.I. Kingston utilizing taxol as a substrate was undertaken.

Taxol is a novel diterpenoid isolated from the Pacific yew, **Taxus brevifolia**. Wani et al. isolated taxol from the stem bark of the Pacific yew in 1971 [4]. Taxol shows considerable antileukemic and tumor inhibitory properties. It was the first taxane ring containing compound which has shown such activity. The structure of taxol is shown below:

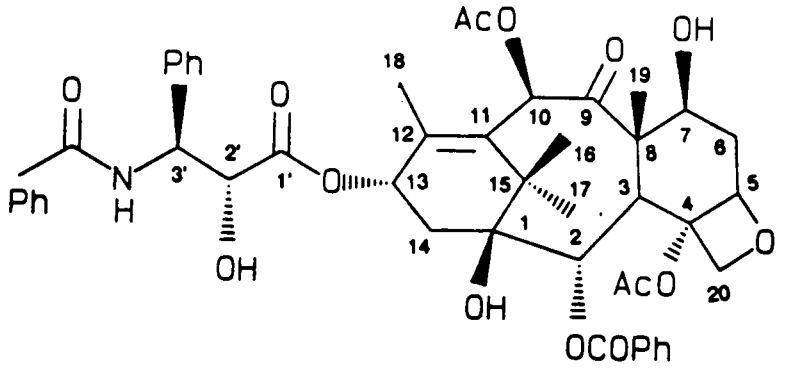

It has a molecular weight of 854 g/mole.

This chapter will discuss the ^1H DNP enhancements obtained for taxol using the SLIT DNP transfer experiment.

The taxol sample was kindly provided by Dr. Kingston. The sample was purified using flash chromatography, followed by recrystallization from ethyl acetate/hexanes, and finally another chromatography to remove solvent impurities. The ^1H DNP enhancement data were acquired using 0.5 g of taxol in 20 mL of $CDCl_3$. Figure 5.1 illustrates the 270 MHz ^1H NMR of the purified taxol. The doublet at 3.6 ppm is due to an impurity. The ^1H NMR T_1s of taxol were measured. The pulse sequence used was the inversion recovery pulse sequence. Figure 5.2 is the static 200 MHz ^1H NMR spectrum in the flow transfer system. Obviously resolution is not as good as with the spinning sample, but most peaks can be distinguished. The NMR detector volume of this sample was 20 μL. At a flow rate of 9.0 mL/min the 200 MHz ^1H NMR spectrum is illustrated in Figure 5.3. The resolution is not as good as with the static sample but again most of the peaks are distinguishable. The resolution of this spectrum is between 5 - 10 Hz. Results obtained when the microwave source was turned on and DNP enhancements were measured (the ^1H DNP spectrum

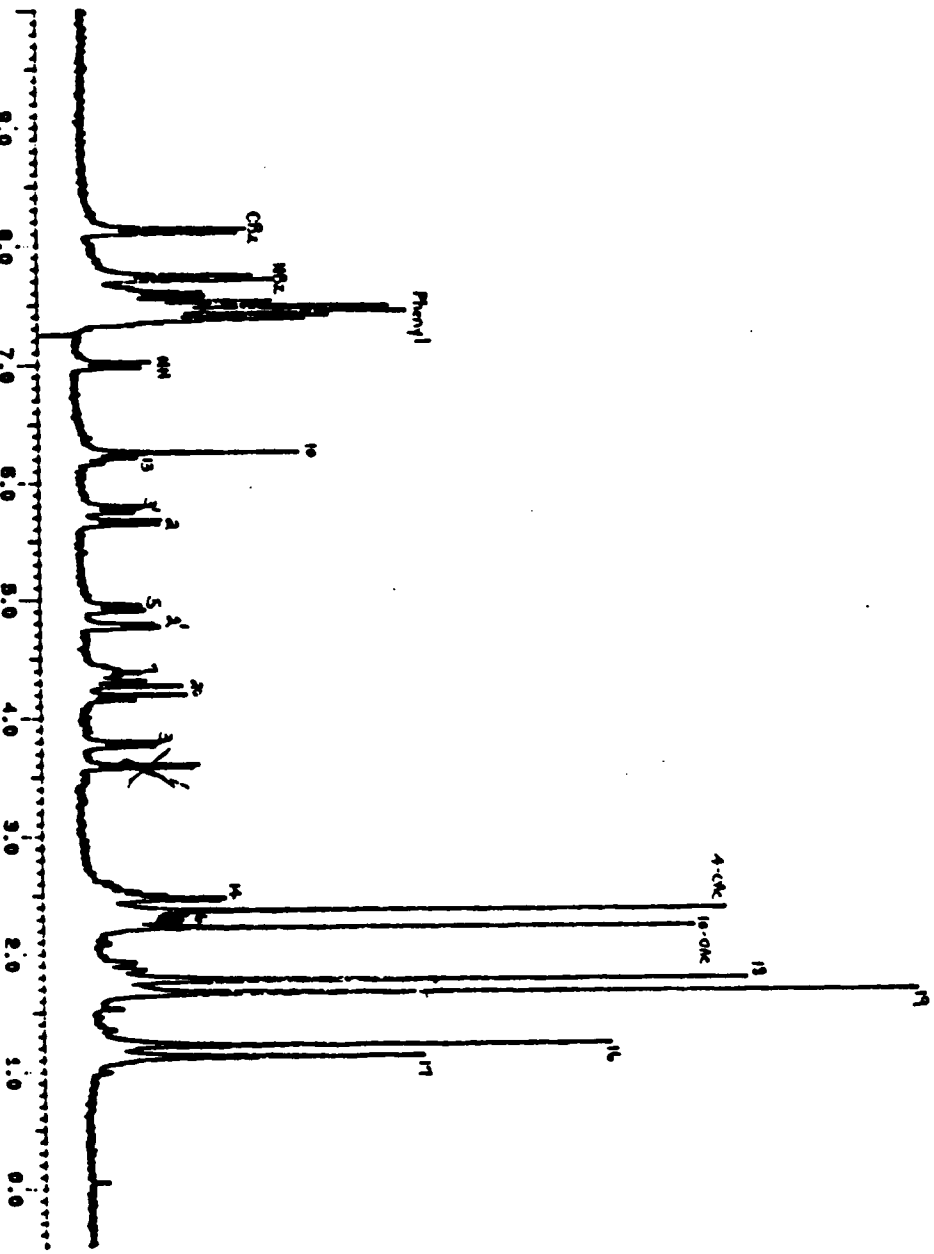

Figure 5.1 The 270 MHz ^1H NMR spectrum for taxol.

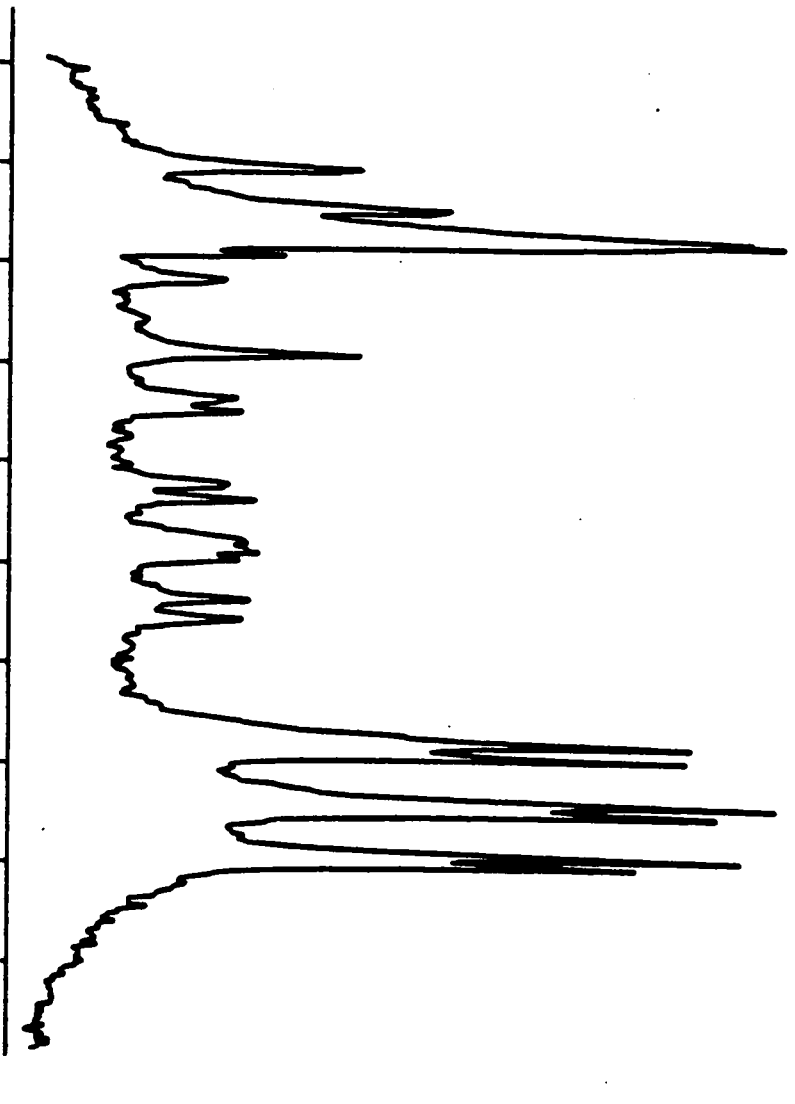

Figure 5.2 The static 200 MHz ^1H NMR spectrum for taxol.

Figure 5.3 The flow 200 MHz ^{1}H NMR signals for taxol.

for a flow rate of 9.0 mL/min) are shown in Figure 5.4. Several interesting observations are seen in this figure. The two acetoxy hydrogens (at 2.2 ppm and 2.4 ppm) clearly exhibit different DNP enhancements. The peak at 2.2 ppm (10-acetoxy) has a larger DNP enhancement than the peak at 2.4 ppm (4-acetoxy), even though they have very similar ^1H relaxation times (see Table 5.1). This would indicate that one acetoxy group is more accessible to the silica gel nitroxide spin label. Another interesting observation is that all of the phenyl groups have relatively large enhancements which suggest greater contact with the immobilized nitroxide radicals. The possible interaction of the taxol molecule with the immobilized nitroxide radicals is illustrated in Figure 5.5.

A typical plot of how the observed enhancements are obtained is given in Figure 5.6. The peaks monitored for Figure 5.6 are the methyl hydrogens at C-16, C-18 and C-19, the acetoxy hydrogens at C-4 and C-10, and all of the aromatic hydrogens. The method used in obtaining observed enhancements involves the use of a variation of equation 34. This equation can be rewritten in a form to incorporate the volumes of each region and the flow rate. In the flow transfer experiments, τ_a, τ_b, and τ_c are equal to v_a/F, v_b/F, and v_c/F respectively, where F is the flow rate and v_a, v_b, and v_c are the volumes in regions A, B, and C respectively. Therefore, equation 34 can be rewritten as

$$\frac{\langle M_Z^{DNP}\rangle - \langle M_Z^{HL}\rangle}{\langle M_0^H\rangle} = \frac{A\left(1 - e^{-v_a / F T_1}\right) e^{-(\tau_b + \tau_c) / F T_1}}{K} \qquad (35)$$

At low flow rate, $v_a/F \gg T_1$ (magnetization is fully built up) and $E_{1a} = 0$. Equation 35 then reduces to:

$$\frac{\langle M_Z^{DNP}\rangle - \langle M_Z^{HL}\rangle}{\langle M_0^H\rangle} = \frac{A\, e^{-(\tau_b + \tau_c) / F T_1}}{K} \qquad (36)$$

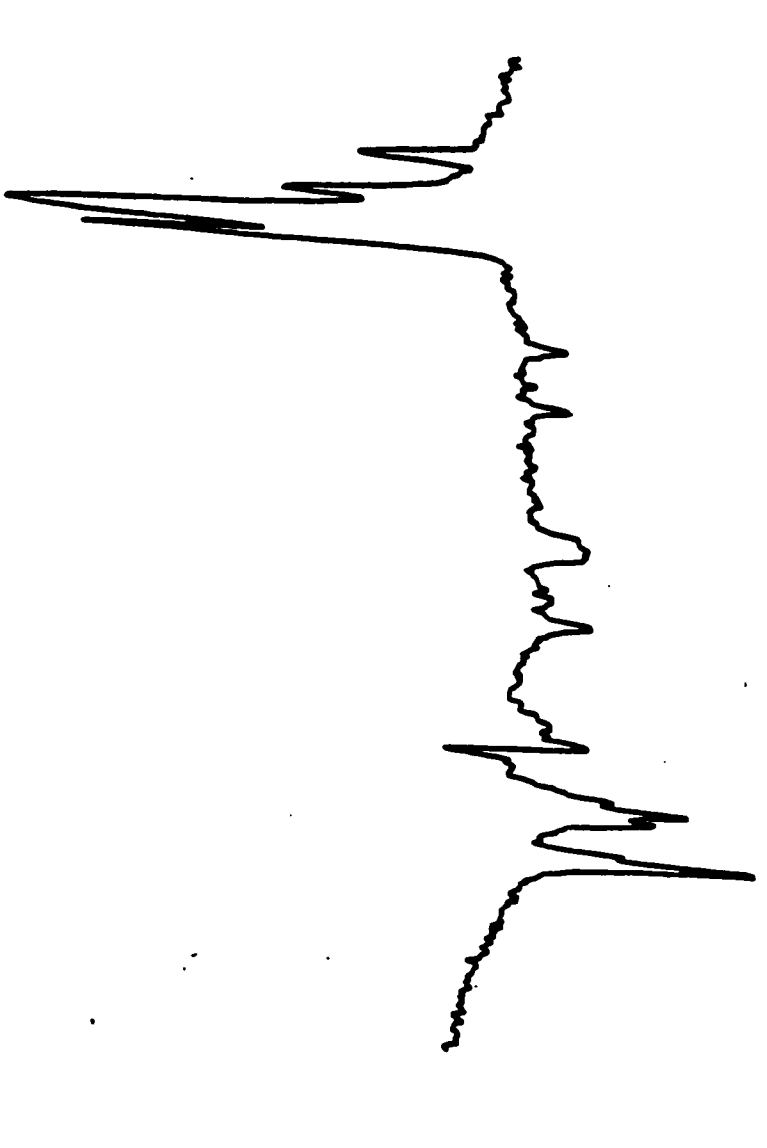

Figure 5.4 The flow SLIT ^1H DNP for taxol.

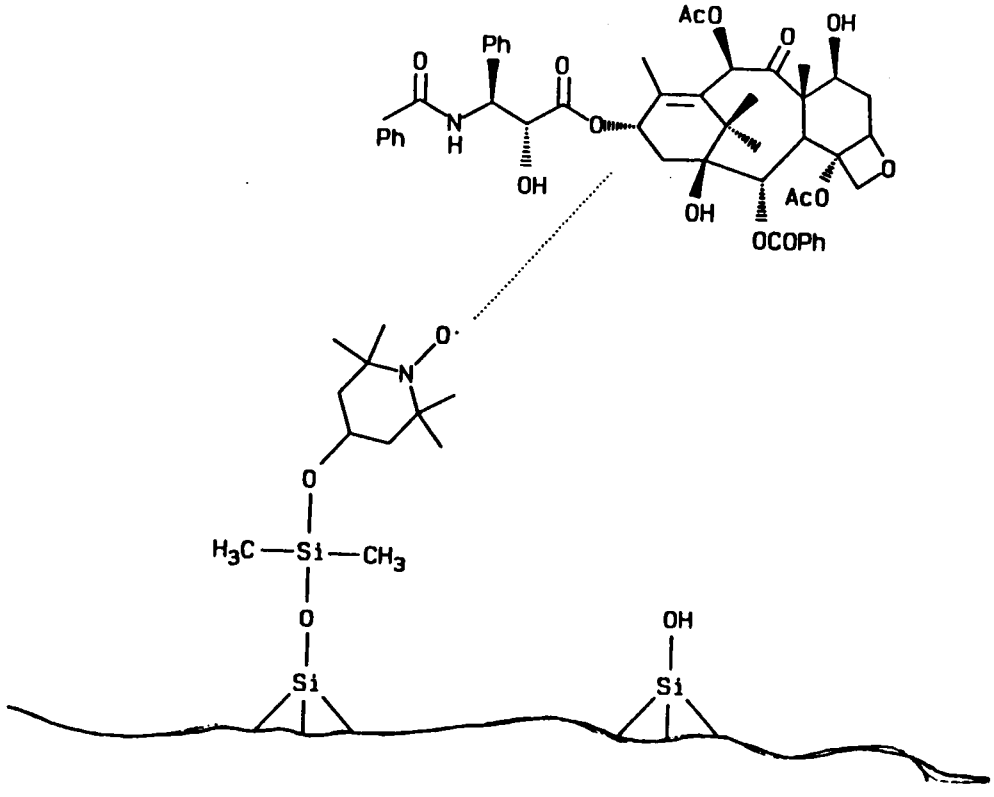

Figure 5.5 The possible surface interaction between taxol and immobilized nitroxide radicals.

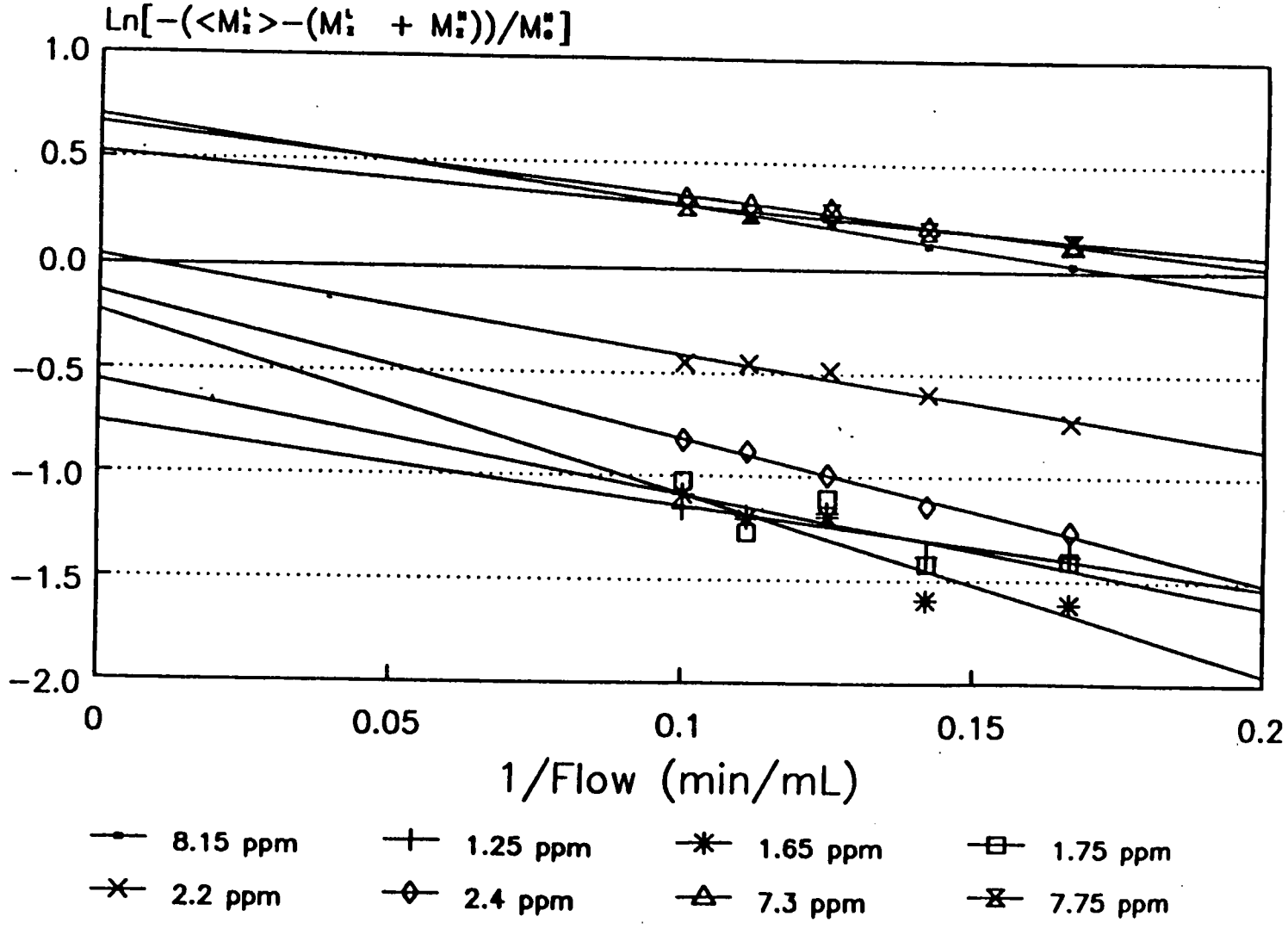

Figure 5.6 The observed enhancements vs. 1/flow plot for taxol.

Table 5.1 SLIT ^1H DNP Enhancements and Relaxation Data For Taxol

Hydrogen Number (types)	T_1 (seconds) (@ 4.7 T)	$(A/M_0^H)^a$	$A\infty^b$
2	0.24		
3	0.36		
4-OAc	0.50	-0.57	-14
5	0.65		
6	0.21		
7	0.17		
10	0.30		
10-OAc	0.58	-1.0	-29
13	0.38		
14	0.54		
16	0.36	-1.9	
17	0.13	-2.0	
18	0.45	-0.88	-20
19	0.69	-1.7	
20	0.17		
2'	0.60		
3'	0.50		
NH	0.41		
Phenyl	1.25	-0.8	-17
NBz	1.29	-0.47	-10
OBz	1.10	-0.6	-13
$CHCl_3$		-2.1	-48

a) These values are referenced to the high field magnetization (M^H) and corrected for relaxation losses. However, they are not corrected for saturation (s) and leakage factor (f).

b) $A\infty$ values are corrected for saturation (s = 1), leakage factor (f = 1), and referenced to M^L (x 14.4). Estimated error is ~ 25%. $A\infty$ for benzene is 69.

Taking the natural logarithm of equation 36,

$$\ln \frac{\langle M_Z^{DNP}\rangle - \langle M_Z^{HL}\rangle}{\langle M_0^{H}\rangle} = \ln\,(A/K) - 1/F\,(v_a + v_b / T_1) \qquad (37)$$

Therefore a plot of ln ($[\langle M_Z^{HL}\rangle - \langle M_Z^{HL}\rangle]/\langle M_0^{HL}\rangle$) vs. 1/F at low flow rates, usually below 5.0 mL/min, would yield a straight line with an intercept of to ln (A/K). Since K is a known value, A can be determined. The A determined by this method has not been corrected for saturation or leakage. Table 5.1 summarizes the ^1H T_1s for taxol, their observed enhancements, and extrapolated enhancements. The values for $CHCl_3$ are also included since the solvent used for this system is $CDCl_3$, therefore, the residual $CHCl_3$ peak can be observed in this system. One important observation from Table 5.1 needs to be noted. Even though the molecular weight of taxol is 7 times greater than that of $CHCl_3$, the ^1H DNP enhancements are not much smaller than for $CHCl_3$. In the most favorable case, the difference is -30 vs. -48. This indicates that the size of the molecule will likely not play an important role in determining the ultimate enhancements obtained using the flow transfer system. This observation is important, in that presumably $CHCl_3$ being a smaller molecule can access the immobilized nitroxide radical much more efficiently than the taxol molecule, but the ultimate enhancements for $CHCl_3$ and taxol indicate this does not occur. This means that there are selective ^1H DNP enhancements between the taxol molecule and the stationary surface. Another interesting observation from Table 5.1 is that the relaxation times for most of the hydrogens excluding the aromatics were all very similar (0.13 to 0.69) but the enhancements were different. This also indicates that there are selective ^1H DNP enhancements occurring for taxol with the immobilized nitroxide radical. From this study, several conclusions can be drawn. First, relatively large dipolar ^1H DNP enhancements are observable. Second, with the present apparatus, ^1H DNP enhancements can be monitored with T_1s as short as ~ 0.3 second (for SLIT experiments) with resolution of 5 - 10 Hz. Third, there seems to be selective ^1H

DNP enhancements for taxol at the "nonpolar" (benzyl and phenyl) region of the molecule with the immobilized nitroxide radicals. However, there is also steric accessibility at the taxol/nitroxide radical interface. This can be seen for the C-10 and C-4 acetoxy hydrogens, where C-10 acetoxy hydrogens have higher ^{1}H DNP enhancement than the C-4 analogs. Previous studies [82] indicate that the C-10 acetoxy group is also more readily hydrolyzed. However, this could be due to factors different than those observed in the present study. In any case, X-ray structural data for taxol would help confirm (or refute) the proposed structural inferences obtained form this study.

Experimental

Purification of Taxol. The column used for first flash chromatography was 6 cm in diameter and contained silica gel (Kieselgel 60, > 230 mesh) to a height of 29 cm. Solvent flow rate was 60 - 70 mL/min. A 5 g portion of sample was used. A gradient solvent system was employed (1-butanol/CH_2Cl_2). The solvent mixture went from 2% (750 mL), 3% (1350 mL), 5% (1350 mL), 7% (1875 mL), and finally 8% 1-butanol in methylene chloride. 0.70 g of pure taxol was recovered. This material was recrystallized from ethyl acetate/hexanes (0.55 g), with column chromatography ($CHCl_3$) being employed to remove any solvent impurities. The final weight of recovered taxol was 0.5 g.

DNP NMR experiments. The variable low field magnet and microwave TE_{102} cavity were part of a modified Varian E-3 EPR spectrometer. The microwave frequency (9.3 GHz) was generated in a low level klystron and amplified to ~ 4 - 10 watts using a Varian TWT amplifier to provide a B_{1e} field for the DNP experiments of 0.34 T. The high magnetic field (B_0^H) NMR detector was a JEOL FX-200 NMR spectrometer with a homebuilt flow probe. A presaturation coil was connected outside the microwave cavity. In all experiments, the liquids were deoxygenated with N_2 for at least 30 minutes prior to the start of the experiment. During the experiment N_2 is continuously bubbled through the solution to exclude oxygen. An ambient temperature of ~ 22 °C was employed in all experiments. The total volume of region A was ~ 160 μL. The transfer tubing in region B was ~ 1.5m of 0.18 mm inner diameter Teflon® tubing with an estimated transfer volume of ~ 40 μL. The volume in the high magnetic region before detection was ~ 10 μL. The active NMR volume in the detector region was ~ 20 μL. The pump employed in these experiments was a SSI Model 200 HPLC pump.

Chapter 6

Lanthanide Shift Reagent-Dynamic Nuclear Polarization Studies

Results and Discussion

From the taxol studies, it can be seen that the radical and solute in the DNP system give rise to site specific intermolecular interactions. This in turn results in different DNP enhancements for the nuclei monitored in the solute depending on the extent of interaction. From the LIS and LIR studies, structural information can be obtained through the complexation of lanthanide shift reagent with the molecule of interest (which has a nucleophilic site).

Ideally, it would be desirable to synthetically design a new reagent which would have a relatively narrow EPR signals as well as Lewis acid properties for nucleophilic site complexation (e.g., LSR's). In this manner, such a reagent would be useful for DNP studies involving specific intermolecular sites in complex molecules.

The combination of a radical (e.g. nitroxide radicals) with a metal chelating reagent in the same molecule have been proposed by many people [83]. Some representative examples are shown in Table 6.1. None have been used for DNP NMR studies. These systems have been employed for: 1) metal concentration detection by observing the ESR spectra of the molecule after it has been complexed with a solution containing the metal, 2) as spin labels for biological systems, and 3) as contrasting agent in magnetic resonance imaging (MRI) [84].

This chapter will discuss the synthesis of several radical systems, and some preliminary results of the DNP NMR studies using the combined radical-LSR systems.

Table 6.1 Compounds That Contain a Nitroxide Radical Moiety and a Chelating Functionality

Name	Structure
2,2,6,6-tetramethyl-4-(4,4,4-trifluoro-1,3-dioxobutyl)-1-piperidinyloxy	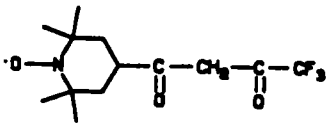
4-([3-carbonxy-1-oxo-2-propenyl] oxy)-2,2,6,6-tetramethyl-1-piperidinyloxy	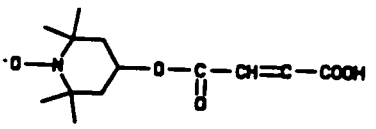
4,4'-(1,2-ethanediylidenebis-[nitrilomethylene])bis(2,2,6,6-tetramethyl-1-piperidinyloxy)	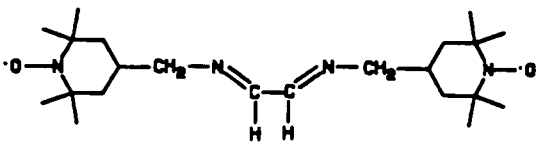
4-([aminothioxomethyl]hydrazono)-2,2,6,6-tetramethyl-1-piperidinyloxy	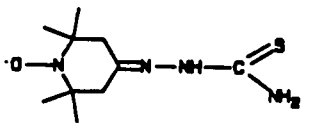
4-([dithiocarboxy]oxy)-2,2,6,6-tetramethyl-1-piperidinyloxy-potassium salt	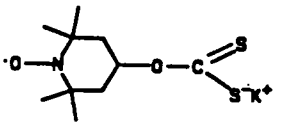

LSR-Radical Synthesis

The first radical-chelating molecule we tried to synthesize was based on the work of Sosonovsky et al [84]. He employed this system as a contrasting agent for magnetic resonance imaging (MRI). The synthesis involved heating diethylenetriamine-N,N,N',N",N"-pentaacetic(DTPA)anhydrideand4-amino-2,2,6,6-tetramethylpiperidine-1-oxyl(4-amino-TEMPO) to form the amide shown below:

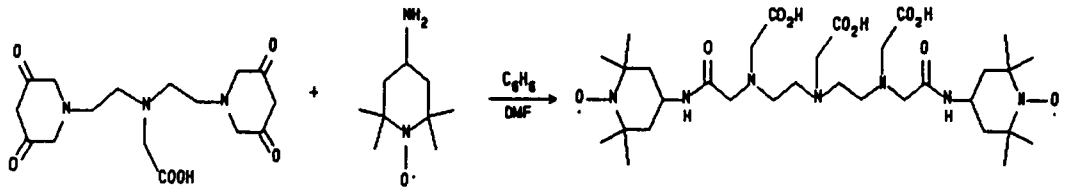

The free carboxylic acid groups were then used to chelate the desired metal, The resulting molecule would possess both free radical and metal chelating functionalities. The metals chelated with the DTPA-diradical system are Yb^{+3}, Gd^{+3}, and Cr^{+3}. The reasons that these metals were chosen are their availability and different electron relaxation times (τ_e), which we believed would be crucial to the T_{1n} observed in the DNP system. Once compounds were chelated with the metals, the corresponding ESR spectra were obtained. The spectra shown in Figures 6.1 - 6.4 also include the DTPA-diradical in the absence of metal. All ESR spectra were taken using solid samples rather than dissolved samples because these compounds are soluble only in water or water-methanol solvent systems. The ESR spectrometer used in this study cannot be used to obtain EPR spectra for solutions with high dielectric constants.

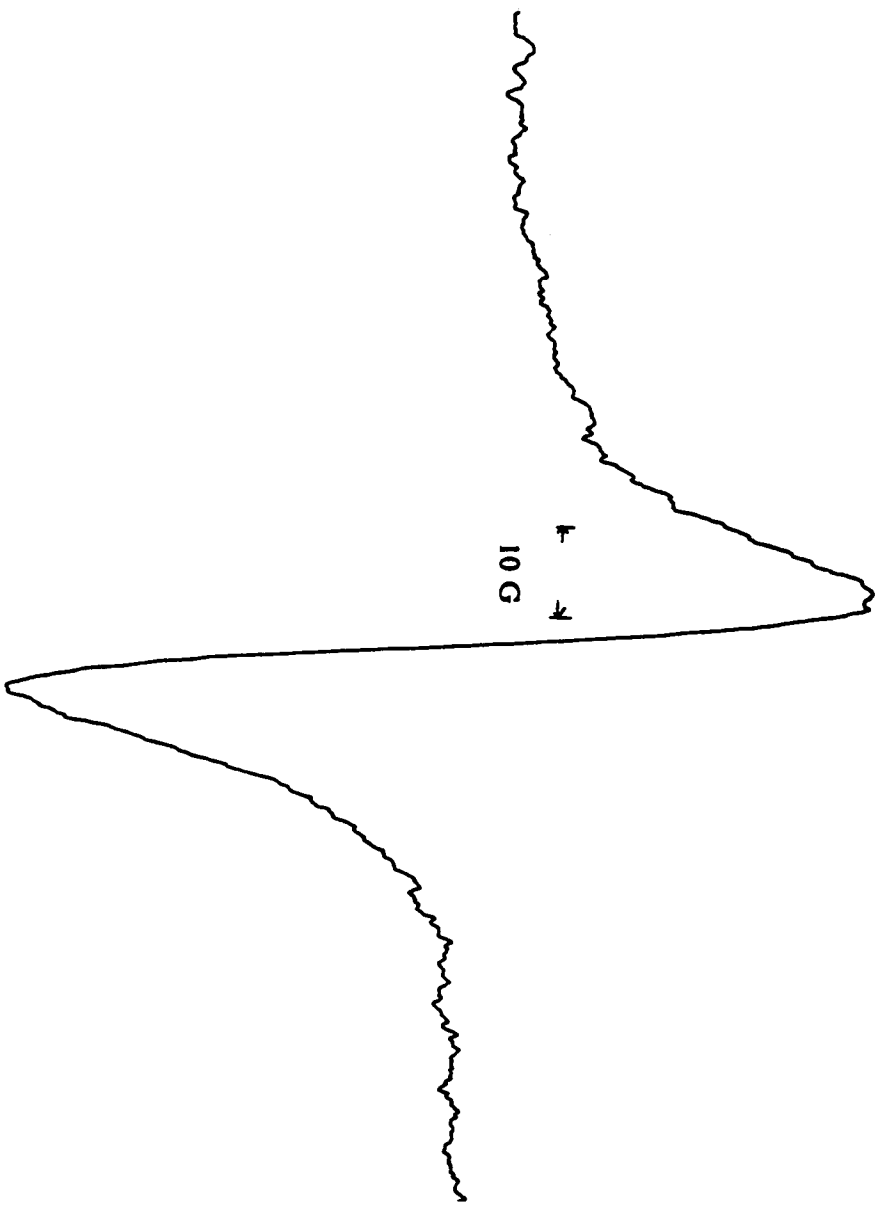

Figure 6.1 The ESR spectrum of DTPA-diradical.

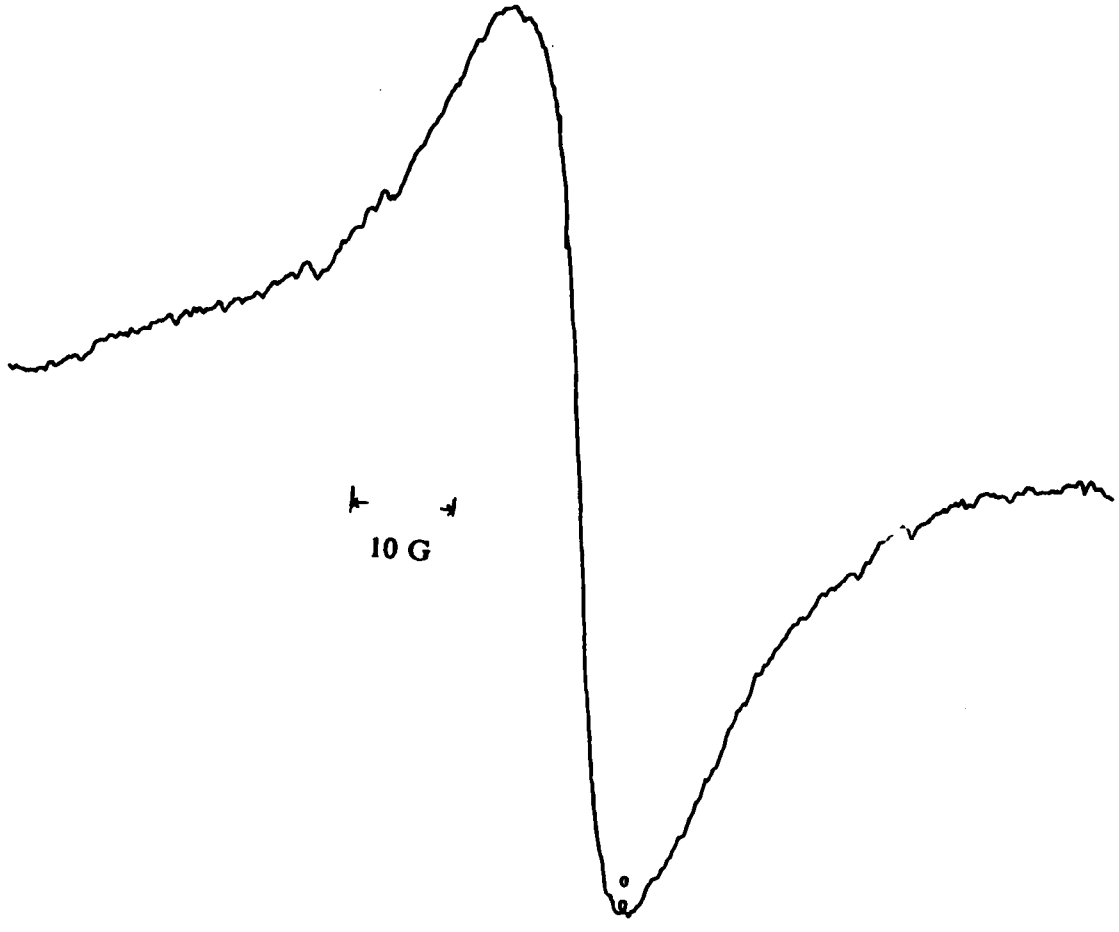

Figure 6.2 The ESR spectrum of DTPA-diradical-Yb^{+3} complex.

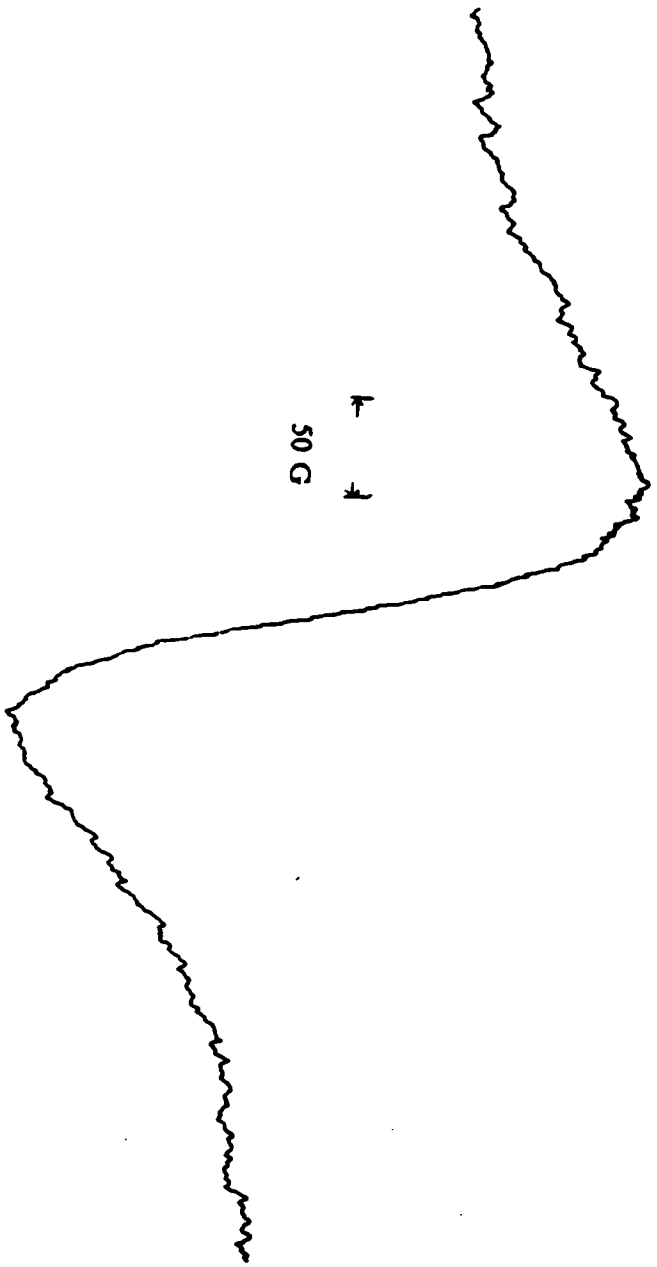

Figure 6.3 The ESR spectrum of DTPA-diradical-Cr^{+3} complex.

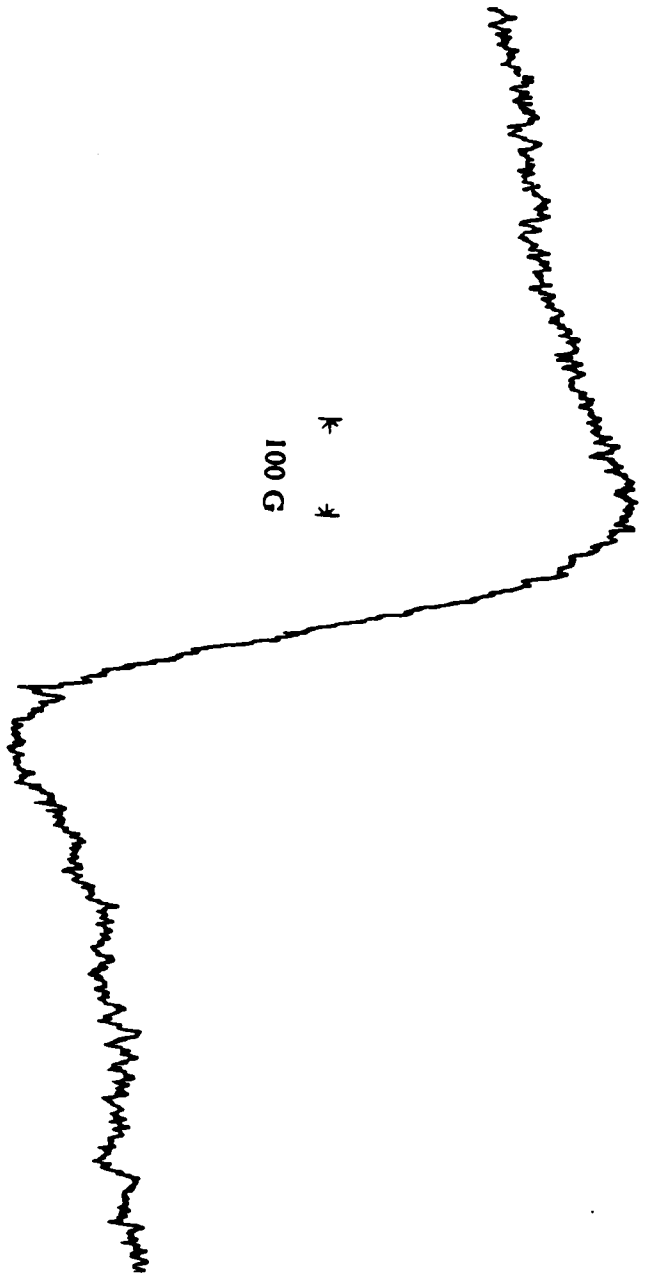

Figure 6.4 The ESR spectrum of DTPA-diradical-Gd^{+3} complex.

As can be seen, all spectra are singlets rather than triplets. This results from the usual hyperfine interactions being obscured by the metal free electron system and electron-electron interactions. The linewidth of the Yb^{+3} chelated compound is somewhat broader than the diradical without any metal. The difference becomes more dramatic with Gd^{+3} and Cr^{+3}. At first glance, the spectra look the same, but the scales are different. The line width of the ESR spectra for Gd^{+3} and Cr^{+3} chelated diradicals are more than 100 gauss. From the ESR spectra, it is obvious that for this diradical system, the Gd^{+3} and Cr^{+3} chelated diradicals are not feasible for DNP NMR experiments due to the fact that the power needed to saturate the ESR transition would be very high. The Yb^{+3} chelated diradical can probably be used, but with the present instrumentation, we cannot readily obtain DNP results because of the high dielectric constant solvents required. As stated previously, the present DNP instrumentation can only handle low dielectric constant solvents such as $CHCl_3$, CCl_4, and benzene.

Since the diradical synthesized above cannot be used for LLIT DNP studies *vide supra*, modification of this synthesis was employed in order to prepare an immobilized metal chelate-spin labelled system. In this way, a system which could be used in SLIT DNP experiments would be available. The monoradical synthesis outlined below was attempted.

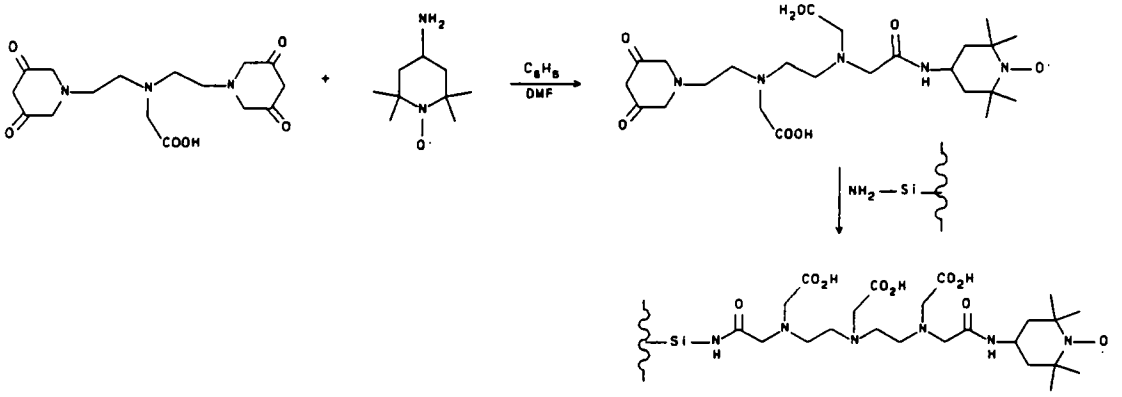

The first step of the synthesis is the same as the previous diradical synthesis except for the ratios of the starting materials. The ratio of DTPA anhydride to 4-aminoTEMPO is 1 : 1 instead of 1: 2. The resulting monoradical can then be treated with amino capped silica gel to produce an immobilized free radical. The immobilized monoradicals can then be chelated with metals. The approach failed in the first step of the reaction scheme. We were never able to prepare exclusively the monoradicals, with the reaction always giving the diradical and hydrolyzed DTPA anhydrides.

Since the immobilized monoradicals could not be obtained, we decided to physically adsorb the diradicals on to the silica gel. The diradicals without metal and Yb^{+3} chelated diradicals were physically adsorbed onto silica gel to make an immobilized system. The ESR spectra of the two compounds are shown in Figures 6.5 - 6.6. Again, the ESR spectra were obtained for solid samples. The ESR spectra of both compounds indicate that by adsorbing the radicals on the silica gel the signals become broader and which in turn makes them difficult to saturate for DNP NMR studies.

Due to the instrumental limitation alluded to earlier, we turned our attention in synthesizing a system that would be soluble in hydrocarbons (e.g., $CHCl_3$, and CCl_4). The first attempt was to chelate 4-phenacylidene-2,2,5,5-tetramethylimidazolidin-1-yloxyl (structure shown below) with the metals previously used.

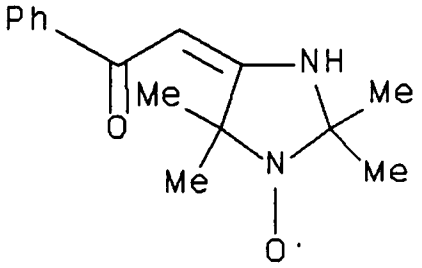

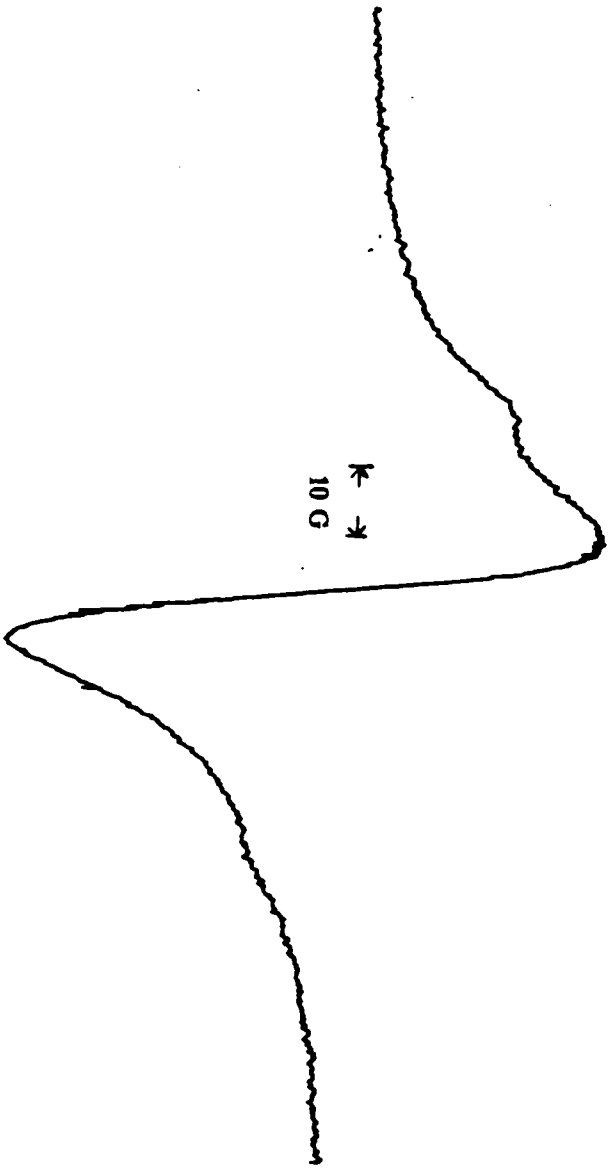

Figure 6.5 The ESR spectrum of DTPA-diradical adsorbed on silica gel.

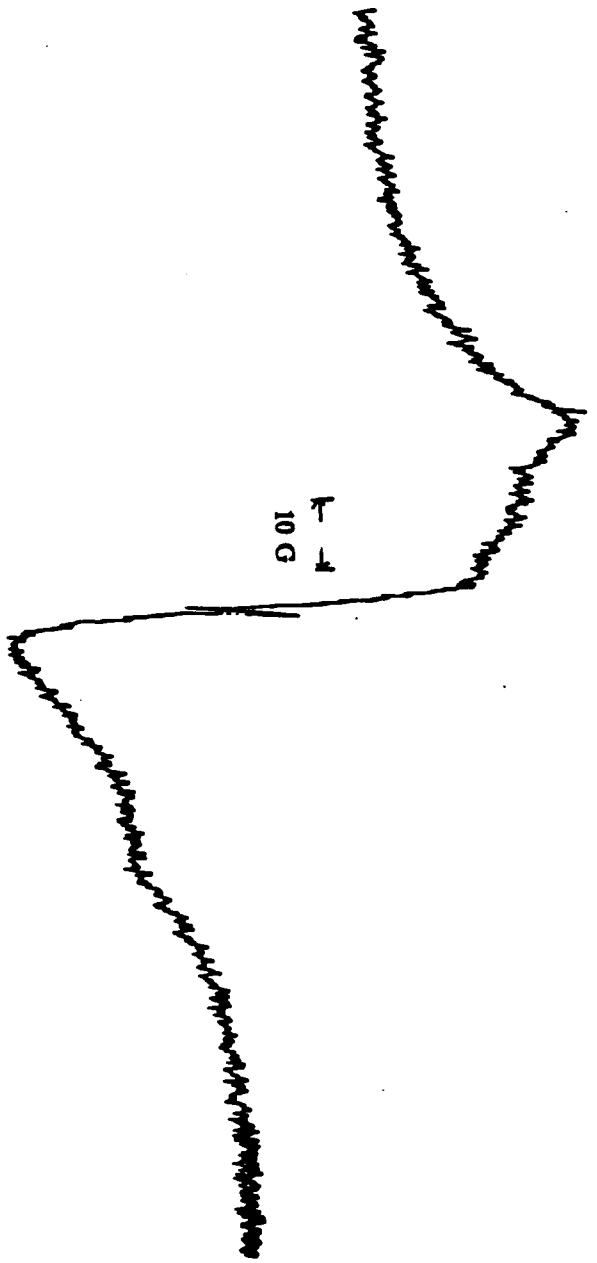

Figure 6.6 The ESR spectrum of DTPA-diradical-Yb^{+3} complex adsorbed on silica gel.

This compound was commercially available and has been used to chelate Cu^{+2}, Zn^{+2}, and Cr^{+2} [85]. Different procedures were attempted to chelate this compound. The first approach was to dissolve the chelating radical in methanol and add a slight excess of the aqueous metal solution portionwise at 60 °C. The solids that were recovered from this reaction were the starting chelating radicals with no complex being formed. The second method involved adding 1 equivalent of base to a solution of the chelating radicals and then adding the dissolved metal solution. The base was added to deprotonate the amine nitrogen and perhaps delocalize the anion's electron density to the carbonyl oxygen. Unfortunately, the solids recovered from this attempt were again the chelating radicals and metal hydroxides with no trace of the desired products. The third method used an excess of base in the chelating radical solution followed by addition of the metal solution. This method also failed. In fact, the chelating radicals were destroyed by this approach. The final attempt at chelation adapted the method developed by Fernelius and Blanch [86] for the preparation of chromium acetylacetonate. Metals chlorides were dissolved in water and heated in a boiling water bath with the chelating radicals and urea. In this way, the base is generated in situ and could react as it is formed. Again, however, no complexes were formed. Only the chelating radicals and metal hydroxides were recovered.

After the failure of chelating 4-phenacylidene-2,2,5,5-tetramethylimidazolidin-1-yloxyl, we turned our attention to the synthesis of the compound shown below: [87]

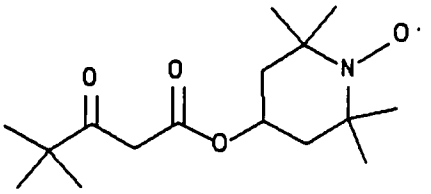

This compound contains a nitroxide radical at one end and a β-ketoester functionality which can chelate with metals at the other end. The synthesis involves first a transesterfication of methyl-4,4-dimethyl-3-oxo-pentanoate with 4-hydroxypiperidinol, followed by oxidation to the nitroxide radical and finally chelation. The overall reaction scheme is shown below.

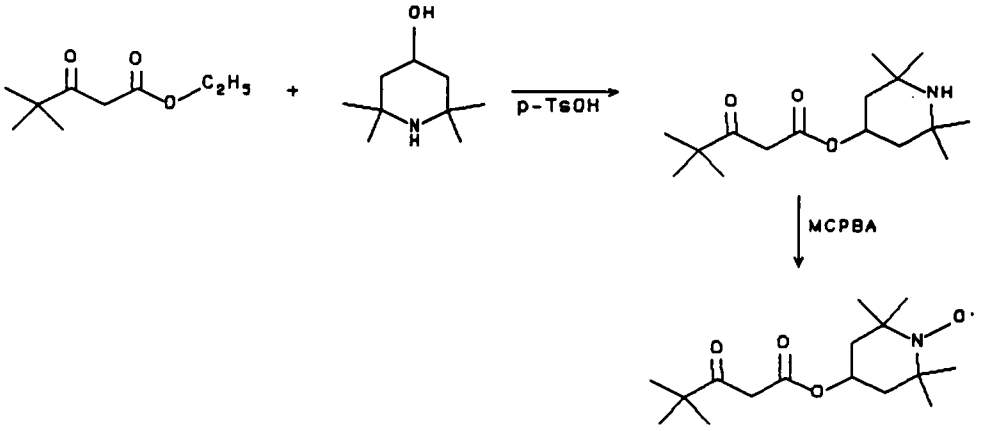

Initial attempts at the transesterfication were not successful because the p-toluenesulfonic acid was not dry. The acid was dried by refluxing in benzene over activated 3Å molecular sieves overnight. The reactants were added to the acid solution and refluxed for 10 hours over 4Å molecular sieves to remove the methanol that formed during the course of the reaction. The desired product was obtained by this method. The resulting β-ketoester was then oxidized with m-chloroperbenzoic acid to give the nitroxyl moiety. In attempts at

chelation, only Cu^{+2} chelates were formed in detectable amounts (ESR shown in Figure 6.7). The metals that were used for chelation were Zn^{+2} and Yb^{+3}. In all the attempts, only starting chelating reagent was recovered. The method used in chelating Cu^{+2} was to add portionwise the dissolved metal solution (in water, slight excess) to a basic ethanolic-water solution of the chelating reagent (pH ~ 8) at 60 °C. During the addition, the solution is kept at pH ~ 8 with additional base. The Cu^{+2}-complex is recovered by filtering the resulting mixture, dissolved in ethyl ether, and recrystallizing from heptane. For the Yb^{+3} and Zn^{+2} metal solutions, the above method was not successful. Sievers et al.'s [88] method of chelating H(fod) with metals was also tried. In this case, exactly one equivalent of base (NaOH) was added to the methanolic solution of the chelating β-ketoester, followed by dropwise addition of the metal solution (aqueous) over a period of 1 hour at room temperature. Again this method was not successful. Only the chelating β-ketoester and metal hydroxides were recovered. The reason chelation did not occur well with these metals might be due to the difference in the pKa's of the β-ketoester and β-diketone. Most of the shift (or relaxation) reagents contain the β-diketone moiety, which has a pKa of ~ 8. The pKa of a β-ketoester is ~ 11. This means that the methylene protons in β-diketone are more easily removed than in the β-ketoester, therefore chelation occurs more smoothly for β-diketones. By the same token, β-ketoesters under the same conditions, do not chelate as smoothly. When the metal solution is added, apparently the metals react with the free OH^- ion and form only metal hydroxides instead of the desired β-ketoester chelates. Under more basic conditions, the β-ketoester will hydrolyze.

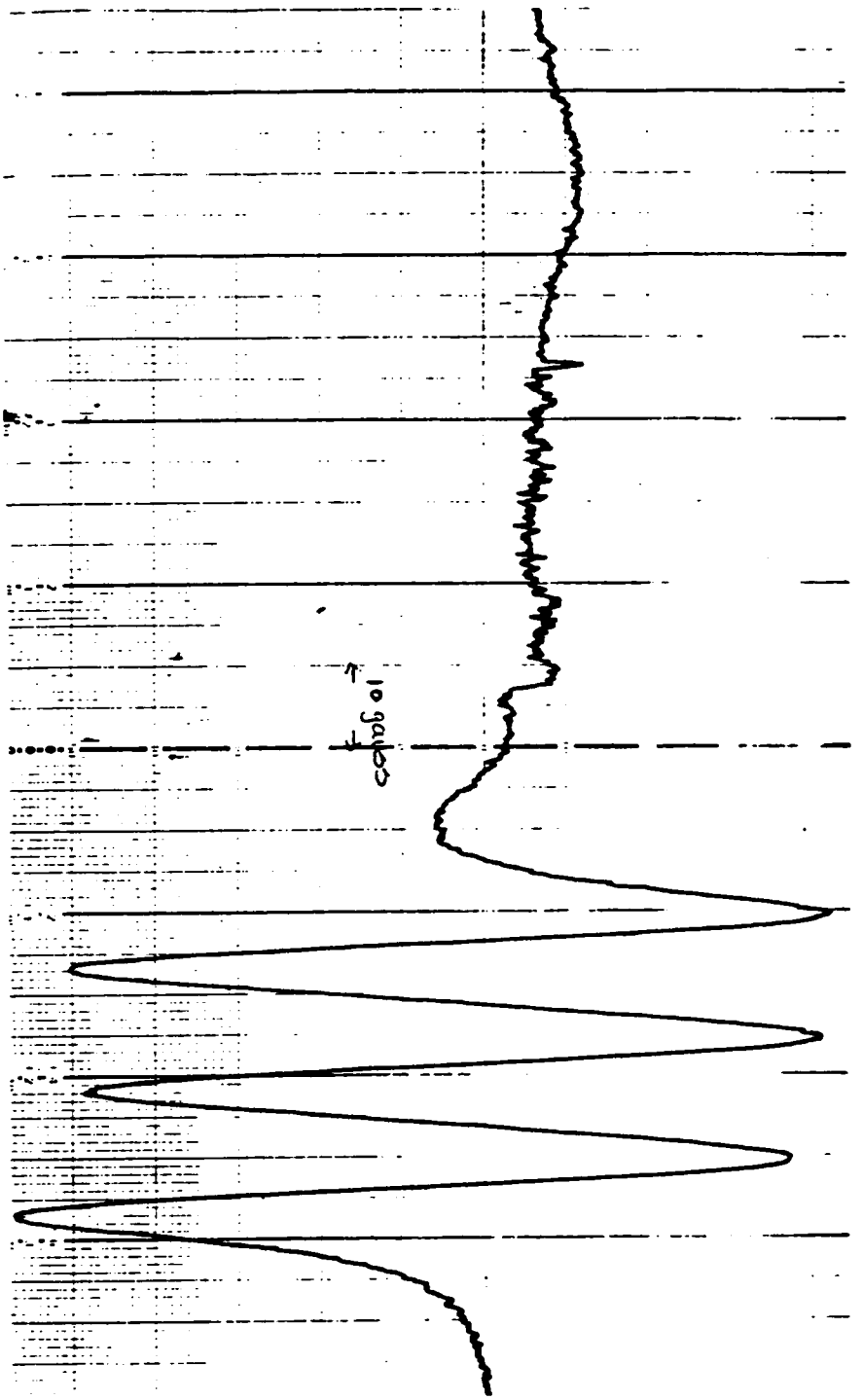

Figure 6.7 The ESR spectrum of Cu^{+2}-2,2,6,6-tetramethyl-4-piperidinyl, 4,4-dimethyl-3-oxo-pentanoate complex in heptane.

Section 2: LSR-DNP Enhancement Studies

After these several attempts, we had in hand only one compound with an intramolecular nitroxide radical and metal chelate system. In the taxol studies, we observed selective DNP enhancements with the nitroxide radicals. We decided to monitor the intermolecular nitroxide radical-LSR interaction for the DNP NMR studies. Specifically, can the intermolecular nitroxide radical-LSR interaction selectively destroy or enhance the observed DNP enhancements at the nucleophilic site.

For the DNP NMR experiments, the LLIT DNP transfer system was employed. The instrumentation was exactly the same as in the the SLIT DNP transfer experiment except the radicals were dissolved in a solvent instead of being immobilized on silica gel. 4,6-Dimethyl-2-methoxyacetophenone (4) was the compound monitored. This compound was used because we have previously acquired LIS data, and the acetyl functionality can complex with the lanthanide shift reagents. First, DNP enhancements of compound 4 over different nitroxide radical (4-hydroxy-TEMPO) concentrations were measured without LSR at different flow rates. The concentrations was used were 1×10^{-3} , 2.5×10^{-3} , 3.5×10^{-3} , and 5×10^{-3} M. Compound 4 has six ^{1}H NMR signals, and their T_1s were measured before radical was added. The T_1s for the 6 signals at the four concentrations were also measured. All of the measured T_1s are shown in Table 6.2. From Table 6.2 it can be seen that the T_1s are not long for the compound without any radical present and as more and more radical is added, the T_1s become very short. This reduces the overall ^{1}H DNP enhancements for these 6 signals because in the LLIT ^{1}H DNP transfer experiment, transfer time is dependent on T_{1n}. If T_{1n} is short then the transfer time for the present system might not be rapid enough resulting in most of the magnetization of the flowing bolus being lost during transfer. For this reason, the observed ^{1}H DNP enhancements were very small. A typical plot of observed enhancements vs. 1/flow rate at different concentrations at 3.80 ppm (methoxy hydrogens) is shown in Figure 6.8

Table 6.2 T_1s[a] for Compound 4 as a Function of Added Radical Concentration

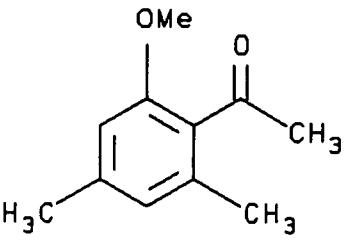

Concentration (M)	PPM 2.21	2.31	2.47	3.80	6.60	6.62
0	2.9	2.9	3.9	2.3	3.9	3.9
1.0×10^{-3}	2.2	2.2	2.6	1.4	3.6	3.6
2.5×10^{-3}	1.4	1.4	1.4	0.9	1.4	1.4
3.5×10^{-3}	1.2	1.2	1.2	0.8	1.2	1.2
5.0×10^{-3}	0.9	0.9	1.0	0.7	0.9	0.9

a) The unit for the T_1s is in seconds, and the experimental error for all the measured T_1s is ± 0.1

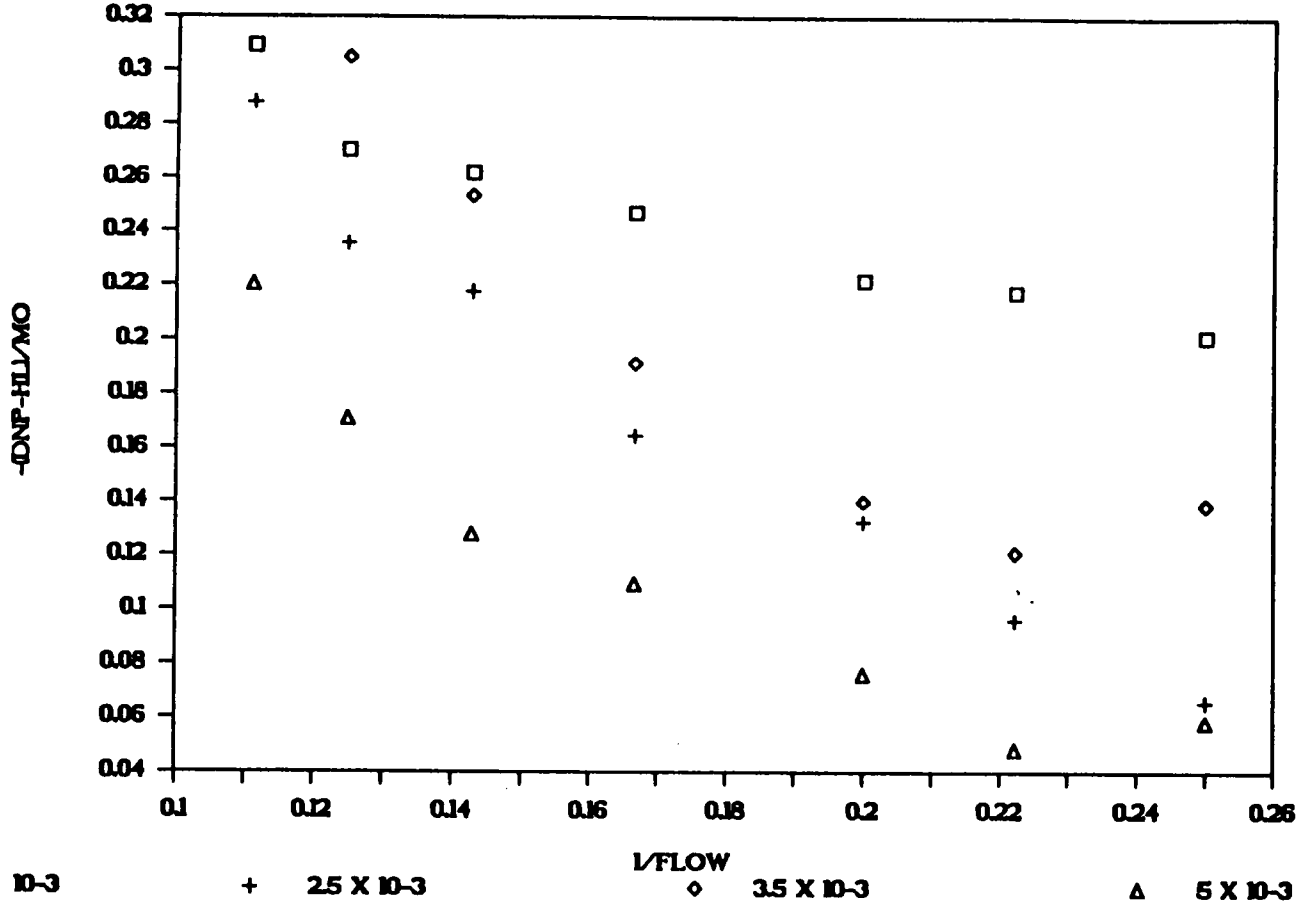

Figure 6.8 The observed ^{1}H DNP enhancements at 3.80 PPM vs. 1/flow plot of 4,6-dimethyl-2-methoxyacetophenone for different nitroxide radical concentrations.

The observed enhancements without correction for saturation and leakage are fairly low (on the order of 0.1 - 0.2). The observable ^1H DNP enhancements can only be observed at a flow rate of 4.0 mL/min or higher. Due to the fact that T_1s are so short, most of the magnetization is lost during transfer, and DNP enhancements cannot be observed at low flow rates making it impossible to extrapolate A_∞ for any of the 6 signals. Even though the T_1s for taxol were similar to compound 4 (some were even shorter), the DNP enhancements were higher because the SLIT ^1H DNP transfer experiment was used instead of the LLIT ^1H DNP experiment. This illustrates the advantage SLIT DNP transfer system has over the LLIT DNP transfer system. Since A_∞ were not obtained for the molecule, only qualitative conclusions can be made when LSR's are added to the radical-compound 4 solutions.

For the intermolecular LSR-nitroxide radical DNP studies, the concentration we chose to use was 2.5×10^{-3} M. We chose this concentration because that the T_1s are not too short and some DNP enhancement can be observed for most of the flow rates. For the Cu-intramolecular complex the concentration of the solution was 1.25×10^{-3} M because the T_1s at this concentration are the same as for the 2.5×10^{-3} M solution. The LSRs used for this study were $La(thd)_3$, $Yb(thd)_3$, and $Eu(thd)_3$. Again, they were chosen for their different electron relaxation times. The electron relaxation time for Yb^{+3} is on the order of 10^{-13} seconds and for Eu^{+3} is 10^{-10} seconds [25]. La^{+3} does not have a electron relaxation time because it is diamagnetic. When equal molar amounts of LSRs (with respect to the radical concentration) were added to the nitroxide containing solution, the T_1s did not change within experimental error for any of the signals. This was somewhat surprising. We expected no change in T_1s when $La(thd)_3$ was added because it is a diamagnetic molecule. For $Yb(thd)_3$ and $Eu(thd)_3$, however, we expected changes in T_1s at least for $Eu(thd)_3$ due to the fact that its electron relaxation time falls above the spectral density region where the condition $\omega_e\tau_c \ll 1$ is met. The electron relaxation time for the nitroxide radicals is on the order of 10^{-6} to 10^{-7} seconds. This may indicate that the observed enhancements for these systems should be

similar to the system without the metals added. The plots of observed enhancements vs. 1/flow rate for the four metal containing solutions and one solution without metal for the 6 signals of the molecule monitored are shown in Figures 6.9 - 6.14. Several observations can be drawn from these figures. First, the Cu^{+2}-intramolecular complex is not a good radical to use for DNP NMR studies. The observed enhancement is almost non-existent for the Cu^{+2}-complex and falls off rapidly for the entire signal. This is probably due to the electron-electron interaction between Cu^{+2} (electron relaxation time 10^{-7} s.) and the nitroxide electron. This interaction is apparently made more efficient when the Cu^{+2} and the nitroxide radical are in the same molecule. Another observation from the figures that is interesting concerns the $Yb(thd)_3$ enhancements. For the signals that are closer to the complexation site, the signals at 2.47 PPM (the methyl hydrogens adjacent to the carbonyl functionality) and at 3.80 PPM (the methoxy hydrogens), the enhancements are lowered as compared to the other systems excluding the Cu^{+2}-complex. This seems to indicate that the Yb^{+3} metal can selectively destroy enhancements at the complexation site. This type of interaction was not observed for Eu^{+3} or La^{+3} systems. Another effect that was observed for Yb^{+3} system and not for La^{+3} and Eu^{+3} systems is illustrated in Figure 6.15. This figure shows the ^1H NMR spectra for the molecule at 2.5 x 10^{-3}M of nitroxide radical without any metal and with Yb^{+3}, La^{+3} and Eu^{+3} metals are plotted out. Only the Yb^{+3} containing system exhibits a shift in the signals where complexation is occurring (at 2.47 PPM and 3.80 PPM). This preliminary studies of nitroxide radical-LSR intermolecular system seems to indicate that the Yb^{+3} containing system might show promise in selectively destroying enhancements at the complexation sites and in exhibiting lanthanide induced shifts.

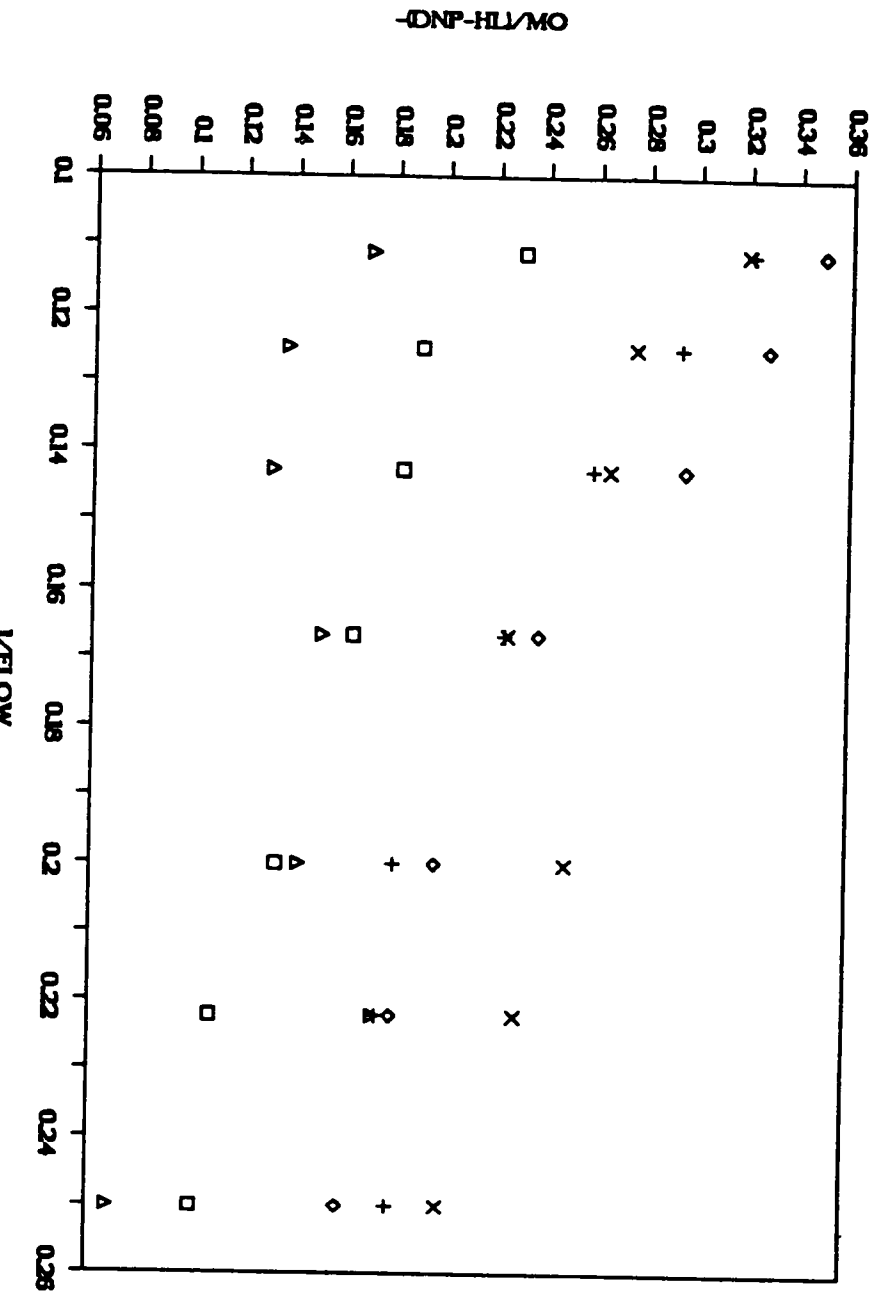

Figure 6.9 The observed ^1H DNP enhancements at 2.21 PPM vs. 1/flow plot of 4,6-dimethyl-2-methoxyacetophenone for different added LSR and Copper complex.

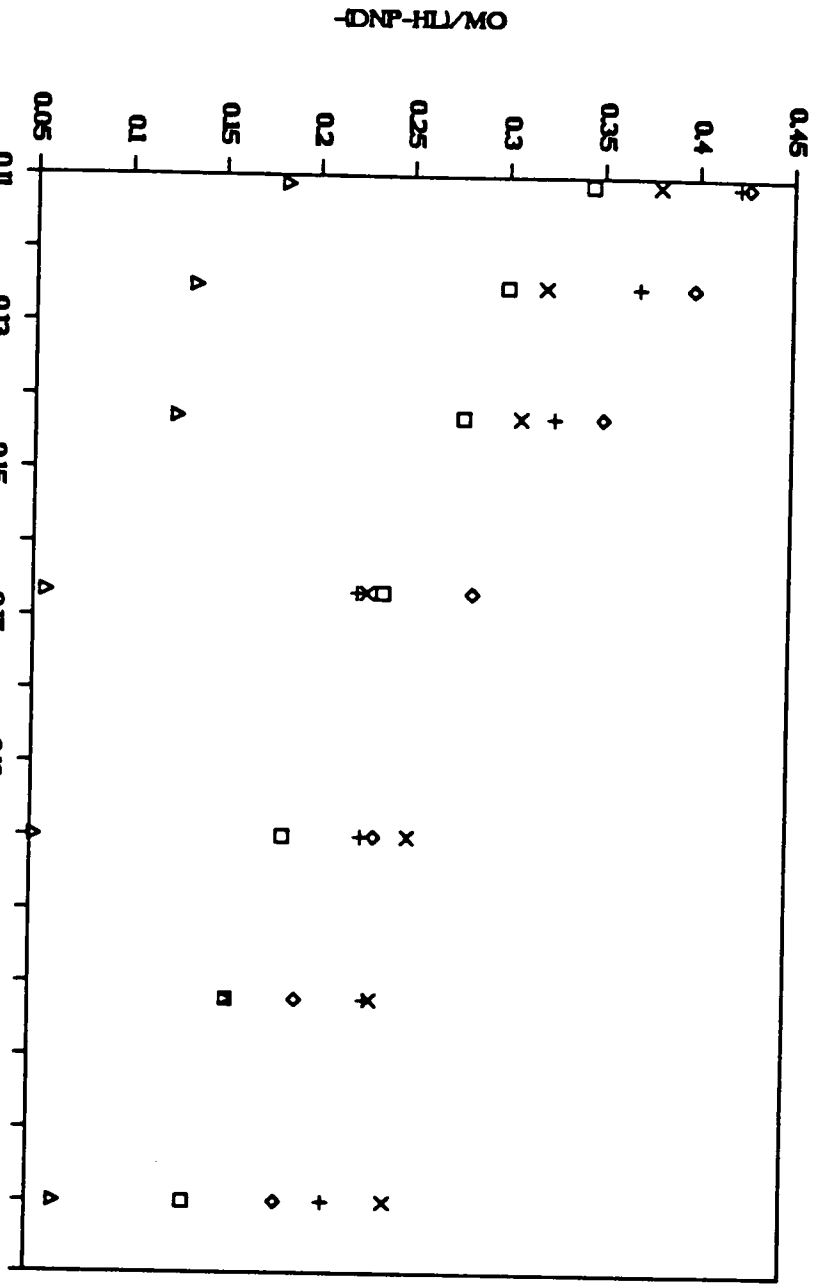

Figure 6.10 The observed ^{1}H DNP enhancements at 2.31 PPM vs. 1/flow plot of 4,6-dimethyl-2-methoxyacetophenone for different added LSR and Copper complex.

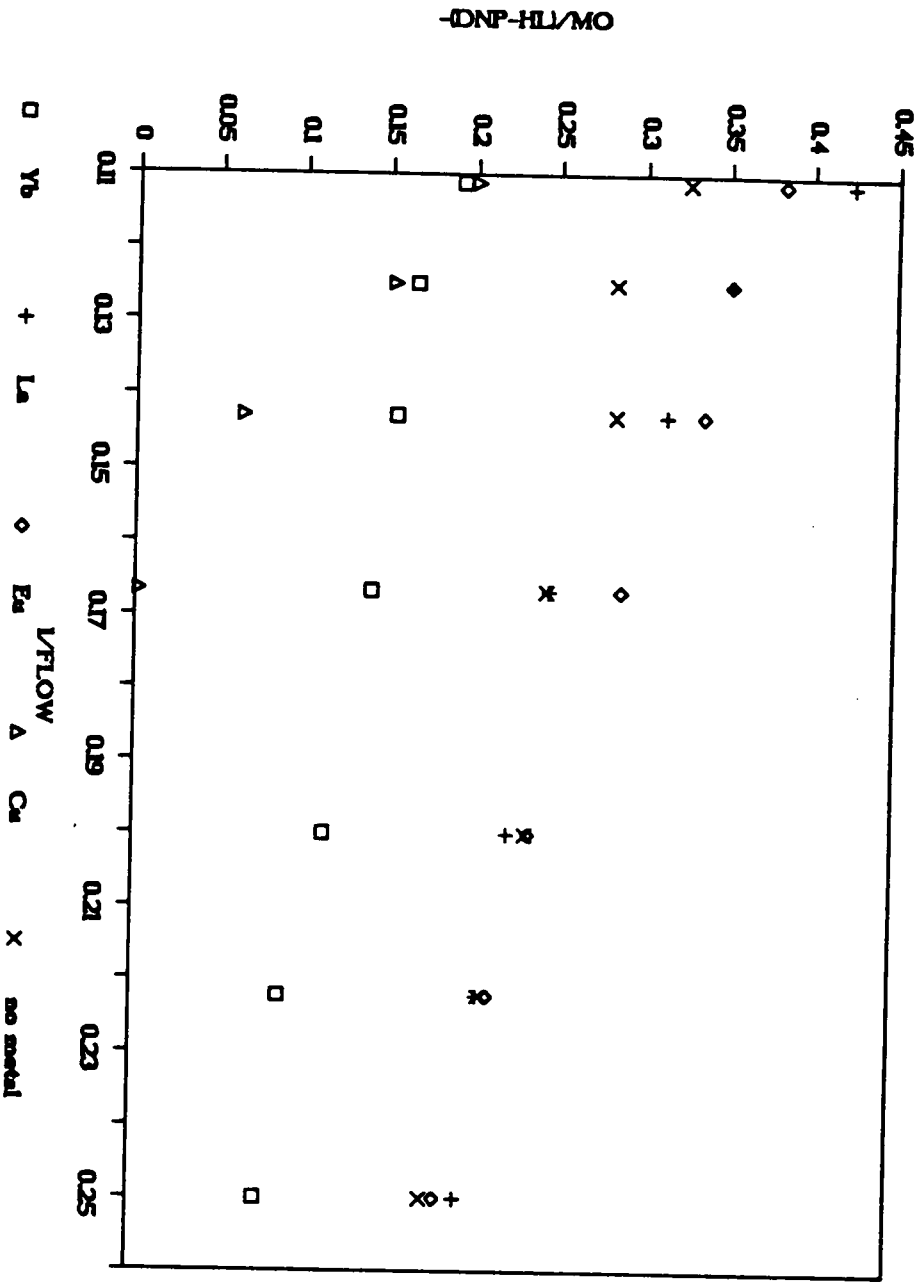

Figure 6.11 The observed ^1H DNP enhancements at 2.47 PPM vs. 1/flow plot of 4,6-dimethyl-2-methoxyacetophenone for different added LSR and Copper complex.

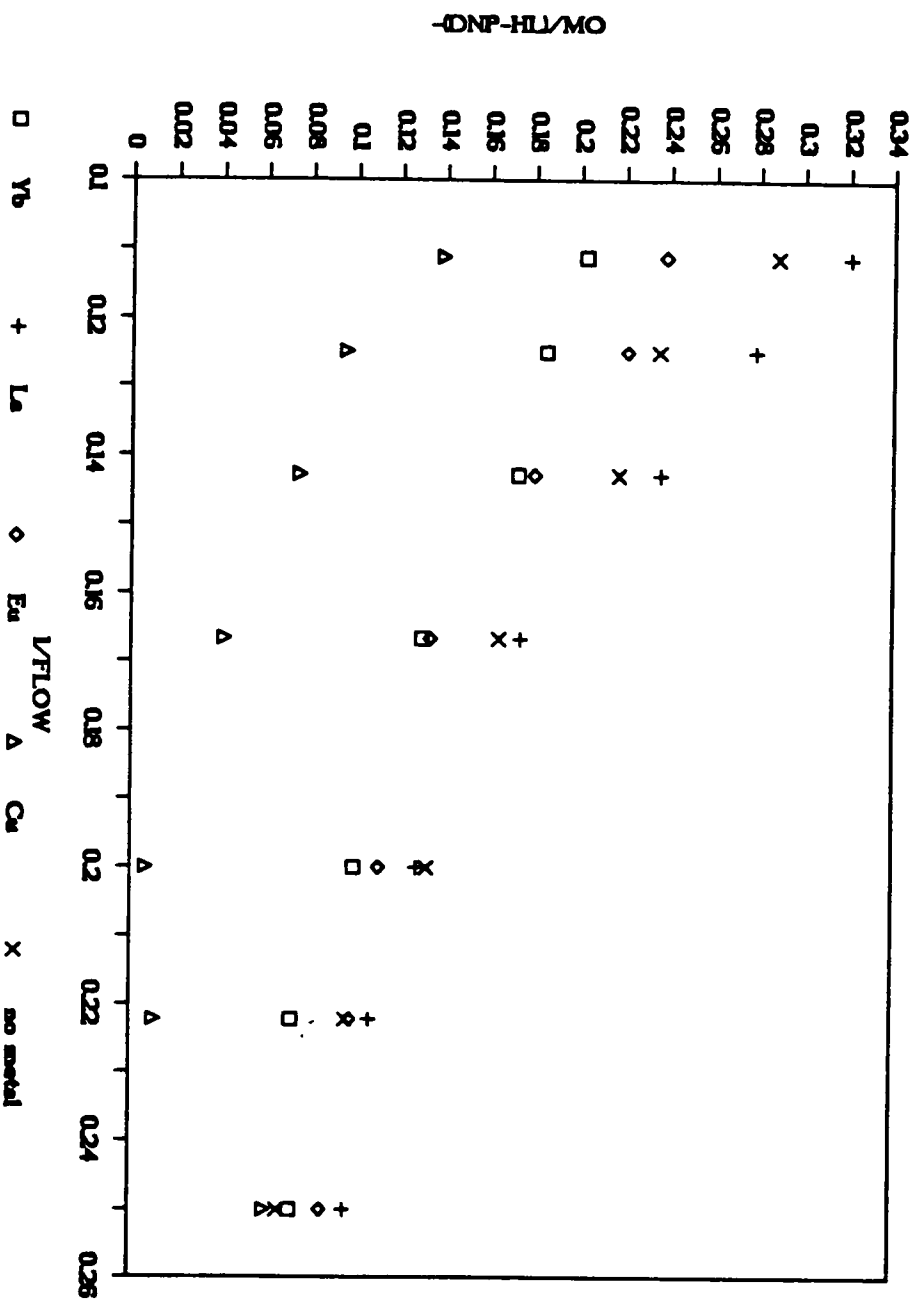

Figure 6.12 The observed ^1H DNP enhancements at 3.80 PPM vs. 1/flow plot of 4,6-dimethyl-2-methoxyacetophenone for different added LSR and Copper complex.

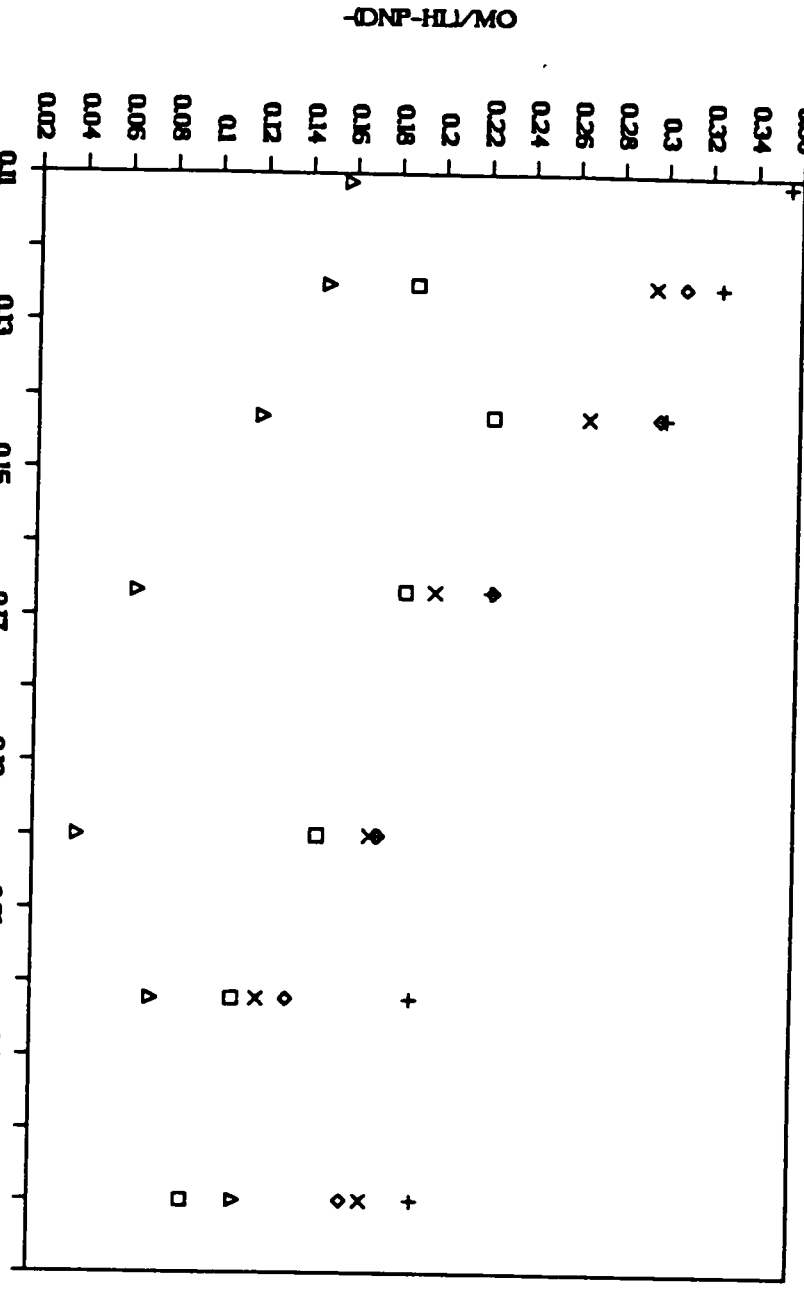

Figure 6.13 The observed ^{1}H DNP enhancements at 6.60 PPM vs. 1/flow plot of 4,6-dimethyl-2-methoxyacetophenone for different added LSR and Copper complex.

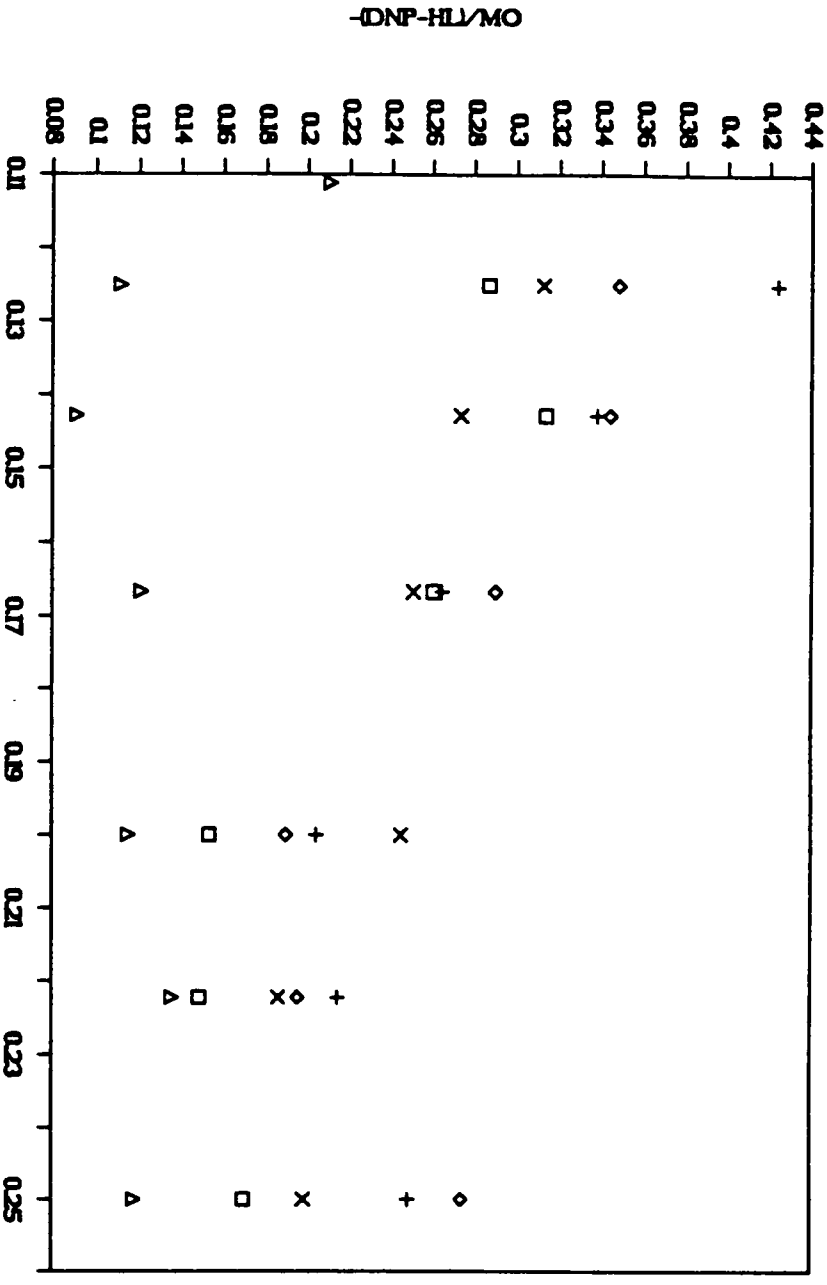

Figure 6.14 The observed ^1H DNP enhancements at 6.62 PPM vs. 1/flow plot of 4,6-dimethyl-2-methoxyacetophenone for different added LSR and Copper complex.

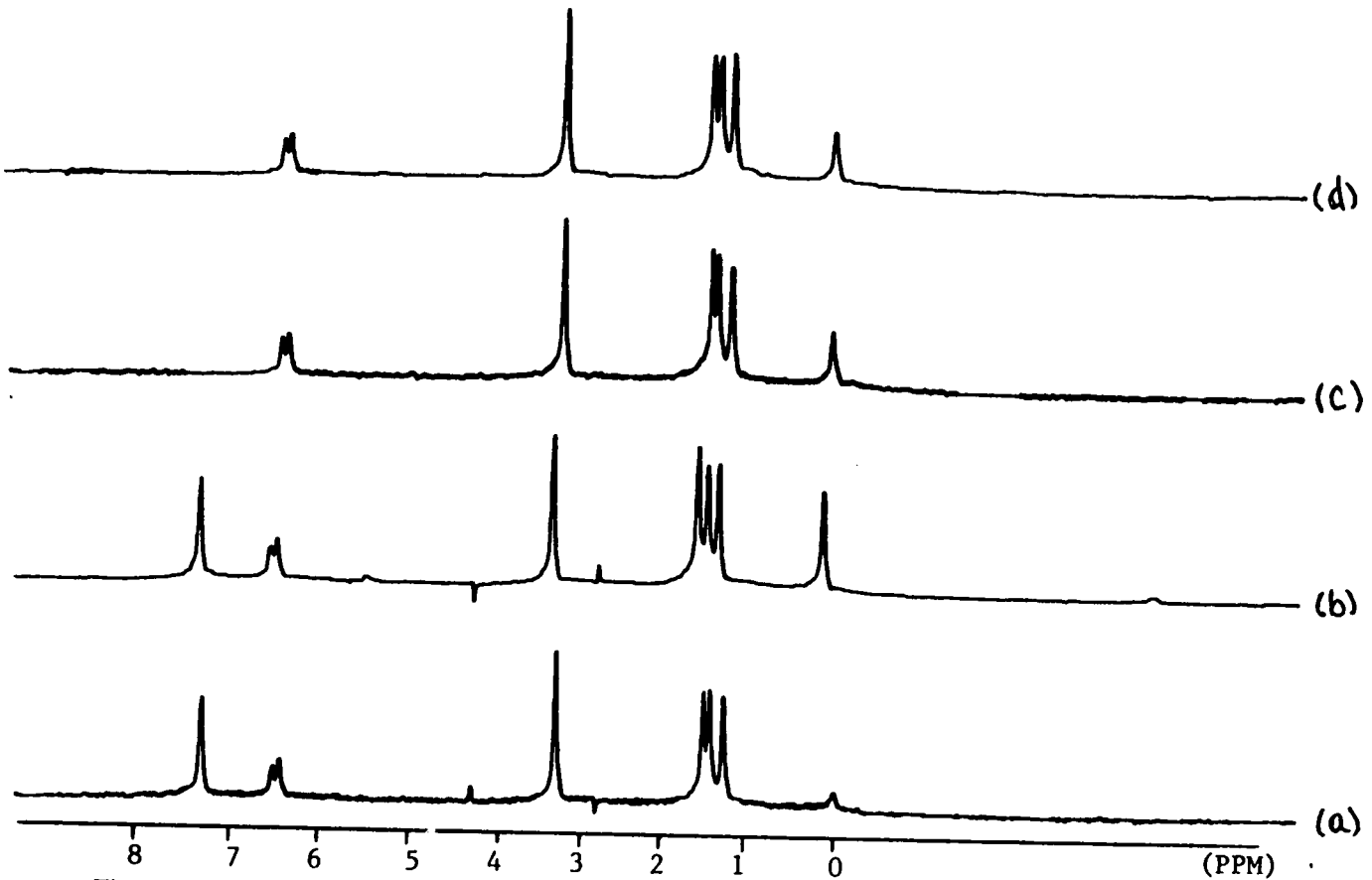

Figure 6.15 The static 200 MHz ^1H NMR spectra of 4,6-dimethyl-2-methoxyacetophenone :

a) 2.5 x 10^{-3} M of 4-hydroxy-TEMPO
b) 2.5 x 10^{-3} M of 4-hydroxy-TEMPO and Yb(thd)$_3$
c) 2.5 x 10^{-3} M of 4-hydroxy-TEMPO and La(thd)$_3$
d) 2.5 x 10^{-3} M of 4-hydroxy-TEMPO and Eu(thd)$_3$

Experimental

DTPA-bis(1-oxyl-2,2,6,6-tetramethyl-piperidinyl-4-amide) (DTPA-diradical). Diethylenetriaminepentaacetic anhydride (0.97 g, 2.7 mmol) and 4-aminoTEMPO (0.93 g, 5.4 mmol) were dissolved in 1 mL dry benzene and 2 mL dry dimethylformamide in a 10 mL, 1 necked, round bottomed flask fitted with a water cooled condenser and a magnetic stir bar. The solution was heated at 70 °C for 3 hours. The solvent was removed *in vacuo*. The residue was purified by flash chromatography (Kieselgel 60. > 230 mesh) using CH_2Cl_2/CH_3OH (1 : 1 v/v) as eluant. The solvent was removed *in vacuo* and afforded 0.95 g (46% yield) of product. M.P. 210 - 213 °C (dec.)

DTPA-diradical gadolinium complex. To a solution of gadolinium nitrate pentahydrate (0.1552 g, 0.3 mmol) in 1.5 mL of water was added a solution of DTPA-diradical (0.2100 g, 0.3 mmol) in 1.5 mL methanol. This mixture was placed in a 10 mL, 1-necked, round bottomed flask fitted with a water cooled condenser. The reaction mixture was heated on a steam bath for 20 minutes, and the solvent was removed *in vacuo*. The orange residue was washed with acetone to remove the unreacted chelating reagent. The orange crystals weighed 0.32 g (88% yield). M.P. > 300 °C.

DTPA-diradical chromium complex. To a solution of chromium acetate hydrate (0.0742 g, 0.3 mmol) in 1.5 mL of water was added a solution of DTPA-diradical (0.2100 g, 0.3 mmol) in 1.5 mL methanol. This mixture was placed in a 10 mL, 1-necked, round bottomed flask fitted with a water cooled condenser. The reaction mixture was heated on a steam bath for 20 minutes, and the solvent was removed *in vacuo*. The purple residue was washed with acetone to remove the unreacted chelating reagent. The purple crystals weighed 0.25 g (88% yield). M.P. > 300 °C.

DTPA-diradical ytterbium complex. To a solution of ytterbium chloride hexahydrate (0.1163 g, 0.3 mmol) in 1.5 mL of water was added a solution of DTPA-diradical (0.2100 g,

0.3 mmol) in 1.5 mL methanol. This mixture was placed in a 10 mL, 1-necked, round bottomed flask fitted with a water cooled condenser. The reaction mixture was heated on a steam bath for 20 minutes, and the solvent was removed *in vacuo*. The orange residue was washed with acetone to remove the unreacted chelating reagent. The orange crystals weighed 0.25 g (77% yield). M.P. > 300 °C.

DTPA-1-oxyl-2,2,6,6-tetramethyl-piperidinyl-4-amide (DTPA-monoradical). Diethylenetriaminepentaacetic anhydride (0.97 g, 2.7 mmol) and 4-aminoTEMPO (0..46 g, 2.7 mmol) were dissolved in 1 mL dry benzene and 10 mL dry dimethylformamide in a 25 mL, 1 necked, round bottomed flask fitted with a water cooled condenser and a magnetic stir bar. The solution was heated at 70 °C for 3 hours. The solvent was removed *in vacuo*. The residue was purified by flash chromatography (Kieselgel 60. > 230 mesh) using CH_2Cl_2/CH_3OH (2 : 1 v/v) as eluant. When the eluant was added to the residue, there were some white solids that were not soluble. The solvent was removed *in vacuo* and afforded 4-aminoTEMPO.

Adsorbing DTPA-diradical on silica gel. DTPA-diradical (0.15 g) was dissolved in deionized water in a 50 mL, 1-necked, round bottomed flask. Silica gel (0.60 g, Kieselgel 60 , washed with HCl and dried) was added to the dissolved DTPA-diradical solution. Water was removed *in vacuo*. Addition and removal of H_2O was repeated until the silica gel acquired light orange color uniformally throughout.

Adsorbing DTPA-diradical ytterbium complex on silica gel. DTPA-diradical ytterbium complex (0.15 g) was dissolved in deionized water in a 50 mL, 1-necked, round bottomed flask. Silica gel (0.60 g, Kieselgel 60 , washed with HCl and dried) was added to the dissolved DTPA-diradical solution. Water was removed *in vacuo*. Addition and removal of H_2O was repeated until the silica gel acquired light orange color uniformally throughout.

Chelation of 4-phenacylidene-2,2,5,5-tetramethylimidazolidin-1-yloxyl with Ytterbium - method A. 4-Phenacylidene-2,2,5,5-tetramethylimidazolidin-1-yloxyl (0.10 g,

0.39 mmol) was dissolved in methanol in a 10 mL, 1-necked, round bottomed flask fitted with a water cooled condenser and a magnetic stir bar. The solution was heated to 60 °C. A solution of ytterbium chloride hexahydrate dissolved in 3 mL of water was added portionwise to the heated solution. After this addition, the solution was maintained at 60 °C for 1/2 hour. The solution was cooled, solids were filtered, washed with water, and dissolved in ethyl ether. The ether was removed *in vacuo*. The yellow solid was dried overnight and a melting point was taken. It had the same melting point as the starting radical. Mixed melting point confirmed this material was 4-phenacylidene-2,2,5,5-tetramethylimidazolidin-1-yloxyl.

Chelation of 4-phenacylidene-2,2,5,5-tetramethylimidazolidin-1-yloxyl with Ytterbium - method B. 4-Phenacylidene-2,2,5,5-tetramethylimidazolidin-1-yloxyl (0.10 g, 0.39 mmol) and 1 equivalent of NaOH were dissolved in methanol in a 10 mL, 1-necked, round bottomed flask fitted with a water cooled condenser and a magnetic stir bar. The solution was heated to 60 °C. A solution of ytterbium chloride hexahydrate dissolved in 3 mL of water was added portionwise to the heated solution. After this addition, the solution was maintained at 60 °C for 1/2 hour. The solution was cooled, the solids were filtered, washed with water, and dissolved in ethyl ether. The ether was removed *in vacuo*. The yellow solid was dried overnight and a melting point was taken. It had the same melting point as the starting radical. Mixed melting point confirmed this material was 4-phenacylidene-2,2,5,5-tetramethylimidazolidin-1-yloxyl.

Chelation of 4-phenacylidene-2,2,5,5-tetramethylimidazolidin-1-yloxyl with Ytterbium - method C. 4-Phenacylidene-2,2,5,5-tetramethylimidazolidin-1-yloxyl (0.10 g, 0.39 mmol) and 10 equivalents of NaOH were dissolved in methanol in a 10 mL, 1-necked, round bottomed flask fitted with a water cooled condenser and a magnetic stir bar. The solution was heated to 60 °C. A solution of ytterbium chloride hexahydrate dissolved in 3 mL of water was added portionwise to the heated solution. After this addition, the solution was

maintained at 60 °C for 1/2 hour. The solution was cooled, the solids were filtered, washed with water, and dissolved in ethyl ether. The ether was removed *in vacuo*. The yellow solid was dried overnight and a melting point was taken. M.P. 45 - 47 °C. The ESR spectrum indicated no radicals were present.

Chelation of 4-phenacylidene-2,2,5,5-tetramethylimidazolidin-1-yloxyl with Ytterbium - method D. Ytterbium chloride hexahydrate (0.25 g, 0.65 mmol) was dissolved in 10 mL of distilled water in 25 mL Erlenmeyer flask. Urea (0.2 g) and 4-phenacylidene-2,2,5,5-tetramethylimidazolidin-1-yloxyl (0.10 g, 0.39 mmol) was added to the solution. The flask was covered with a watch glass and heated at 100 °C in a water bath for 2 hours. Compound melted and the solution became yellow. The reaction flask was cooled to room temperature and the yellow solid was filtered, washed with several portions of water and dissolved in ethyl ether. The ether was yellow and there were some white solids left in the funnel. The ether was removed *in vacuo*. The yellow solid was dried overnight and a melting point was taken. It had the same melting point as the starting radical. Mixed melting point confirmed this material was 4-phenacylidene-2,2,5,5-tetramethylimidazolidin-1-yloxyl.

2,2,6,6-tetramethyl-4-piperidinyl, 4,4-dimethyl-3-oxopentanoate. A mixture of methyl-4,4-dimethyl-3-oxopentanoate (1.58 g, 0.01 mol), 2,2,6,6-tetramethyl-4-piperidinol (0.40 g, 0.0023 mol), and p-toluenesulfonic acid monohydrate (0.44 g, 0.0023 mol) were heated in a 50 mL, 1-necked, round bottomed flask fitted with a short path water cooled condenser and a magnetic stir bar. The acid was dried by repeated addition and removal of dry benzene. This process was repeated until the acid crystals were white and fluffy. The methanol that formed were distilled off. After cooling, 10 mL water was added to the reaction flask. The resulting solution was extracted with ethyl ether. The aqueous layer was separated and rendered basic (pH - 9) with 5% NaOH. The aqueous layer was extracted twice with 20 mL ethyl ether. The ether layers were combined and dried over K_2CO_3. Ether was removed *in vacuo* to afford very small amount of white solid. The solid had the same melting

point and ^1H NMR as 2,2,6,6-tetramethyl-4-piperidinol.

2,2,6,6-tetramethyl-4-piperidinyl, 4,4-dimethyl-3-oxopentanoate. P-toluenesulfonic acid monohydrate (2.70 g, 0.014 mol) was refluxed in 40 mL dry benzene in a 100 mL, 3-necked, round bottomed flask fitted with a Soxhlet extractor filled with activated 3Å molecular sieves, a water cooled condenser, and a magnetic stir bar under N_2. The mixture was refluxed for overnight. The 3Å molecular sieves was replaced by activated 4Å molecular sieves and methyl 4,4-dimethyl-3-oxopentanoate (10.00 g, 0.063 mol) and 2,2,6,6-tetramethyl-4-piperidinol (2.50 g, 0.014 mol) in 20 mL dry benzene were added to the flask. The mixture was refluxed for 10 hours. After cooling, 10 mL water was added to the reaction flask. The resulting solution was extracted with ethyl ether. The aqueous layer was separated and rendered basic (pH - 9) with 5% NaOH. The aqueous layer was extracted twice with 20 mL ethyl ether. The ether layers were combined and dried over K_2CO_3. The ether was removed *in vacuo* and to afford 2.40 g (60% crude yield) of a colorless oil. This material was used without further purification and afforded the following spectroscopic data. ^1H NMR δ 1.12 (s, 6H), 1.17 (s, 9H), 1.22 (s, 6H), 1.80 - 2.0 (m, 4H), 3.46 (s, OC-CH_2-CO), 4.97 (s, HOC=CH-C=O), 5.23 (m, 1H).

2,2,6,6-tetramethyl-1-oxyl-4-piperidinyl,4,4-dimethyl-3-oxopentanoate. 2,2,6,6-tetramethyl-4-piperidinyl, 4,4-dimethyl-3-oxopentanoate (1.0 g, 3.5 mmol) was oxidized with m-chloroperbenzoic acid (55%) (1.8 g, 5.8 mmol) in 100 mL ethyl ether in a 1-necked, 250 mL, round bottomed flask fitted with a water cooled condenser at 0 °C for 2 hours. The solution was washed twice with 50 mL 5% NaOH. The organic layer was dried over $MgSO_4$ and the solvent was removed *in vacuo*. The residue was purified by chromatography (Woelm Act. III. with 50 : 50 ethyl ether : petroleum ether). This afforded 0.6 g (57% yield) orange crystals. M.P. 89 °C.

Copper complex of the β-ketoester radical. 2,2,6,6-tetramethyl-1-oxyl-4-piperidinyl-4,4-dimethyl-3-oxopentanoate (1.0 g, 3.35 mmol) was dissolved in ~ 5 mL of a

mixture of water-ethanol (50-50 by volume) in a 25 mL. 1-necked, round bottomed flask fitted with a water cooled condenser and a magnetic stir bar. The mixture was heated to 60 °C and a solution of Copper acetate (0.35 g, 1.9 mmol) in 10 mL water was added portionwise. During the addition, the pH of the solution was maintained at 8 using 5% NaOH. The brown precipitate was filtered, washed with water and dissolved in ethyl ether. The ether was removed *in vacuo* and to afford dull green crystals. The product was recrystallized from heptane and to afford 0.3 g (27% yield). M.P. 247 - 249 °C.

Ytterbium complex of the β-ketoester radical - method A. 2,2,6,6-tetramethyl-1-oxyl-4-piperidinyl-4,4-dimethyl-3-oxopentanoate (1.0 g, 3.35 mmol) was dissolved in ~ 5 mL of a mixture of water-ethanol (50-50 by volume) in a 25 mL. 1-necked, round bottomed flask fitted with a water cooled condenser and a magnetic stir bar. This mixture was heated to 60 °C and a solution of Ytterbium chloride hexahydrate (0.74 g, 1.9 mmol) in 10 mL water was added portionwise. During the addition, the pH of the solution is maintained at 8 using 5% NaOH. The orange precipitate was filtered, washed with water and dissolved in ethyl ether. The ether was removed *in vacuo* and to afford orange crystals. A melting point was taken and it was concluded that the orange crystals were the starting radical.

Zinc complex of the β-ketoester radical - method A. 2,2,6,6-tetramethyl-1-oxyl-4-piperidinyl-4,4-dimethyl-3-oxopentanoate (1.0 g, 3.35 mmol) was dissolved in ~ 5 mL of a mixture of water-ethanol (50-50 by volume) in a 25 mL. 1-necked, round bottomed flask fitted with a water cooled condenser and a magnetic stir bar. This mixture was heated to 60 °C and a solution of Zinc acetate dihydrate (0.42 g, 1.9 mmol) in 10 mL water was added portionwise. During the addition, the pH of the solution is maintained at 8 using 5% NaOH. The orange precipitate was filtered, washed with water and dissolved in ethyl ether. The ether was removed *in vacuo* and to afford orange crystals. A melting point analysis determined that the orange crystals were the starting radical.

Ytterbium complex of the β-ketoester radical- method B. 2,2,6,6-tetramethyl-1-oxyl-4-piperidinyl-4,4-dimethyl-3-oxopentanoate (1.0 g, 3.35 mmol) and 1 equivalent of NaOH were dissolved in ~ 5 mL of methanol in a 25 mL. 1-necked, round bottomed flask fitted with a water cooled condenser and a magnetic stir bar. The mixture was heated to 60 °C and a solution of Ytterbium chloride hexahydrate (0.74 g, 1.9 mmol) in 10 mL water was added portionwise. The orange precipitate was filtered, washed with water and dissolved in ethyl ether. The ether was removed *in vacuo* and to afford orange crystals. A melting point determined that the orange crystals were the starting radical.

Zinc complex of the β-ketoester radical - method B. 2,2,6,6-tetramethyl-1-oxyl-4-piperidinyl-4,4-dimethyl-3-oxopentanoate (1.0 g, 3.35 mmol) and 1 equivalent of NaOH were dissolved in ~ 5 mL of methanol in a 25 mL. 1-necked, round bottomed flask fitted with a water cooled condenser and a magnetic stir bar. The mixture was heated to 60 °C. and a solution of Zinc acetate dihydrate (0.42 g, 1.9 mmol) in 10 mL water was added portionwise. The orange precipitate was filtered, washed with water and dissolved in ethyl ether. The ether was removed *in vacuo* and to afford orange crystals. A melting point determined that the orange crystals were the starting radical.

DNP NMR experiments. The variable low field magnet and microwave TE_{102} cavity were part of a modified Varian E-3 EPR spectrometer. The microwave frequency (9.3 GHz) was generated by a low level klystron and amplified to ~ 4 - 10 watts using a Varian TWT amplifier to provide a B_{1e} field for the DNP experiments of 0.34 T. The high magnetic field (B_0^H) NMR detector was a JEOL FX-200 NMR spectrometer with an in house probe. An ambient temperature of ~ 22 °C was employed in all experiments. The total volume of region A was ~ 160 μL. The transfer tubing in region B was ~ 2.0 m of 0.18 mm inner diameter teflon tubing with an estimated transfer volume of ~ 50 μL. The volume in the high magnetic region before detection was ~ 10 μL. The active NMR volume in the detector region was ~ 20 μL. The pump employed in these experiments was a Waters 6000A dual piston pump.

Conclusions

From the NMR experiments utilizing LIS and LIR data, it is shown that the trifluoroethyl moiety is shown to be a good deactivating group toward lanthanide induced complexation for hydroxyl and carbonyl functionalities. It can be used selectively to deactivate a polyfunctional molecule and certain molecular information can be obtained from the LIS data. Structural information (e.g. distance ratios) can also be obtained with the use of LIR data.

The DNP experiments yielded several interesting observations. First, by deuterating the TTBP and GALV radicals, the microwave power needed for saturation did not decrease. With deuterated, ^{15}N labelled 4-hydroxy-TEMPO, an increase in the observed enhancements was observed at low concentration of the nitroxide radical as compared to the nondeuterated, ^{14}N labelled 4-hydroxy-TEMPO due to electron-electron exchange interaction. Second, there are selective ^{1}H DNP enhancements between the taxol molecule and the immobilized nitroxide radical surface utilizing the low-to-high field SLIT DNP experiments. The low-to-high field SLIT DNP experiment offers the advantage over LLIT DNP experiment of not only fairly high observable DNP enhancements for nuclei with short T_1s (e.g. 0.3 seconds), but also does not contaminate the solvent/solute system. Therefore, recovery of valuable samples is possible. Third and perhaps most interesting, studies of LSR-nitroxide radicals systems seem to indicate that there is a selective deactivation of the DNP enhancements by Yb^{+3} lanthanide metal near or at the complexation site(s). Future work might involve synthesis of an intramolecular system of Yb^{+3} lanthanide metal and a nitroxide radical moiety which can be immobilized on a silica gel surface in order that, a low-to-high field SLIT DNP experiment can be carried out. This type of experiment would determine if the Yb^{+3} lanthanide metal can selectively deactivate the DNP enhancements at the complexation site of a molecule.

References

1) Wenzel, T.J., "NMR Shift Reagents", CRC Press Inc., Florida, 1987.

2) Müller-Warmuth, W., and Meise-Gresch, K., *Adv. Magn. Reson.*, **1983**, *11*, 1.

3) Wind, R.A., Duijvestijn, M.J., Van der Lugt, C., Maneschijn, A., and Vriend, J., *Prog. NMR Spectrosc.*, **1985**, *17*, 33.

4) Hinckley, C.C., *J. Am. Chem. Soc.*, **1969**, *91*, 5160.

5) Sander, J.K.M., and Williams, D.H., *J. Chem. Soc. Chem. Commun.*, **1970**, 422.

6) Rondeau, R.E., and Sievers, R.E., *J. Am. Chem. Soc.*, **1971**, *93*, 1522.

7) Morrill, T.C., Clark, R.A., Bilobran, D., and Youngs, D.S., *Tetrahedron Lett.*, **1975**, 397.

8) Goering, H.L., Eikenberry, J.N., and Koermer, G.S., *J. Am. Chem. Soc.*, **1971**, *93*, 5913.

9) Fraser, R.R., Petit, M.A., and Saunders, J.K., *J. Chem. Soc. Chem. Commun.*, **1971**, 1450.

10) Evans, D.F., Tucker, J.N., and de Villardi, G.C., *J. Chem. Soc. Commun.*, **1975**, 205.

11) Wenzel, T.J., Bettes, T.C. Sadlowski, J.E., and Sievers, R.E., *J. Am. Chem. Soc.*, **1982**, *102*, 5903.

12) Rabenstein, D.L., *Anal. Chem.*, **1971**, *43*, 1599.

13) Hofer, O., *Top. Stereochem.*, **1976**, *9*, 111.

14) Horrocks, W.D. Jr., *Inorg. Chem.*, **1970**, *9*, 690.

15) McConnell, H.M., and Robertson, R.E., *J. Chem. Phys.*, **1958**, *29*, 1361.

16) Lewis. W.B., Jackson, J.A., Lemons, J.F., and Taube, H., *J. Chem. Phys.*, **1962**, *36*, 694.

17) Reuben, J., "Nuclear Magnetic Resonance Shift Reagents", Sievers, R.E., Ed., Academic Press, New York, 1973, 341.

18) Chiasson, J.B., and Jankowski, K., "Lanthanide Shift Reagents in Stereochemical Analysis", Morrill, T.C., Ed., VCH Publishers, Inc., New York, 1986, p. 19.

19) Roberts, J.D., Hawkes, G.E., Husar, J., Robert, A.W., Roberts, D.W., *Tetrahedron*, **1974**, *30*, 1833.

20) Wilcott, M.R., III., Lenkinski, R.E., and Davis, R.E., *J. Am. Chem. Soc.*, **1972**, *94*, 1742.

21) Sullivan, G.R., *J. Am. Chem. Soc.*, **1976**, *98*, 7162.

22) Bleaney, B., *J. Magn. Reson.*, **1972**, *8*, 91.

23) Reubens, J., Elgavish, G.A., "Handbook of the Phsysics and Chemistry of Rare Earths", Gschneider, K.a., Jr., and Erying, L., Ed., North Holland, New York, 1979.

24) Dwek, R.A., "Nuclear Magnetic Resonance (NMR) in Biochemistry", Clarendon Press, Oxford, 1973.

25) Inagaki, F., and Miyazawa, T., "Progress in NMR Spectroscopy", Pergammon Press Ltd., Great Britain, **1981**, *14*, 67.

26) McLennan, I.J., and Lenkinski, R.E., *J. Am. Chem. Soc.*, **1984**, *106*, 6905.

27) Faller, J.W., Adams, M.A., LaMar, G.N., *Tetrahedron Lett.*, **1974**, 699.

28) Peters, J.A., van Bekkum, H., and Bovee, W.M.M.J., *Tetrahedron*, **1982**, *38*, 331.

29) Cockerill, A.F., Davies, G.L.O., Harden, R.C., and Rackham, D.M., *Chem. Rev.*, **1973**, *73*, 553.

30) Hofer, O., *Top. Stereochem.*, **1976**, *9*, 111.

31) Wright, G.E., and Wei, T.Y.T., *Tetrahedron*, **1973**, *29*, 3775.

32 Crump, D.R., Sanders, J.K.M., and Williams, D.H., *Tetrahedron Lett.*, **1970**, 4994.

33) Raber, D.J., and Propeck, G.J., *J. Org. Chem.*, **1982**, *47*, 3324.

34) Szabo, P., M.S. Thesis 1979, Virginia Polytechnic Institute and State University.

35) Koller, K.L. and Dorn H.C., *Anal. Chem.*, **1982**, *54*, 529.

36) Wild, C., Ph.D. Thesis 1988, Virginia Polytechnic Institute and State University.

37) Abraham, R.J., Fisher, J., and Loftus, P., "Introduction to NMR Spectroscopy", John Wiley & Sons, Chichester, 1988.

38) Roy, J.T., Ph.D. Thesis 1984, Virginia Polytechnic Institute and State University.

39) Hausser, K.H., and Stehlik, D., *Adv. Magn. Reson.*, **1968**, *3*, 79.

40) Dwek, R.A., Richards, R.E., and Taylor, D., *Annu. Rev. NMR Spectrosc.*, **1969**, *2*, 293.

41) Potenza, J.A., *Adv. Mol. Relaxation Processes*, **1972**, *4*, 229.

42) Overhauser, A. W., *Phys. Rev.*, **1953**, *92*, 411.

43) Carver, T.R., and Slichter, C.P., *Phys. Rev.*, **1953**, *92*, 212.

44) Abragam, A., *Phys. Rev.*, **1955**, *98*, 1729.

45) Abragam, A., Landesman, A., and Minter, J.M., *C.R. Acad. Sci.*, **1958**, *247*, 1852.

46) Poindexter, E.H., *J. Chem. Phys.*, **1965**, *43*, 3587.

47) Ryter, C., *Phys. Rev. Lett.*, **1960**, *5*, 10.

48) Codrington, R.S., and Bloembergen, N., *J. Chem. Phys.*, **1958**, *29*, 600.

49) Haupt, J., and Müller-Warmuth, W., *Z. Naturforsch. A*, **1966**, *21*, 158.

50) Richards, R.E., and White, J.W., *Discuss. Faraday Soc.*, **1962**, *34*, 96.

51) Kramer, K.D., and Müller-Warmuth, W., *Z. Naturforsch. A*, **1964**, *19*, 375.

52) Potenza, J.A., and Poindexter, E.H., *J. Am. Chem. Soc.*, **1968**, *90*, 6309.

53) Poindexter, E.H., Dwek, R.A., and Potenza, J.A., *J. Chem. Phys.*, **1969**, *51*, 628.

54) Dwek, R.A., Paddock, N.L., Potenza, J.A., and Poindexter, E.H., *J. Am. Chem. Soc.*, **1969**, *91*, 5436.

55) Dwek, R.A., Richards, R.E., Taylor, D., Penney, G.J., and Sheldrick G.M., *J. Chem. Soc. A*, **1969**, 935.

56) Solomon, I., *Phys. Rev.*, **1955**, *99*, 559.

57) Poindexter, E.H., Stewart, J.R., and Caplan P.J., *J. Chem. Phys.*, **1967**, *47*, 2862.

58) Ohnishi, J., and McConnell, H.M., *J. Am. Chem. Soc.*, **1965**, *87*, 2293.

59) Berliner, L.H., Ed., "Spin Labeling Theory and Applications", Academic Press, New York, NY. 1976.

60) Dwek, R.A., Howarth, O.W., Natusch, D.F.S., and Richards, R.E., *Mol. Phys.*, **1967**, *13*, 457.

61) Helbert, J.N., Poindexter, E.H., and Wagner, B.E., *Chem. Phys. Lett.*, **1977**, *52*, 546.

62) Bates, R.D., Poindexter, E.H., and Wagner, B.E., *J. Chem. Phys.*, **1973**, *59*, 3031.

63) Potenza, J.A., and Linowski, J.W., *J. Chem. Phys.*, **1971**, *54*, 4095.

64) Wagner, B.E., Linowski, J.W., Potenza, J.A., Bates, R.D., Helbert, J.N., and Poindexter, E.H., *J. Am. Chem. Soc.*, **1976**, *98*, 4405.

65) Potenza, J.A., Linowski, J.W., Poindexter, E.H., and Wagner, B.E., *Mol. Phys.*, **1975**, *29*, 1597.

66) Natusch, D.F.S., and Richards, R.E., *Chem. Commun.*, **1966**, 185.

67) Grützediek, H., and Müller-Warmuth, W., *Z. Naturforsch. A*, **1969**, *24*, 459.

68) Stewart, J.R., Poindexter, E.H., and Potenza, J.A., *J. Am. Chem. Soc.*, **1967**, *89*, 6017.

69) Webb, R.H., Van Nghia, N., Pearlman, M.R., Poindexter, E.H., Caplan, P.J., and Potenza, J.A., *J. Chem. Phys.*, **1969**, *50*, 4408.

70) Potenza, J.A., Poindexter, E.H., Caplan, P.J., and Dwek, R.A., *J. Am. Chem. Soc.*, **1969**, *91*, 4356.

71) Dwek, R.A., and Richards, R.E., *Chem. Commun.*, **1966**, 581.

72) Dorn, H.C., Wang, J., Allen, L., Sweeney, D., and Glass, T.E., *J. Magn. Reson.*, **1988**, *79*, 404.

73) Gitti, R., Wild, C., Tsiao, C., Zimmer, K., Glass, T.E., and Dorn, H.C., *J. Am. Chem. Soc.*, **1988**, *110*, 2294.

74) Dorn, H.C., Gitti, R., Tsai, K.H., and Glass, T.E., *Chem. Phys. Lett.*, **1989**, *155*, 227.

75) Tsai, K.H., and Dorn, H.C., 30th Experimental NMR Conference, April 1989, Asilomar, California.

76) Stillson, G.H., Sawyer, D.W., and Hunt, C.K., *J. Am. Chem. Soc.*, **1945**, *67*, 303.

77) Kharasch, M.S., and Joshi, B.S., *J. Org. Chem.*, **1957**, *22*, 1435.

78) Bates, R.D. Jr., *J. Magn. Reson.*, **1982**, *48*, 111.

79) Bates, R.D., Jr., and Drozdoski, W.S., *J. Chem. Phys.*, 1977, *67*, 4038.

80) Motchane, J.L., Erb, E., and Uebersfeld, J., *Compt. Rend. Acad. Sci. (Paris)*, **1958**, *246.*, 833.

81) Wani, M.C., Taylor, H.L., Wall, M.E., Coggon, P., and McPhail. A., *J. Am. Chem. Soc.*, **1971**, *93*, 2325.

82) Mclaughlin, J.L., Miller, R.W., Powell, R.G., and Smith, C.R. Jr., *J. Nat. Prod.*, **1981**, *44*, 312.

83) Nagy, V.Y., Petrukhin, O.M., and Zolotov, Y.A., *CRC Crit. Rev. Anal. Chem.*, **19**, *17*, 265.

84) Sosnovsky, G., Li, S.W., and Uma Maheswara Rao, N., *Z. Naturforsch.*, **1985**, *40b*, 1558.

85) Kelareva, M.P., Gromova, T.A., Bodnya, V.A., Volodarskii, L.B., Reznikov, V.A., and Zolotov, Yu. A., *Zh. Anal. Khim.*, **1982**, *37*, 563.

86) Fernelius, W.C., and Blanch, J.E., *Inorg. Syn.*, **1957**, *5*, 130.

87) Briere, R., Giroud, A.M., Rassat, A., and Rey, P., *Bull. Soc. chim. France II*, **1980**, 147.

88) Springer, C.S. Jr., Meek, D.W., and Sievers, R.E., *Inorg. Chem.*, **1967**, *6*, 1105.

The vita has been removed from the scanned document